An Observationally and Dynamically Determined Basic State for the Study of Synoptic Scale Waves

by

Michael Cottman Morgan

S.B., Mathematics, MIT
(1988)

Submitted to the Department of Earth, Atmospheric, and Planetary Sciences
in partial fulfillment of the requirements for the degree of

DOCTOR OF PHILOSOPHY IN METEOROLOGY

at the

MASSACHUSETTS INSTITUTE OF TECHNOLOGY

September 1994

© Massachusetts Institute of Technology, 1994. All Rights Reserved.

Author _____
Center for Meteorology and Physical Oceanography
Department of Earth, Atmospheric, and Planetary Sciences
22 August 1994

Certified by _____
Professor Kerry A. Emanuel
Thesis Supervisor

Accepted by _____
Professor Thomas H. Jordan
Department Chairman

WITHDRAWN
MASSACHUSETTS INSTITUTE
FROM
MIT LIBRARIES

An Observationally and Dynamically Determined Basic State for the Study of Synoptic Scale Waves

by

Michael Cottman Morgan

Submitted to the Department of Earth, Atmospheric, and Planetary Sciences
on 22 August 1994, in partial fulfillment of the requirements for the degree
of Doctor of Philosophy in Meteorology

Abstract

The principal objective of this thesis is to determine a basic state, constrained by both dynamics and observations, for the study of synoptic scale waves in the atmosphere. Such a basic state may be regarded as the balanced mass and wind fields of a steady flow in which the synoptic scale waves and other transient features have been removed while certain dynamically important features of the observed potential vorticity distribution have been retained.

Isentropic analyses reveal that potential vorticity is nearly uniform in the troposphere and lower stratosphere away from the polar and subtropical jet streams. Maxima in the magnitudes of potential vorticity gradients are found along the tropopause in the vicinity of the jets. Instantaneous analyses of Ertel potential vorticity (Q) and Montgomery potential (M), show a tendency for the isopleths of each field to be nearly parallel - suggesting that a steady component of the flow dominates the instantaneous observed flow. Geostrophic scatter diagrams of Q and M constructed for individual isentropic surfaces suggest that a robust functional relationship between Q and M (*i.e.* $Q = Q(M)$) may be defined for each isentropic surface.

While the condition $Q = Q(M;\theta)$ satisfies the requirement for the basic state to be steady in the interior, steadiness also requires that the advections of potential temperature at the both the lower and upper boundary be zero. (i.e. $M = M(\theta)$). At the lower boundary, a relationship between M and θ is obtained; at the upper boundary, the time mean M is prescribed. The technique used to determine the steady, balanced, basic state essentially involves inverting the potential vorticity field to determine the Montgomery potential, while constraining the solution to obey $Q = Q(M;\theta)$, subject to boundary conditions, one of which satisfies the aforementioned boundary conditions on M. The resulting nonlinear problem is solved iteratively. A geostrophic balance condition is used in the inversion.

The technique is demonstrated by solving for a basic state flow for January 1991. The basic state that is determined is characterized by an equivalent barotropic structure with ridges over the oceans and troughs over the continents and light winds at the surface. These are attributes of the so called "thermally equilibrated" or "resonant response."

In addition to determining this basic state flow, a new expression for the refractive index is

derived in isentropic coordinates making use of the geostrophic momentum approximation. In its simplest form the refractive index is expressed as the gradient of the natural logarithm of the potential vorticity with respect to the Bernoulli function.

Thesis Supervisor: Kerry A. Emanuel
Title: Professor of Meteorology

Table of Contents

ACKNOWLEDGEMENTS

I express my sincere thanks to my thesis advisor, Dr. Kerry Emanuel. I greatly appreciated his guidance, insightful counsel, and patience throughout the course of my thesis research. His allowing me considerable independence to conduct my thesis research will undoubtedly serve me well in my conduct of future research. I thank my thesis committee members Dr. Paola Malanotte-Rizzoli, Dr. John Marshall, Dr. Alan Plumb, and Dr. Frederick Sanders for their thoughtful and helpful criticism and advice.

I also express my gratitude to Dr. Randall Dole, my academic advisor during my first two years as a graduate student, for his encouragement and continued interest in my work.

Among the many friends and fellow students I have had the pleasure to have known, I express my deepest appreciation to John Nielsen-Gammon, Peter Neilley, Chris Davis, Robert Black, and Lars Schade, for their inspiration and friendship. I also thank the many "weather weenies" (including Brad Lyon, Dennis Boccippio, Daniel Kirk-Davidoff, Chris Forest, Marja Bister, James Risbey, Francoise Robe, and Marek Zebrowski) who, through their enthusiasm for all sorts of weather, made my stay here enjoyable.

I wish to also acknowledge my many students and friends in Burton - Conner House, in particular, the residents of English House (Conner 2) where I had the pleasure and good fortune of serving as a graduate resident tutor.

Special thanks go also to the members of CMPO support staff including Jane McNabb, Tracy Stanelun, Eddie Nelson, Diana Spiegel, and Tom Yates for their helpfulness during my stay at MIT.

This thesis is dedicated to my parents, Windsor and Kerlan Morgan, who have provided me many opportunities to develop and explore my scientific interests. Their love and encouragement continue to inspire me to do my best.

Chapter 1

Introduction

The existence of horizontal wave-like structures in the troposphere has been recognized from the time upper tropospheric synoptic charts were analyzed in the early 1930's. These analyses reveal a broad spectrum of spatial scales for these wave-like features. The most prominent observed structures on these charts are associated with planetary waves which have typical zonal and meridional scales of several thousand kilometers. These waves are thought to be forced by topographical and thermal zonal inhomogeneities at the earth's surface (Charney and Eliassen (1949), Smagorinsky (1953), Hoskins and Karoly (1981), Held (1983)). Embedded within this large scale flow are numerous smaller scale disturbances, referred to by synopticians as "short waves". These shorter wavelength features are ubiquitous features of upper tropospheric analyses and are often associated with midlatitude cyclogenesis (Petterssen (1956), Sanders and Gyakum (1980)). Transports of potential vorticity by these waves are believed to be responsible for the formation and maintenance of persistent anomalies as well as atmospheric blocking (Illari and Marshall (1983), Shutts (1984, 1986) Neilley (1990)).

The earliest attempts at explaining the existence of these smaller scale fluctuations focused on attributing them to an instability of the flow in which they are embedded. In order to determine whether this hypothesis is correct, a three-dimensional flow must first be identified that is free of these fluctuations (Pedlosky, 1987). This fluctuation free flow is commonly called a "basic state". The next step is to determine whether the small scale disturbances that arise from this basic state resemble the observed structures seen in the atmosphere.

The most often used candidate for a basic state has been the *time mean* flow. A long time average is constructed from data to filter out the smaller time scale fluctuations, to yield a statistically steady state. The resulting flow, while free of the instantaneous fluxes of heat and momentum associated with the "transient" disturbances is not, in general, the most appropriate flow to use to assess the stability of the basic state, nor is it necessarily steady. It is often observed in dynamical systems that the disturbances that arise from instabilities often adjust the flow toward a neutral state. Another disadvantage of using the time averaged distributions of winds and temperatures as a basic state is that these fields are not guaranteed to resemble the instantaneous flow felt by the disturbances that are to be studied.

An alternative to using averaged quantities as defining the basic state, is to simply prescribe the basic state flow. In this way, one is guaranteed to have a flow that is *by definition* free of the effects of transients. The problem with this approach, however, is relating the chosen basic state to the observed flow. Further, the basic states that are chosen are often chosen to be steady. This raises the questions, "What is maintaining the steadiness of flow?" and "How does that agent which is maintaining the flow's steadiness, effect disturbances to that flow?".

It is clear that while the concept of a basic state is fundamental to the current understanding of the dynamics of the atmosphere, the identification and more importantly the existence of such a basic state has not been clearly established. In this thesis, we address the questions: "*What is an appropriate basic state for the study of the dynamics of synoptic scale eddies*?" and "*How might that basic state be determined on the basis of observations and dynamics?*"

The thesis is organized as follows: Chapter 2 provides the observational and dynamical rationalization for the work that follows. In particular, an analysis and discussion of the

distribution of Ertel potential vorticity in the troposphere and lower stratosphere and its implications for the structure, growth, and propagation of synoptic scale waves is presented. At the close of this chapter, a clear example of the difficulties in choosing a time or space average of potential vorticity is presented. In Chapter 3, further motivation for requiring the basic state to be steady is presented. A description of the date set and its limitations as well as the methodology for determining a basic state is also presented in Chapter 3. Chapter 4 contains a discussion of the implementation of the method used in determining the basic state. In Chapter 5, the derivation, calculation, and interpretation of a refractive index for the study of synoptic scale waves is presented. The primary results of the thesis are summarized in Chapter 6.

Chapter 2

Motivation

In this section the observational and dynamical motivation for this study is presented. The chapter is divided into four sections. Section 1 briefly reviews some background information on Ertel potential vorticity. For a more thorough discussion of potential vorticity (or PV), the reader is urged to refer to Hoskins *et al.* (1985) (hereafter referred to as HMR). Section 2 contains a description of the observed characteristics of the distribution of PV in the troposphere and lower stratosphere and Section 3 discusses the factors which lead to this distribution of PV. In Section 4 a discussion of the theoretical implications that the observed distribution of Ertel potential vorticity should have on the quasi-balanced dynamics of the troposphere is presented. A synthesis of the observations and their dynamical implications is presented in the summary section (Section 5) at the end of this chapter.

2.1 Background

The dynamics of synoptic scale motions are governed by the distribution of Ertel Potential Vorticity, Q, defined as

$$Q = \frac{1}{\rho}\zeta_a \cdot \nabla\theta,$$

where ρ is the density of air, ζ_a is the absolute vorticity, and θ the potential temperature. For a hydrostatic atmosphere, the potential vorticity on isentropic surfaces may be written as

$$Q = -g\frac{\zeta_{a\theta}}{\frac{\partial p}{\partial\theta}}. \tag{2.1}$$

In this expression, p represents pressure, and g the gravitational acceleration. For a value of the Coriolis parameter in midlatitudes of $10^{-4}s^{-1}$ and a stratification of 10K in 100 hPA, Q is approximately 10^{-6} m^2 s^{-1} K kg^{-1}. HMR define this value as a potential vorticity unit (or PVU). Typical values of PV range from .25 PVU to about 1 PVU in the troposphere, to several times those values in the stratosphere. Following Danielsen and Hipskind (1980), a *dynamical tropopause* is defined as the surface Q = 1.5 PVU. The large values in the stratosphere relative to those in the troposphere are principally associated with the differences in stratification between the two regions.

The concepts of invertibility and conservation make potential vorticity a useful diagnostic quantity to study atmospheric motions on the synoptic scale. The distribution of potential vorticity (or vorticity) is related to the streamfunction and geopotential through a three- (or two-) dimensional Laplacian operator, under certain balance assumptions. Given a three dimensional distribution of PV, a balance condition, and boundary conditions, the wind and mass fields consistent with that balance approximation and potential vorticity distribution may be determined. This is known as the *invertibility principle* for potential vorticity.

The Lagrangian time rate of change of Q is given by

$$\frac{dQ}{dt} = \frac{1}{\rho}\zeta_a \cdot \nabla \dot{\theta} + \frac{1}{\rho}(\nabla \times \boldsymbol{F} \cdot \nabla \theta) \quad , \tag{2.2}$$

where $\dot{\theta}$ represents diabatic heating, and $\mathbf{F}$ is a frictional force. From these relations it is seen that for flows in which the heating gradients are weak or nearly orthogonal to the local vorticity vector, and in which friction is negligible, potential vorticity is approximately conserved. Given a time series of analyses of potential vorticity on a set of isentropic surfaces, the nonconservation of PV may be readily diagnosed.

Integrating the product of density and (2.2) over a a material volume, dV, gives

$$\frac{d}{dt}\iiint \rho Q dV = \iint \left(\left(\dot{\theta}\zeta_a + \theta \left(\nabla \times \boldsymbol{F} \right) \right) \cdot \boldsymbol{n} \right) dA \ , \tag{2.3}$$

where $\boldsymbol{n}$ is the outward pointing unit normal vector to the material volume. (2.3) states that the mass weighted integral of potential vorticity over a material volume is conserved in the absence of heating and a curl of the frictional force on the boundary of that volume.

In isentropic coordinates, the conservation of mass-weighted potential vorticity, takes on a more elegant form. In isentropic coordinates, the analog to density is the pseudo- density, $\sigma = \frac{\partial p}{\partial \theta}$. Within an isentropic layer, the conservation theorem (Haynes and McIntyre, 1987) states:

$$\frac{\partial}{\partial t}(\sigma Q) + \nabla \cdot \boldsymbol{J} = 0 \tag{2.4}$$

where $\boldsymbol{J}$ is given by:

$$\boldsymbol{J} = \zeta_a \boldsymbol{u} - \boldsymbol{k} \times \dot{\theta} \frac{\partial \boldsymbol{u}}{\partial \theta} + \boldsymbol{k} \times \boldsymbol{F} \tag{2.5}$$

and is the total flux of potential vorticity (or the flux of vorticity within an isentropic layer).

In the next two sections the observed distribution of potential vorticity is discussed (Section 2.2) and the physical mechanisms that could lead to these distributions are reviewed (Section 2.3).

2.2 Observations

2.2.1 *Potential vorticity distributions on isentropic surfaces*

Fig 2.1 (a,b,c) displays the distributions of Ertel potential vorticity and wind on the 350K, 320K, and 285K isentropic surfaces respectively for 1200 UTC 14 January 1990, for a portion of the Northern Hemisphere. These charts were chosen as they show the intersections of the individual isentropic surfaces with the subtropical jet, the polar jet, and the Earth's surface. Figure 2.1a and 2.1b lie approximately in the "Middleworld" region of

the troposphere, (Hoskins, 1990). The Middleworld region corresponds to those isentropic surfaces which intersect the tropopause. The 285 K surface is in the "Underworld" (those isentropic surfaces which intersect the ground).

The 350K surface (Figure 2.1a) is characteristic of the upper troposphere at middle latitudes during the winter. The band of strong winds along the lower edge of the figure corresponds to the subtropical jet. The most systematic gradients of potential vorticity on this surface are also associated with the jet. North and south of the jet, closed gyres of both high and low PV are found , generally associated with relatively weaker cyclonic and anticyclonic winds, respectively.

The 320K surface for this same time is characteristic of the atmosphere in the upper troposphere and lower stratosphere over midlatitudes. The most striking feature of this chart is the region of very strong gradients near the polar jet. South of the jet on this surface, the potential vorticity tends to be homogenized - with relatively weak gradients of potential vorticity in the subtropics. In midlatitudes, there is a systematic increase in the magnitude of the gradients nearly coincident with the strongest winds at the polar jet core. Further, the isopleths of PV have a propensity to be nearly aligned with the winds. This distribution of winds and potential vorticity make assessments of PV advection difficult. North of the jet, the potential vorticity gradient are weaker in magnitude, and once again, less systematic in direction. The weaker winds in both the subtropical troposphere and middle and high latitude stratosphere are associated with nearly homogeneous potential vorticity.

The 285K is typical of the lower and mid troposphere at middle and high latitudes during the winter. This surface intersects the Earth's surface in the subtropics. On this surface the potential vorticity values are generally around .4 PVU with the exception of the closed

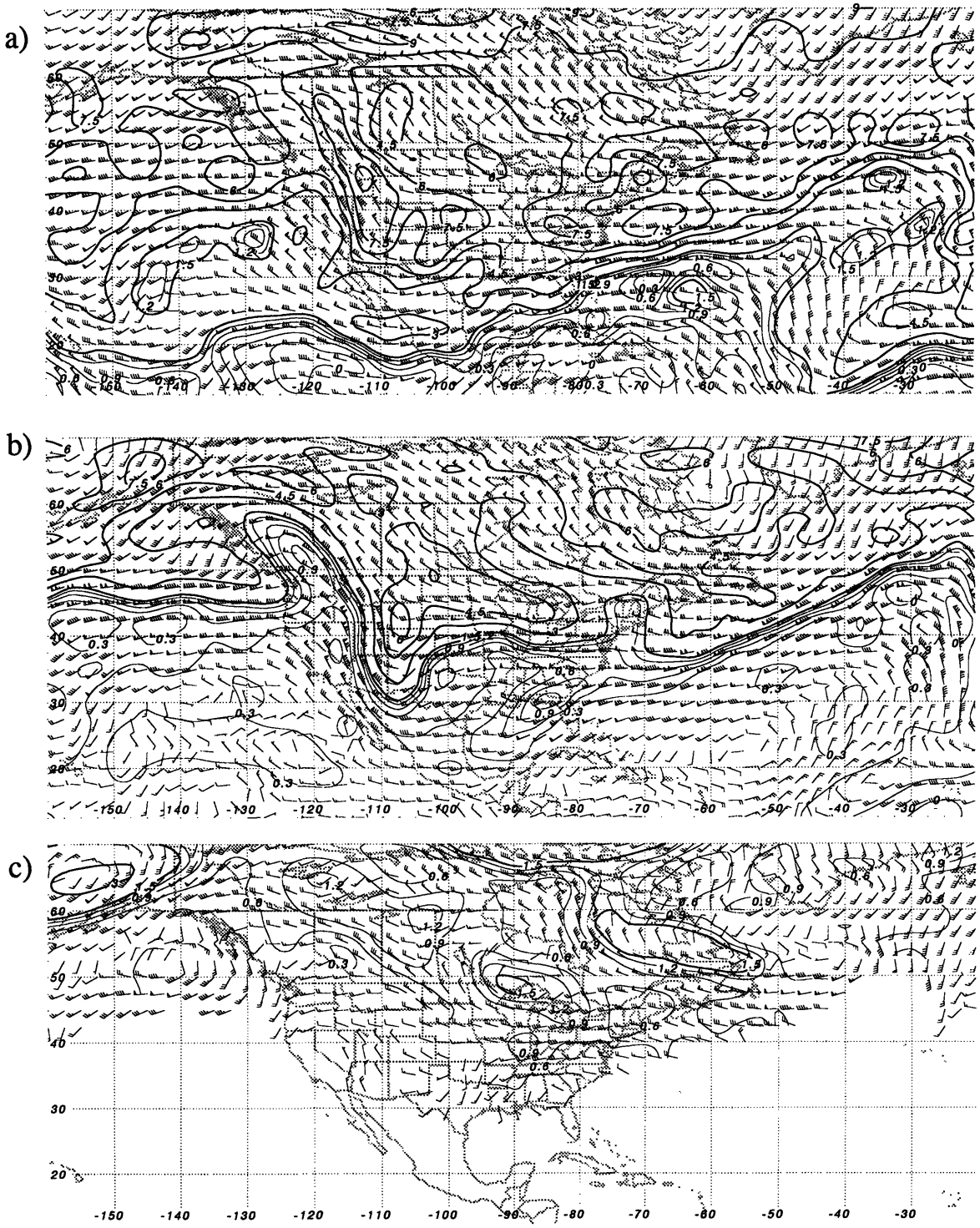

Figure 2.1: Ertel potential vorticity and winds on the (a) 350K, (b) 320K, and (c) 285K isentropic surfaces. Contour interval is .3 PVU (light contour) for $Q < 1.5$ PVU; and 1.5 PVU (heavy contour) for Q 1.5 PVU or greater. Winds in ms^{-1} with short barbs 5 ms^{-1} and long barbs 10 ms^{-1}.

cyclonic gyres within which the PV values are more typical of the stratosphere. Note once more the correspondence between weaker winds and smaller gradients.

The consistent features on each of these three charts which will be of particular interest to this study are 1) the region of strong lateral gradients of PV separating tropospheric values of PV from stratospheric values, that is approximately coincident with the polar and subtropical jets and 2) the fact that the in these regions, winds are nearly parallel to the isopleths of Q.

2.2.2 Cross Sections

Given that the strongest lateral gradients of PV are concentrated near the polar and subtropical jets, one would expect that the largest perturbations can be created here through advection. Attention is now focused on these dynamically significant regions by constructing cross sections through jets and identifying characteristic features within the PV distribution near the jets. Figure 2.2 shows a distribution of PV calculated from radiosonde data on the 320K isentropic surface for 1200 UTC 24 February 1990. The PV was calculated from radiosonde data by first interpolating pressure and wind at each station to isentropic surfaces. The pseudo-density was then calculated as a finite difference of pressure over a layer 10K thick. The vorticity was evaluated using a triangle method. The fields of pseudo-density and vorticity where then objectively analyzed using the Barnes scheme, and the PV was calculated using the objectively analyzed fields.

On this date, the flow over North America was dominated by a jet (with winds in excess of 65 ms^{-1}) lying northwest to southeast from central Canada - exiting North America along the southeast coast of the US. On this date, the 320K surface lies in the lower stratosphere over most of the eastern third of North America.

A mean cross section, Figure 2.3 is taken normal to the jet along the rhumb line shown in Fig 2.2. The cross section extends in the vertical from 260K to 355K. The various quan-

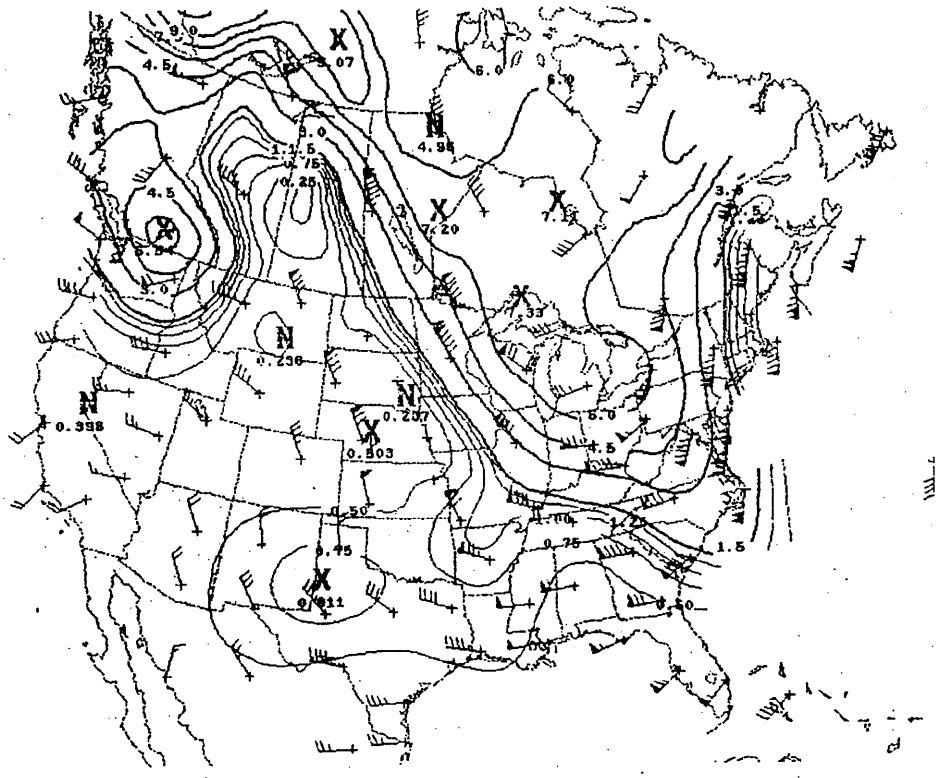

Figure 2.2: Ertel potential vorticity and winds on the 310K surface 24 February 1991. Contour interval is .25 PVU (light contour) for $Q < 1.5$ PVU; and 1.5 PVU (heavy contour) for Q 1.5 PVU or greater. Winds in knots with short barbs 5 knots and long barbs 10 knots.

tities plotted have been averaged over a 1000 km region normal to the section. Figure 2.3a shows the winds normal to the cross section. The jet is readily identified slightly to the left of center of the domain. The earth's surface is seen to slope upward and to the right in the figure. Because of the geometry of the section, this sloping surface is associated with a horizontal temperature gradient at the Earth's surface. Figure 2.3b shows the PV. The tropopause in this section takes on the appearance of a "wall" near the jet core over a layer from approximately 280K to 330K. Away from the jet, the tropopause is nearly horizontal along the 280K and 330K surfaces. The tropospheric values of the PV in this section (ranging from .2 PVU to about .8 PVU) are seen to be associated with hardly any systematic variations. Indeed, Figure 2.3c shows that the gradients in these regions are, in fact, relatively small. The stratospheric values of PV seen lying along the surface are presum-

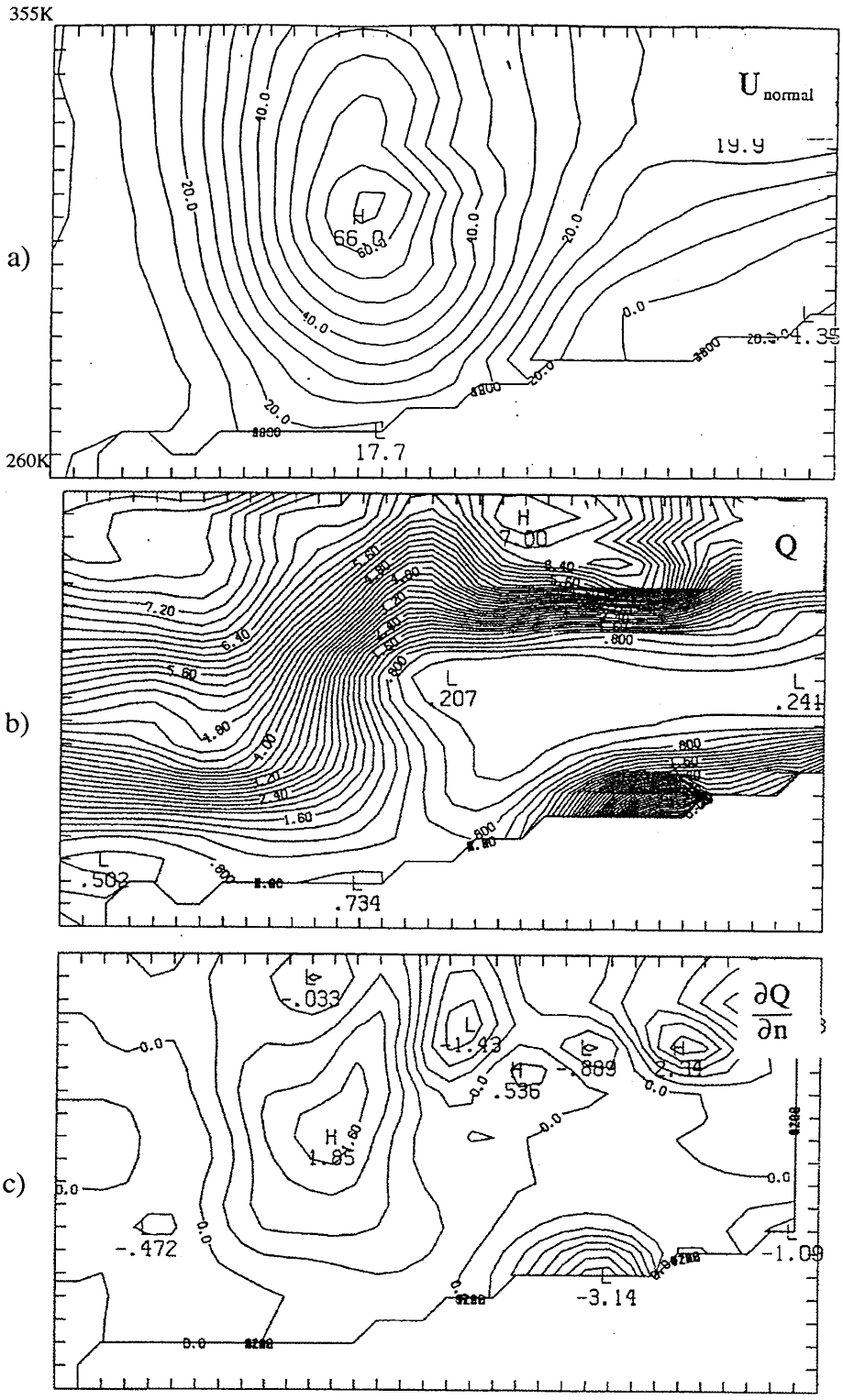

Figure 2.3: Cross sections of (a) wind, (b) Ertel PV, and (c) gradient of PV taken along rhumb line in Figure 2.2. Contour interval for wind is 5 ms^{-1}, for PV .2 PVU, and for PV gradient, .4 PVU(200km)$^{-1}$. Horizontal tick marks represent 100 km, vertical tick marks represent 5K.

ably associated with the effects of radiative cooling the previous night. Aside from the large horizontal gradients associated with the low level PV, the strongest gradients in the section are confined to the vicinity of the tropopause. The broadest region of high gradient is associated with the jet.

2.2.3 *Composite of Cross Sections*

A composite of 14 cross sections taken through 14 different jet events with the tropopause appearing as a wall was constructed to highlight those features seen in the above cross section, which are consistently observed in all of the cross sections. The procedure for constructing the composite was as follows: For each cross section, a subjective identification of where the tropopause was most vertical was made. The cross sections were then aligned with respect to this reference position. To account for the differing "depths" of the wall, the mean tropopause height north and south of the wall were normalized and the PV was then averaged with respect to this normalized coordinate. The resulting distribution was then transformed back into isentropic coordinates. The resulting PV and its gradient along the composite section are shown in Figures 2.4a and 2.4b respectively.

In Figure 2.4b the features described in Figure 2.3d are seen. That the horizontal gradients are nearly zero is evidenced by the "meandering" of the 0.0 PVU $(200\ km)^{-1}$ contour through the domain. The most coherent feature of the 14 individual cases is the presence of a large PV gradient associated with the jet extending along the tropopause into the lower stratosphere.

2.2.4 *Composite of the gradient*

Another technique to determine the characteristic structure of the PV gradient along the tropopause is to composite the gradient, rather than the potential vorticity itself. The approach taken is to construct a "Lagrangian" average of the meridional isentropic potential vorticity gradient with respect to the location of the tropopause. The twice daily NMC analyses (described in Chapter 3) were used to construct isentropic analyses of winds and

a)

b)

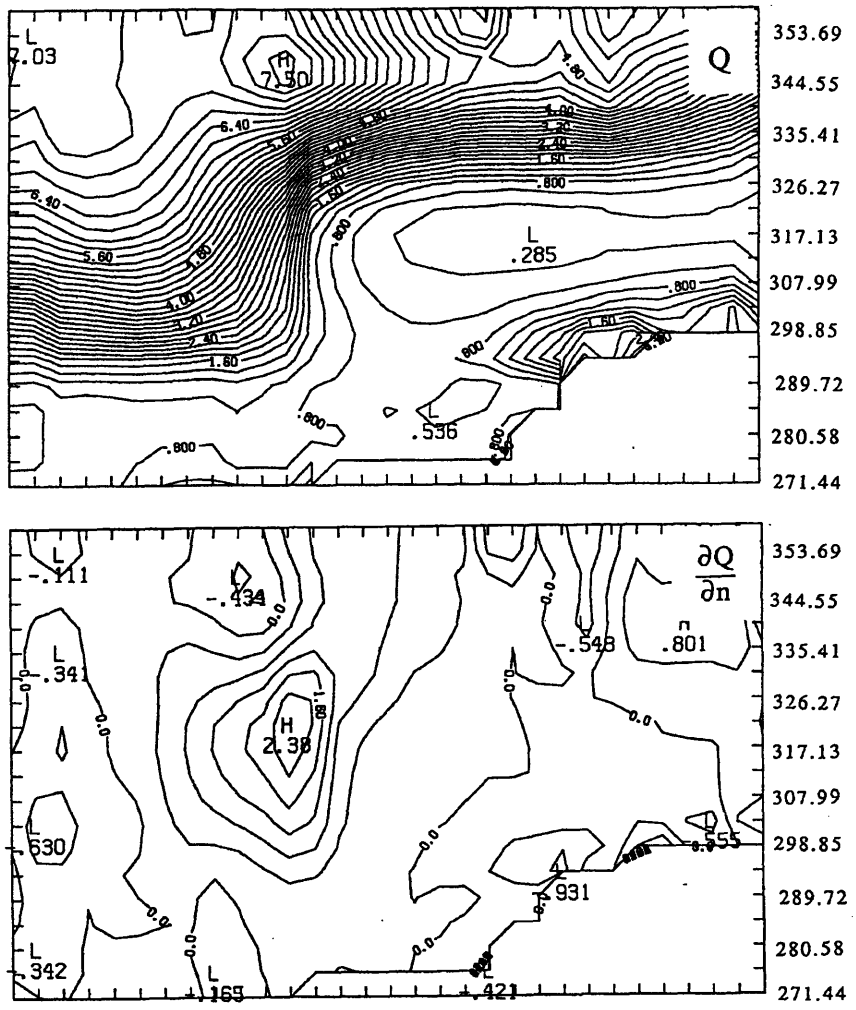

Figure 2.4: (a) Composite Ertel PV and (b) the gradient of the composite PV. Contour interval as in Fig 2.3

pressure from which PV distributions were computed. For the month of January 1991, at each time, the location of the dynamical tropopause was determined for each longitude. The meridional PV gradient was calculated and tabulated at the tropopause and at fixed distance north and south of the tropopause. The results were then zonally and time averaged. The result of this calculation for the 320K and 350K surfaces is shown in Figure 2.5 (a,b) respectively.

The magnitude of the gradient is seen to be maximized near the tropopause. Approximately 8 degrees latitude north of south of the jet, the gradients are considerably smaller.

a)

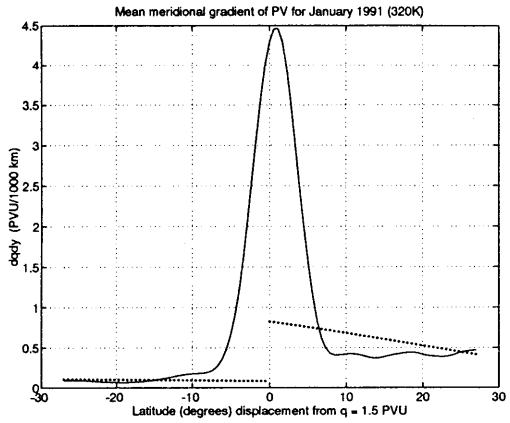

b)

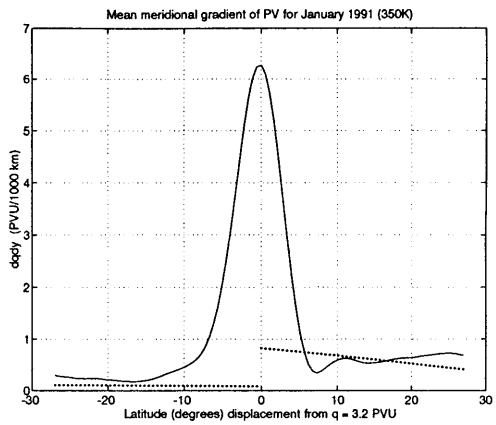

Figure 2.5: Time mean, zonally averaged PV gradient (solid) and the gradient of PV associated with the gradient of planetary vorticity (see text) as a function of distance from that contour of PV along which the PV gradient is maximized on the a) 320K and b) 350K surfaces.

For purposes of comparison, also shown in Figure 2.5 is the meridional gradient in planetary vorticity (β) multiplied by a stratification typical of the lower stratosphere (troposphere) $\theta_p = .5K\ hPA^{-1}$ ($\theta_p = .05K\ hPa^{-1}$). Comparing the two curves, it is apparent that the gradients of PV away from the tropopause are comparable to or smaller than the variations in PV associated with a typical stratification and β. Sun and Lindzen (1994) note that while the PV gradients in the troposphere appear to be distinguishable from zero, due to the resolution of observing systems, these tropospheric gradients might in fact be exaggerated.

2.2.5 *Time mean cross section*

Time and zonal averages of PV tend to smear out the localized, intense gradients of PV seen on instantaneous maps. Figure 2.6, which shows a climatological, zonal mean distribution of PV and potential temperature, illustrates this point. While the PV gradients tend to concentrated near the tropopause in this climatological distribution. The variation of PV along isentropes suggests that the gradients are considerably weaker than the gradi-

ents seen in the composite cross section (Figure 2.4). Furthermore, the gradients appear to exist over a much deeper range of the atmosphere.

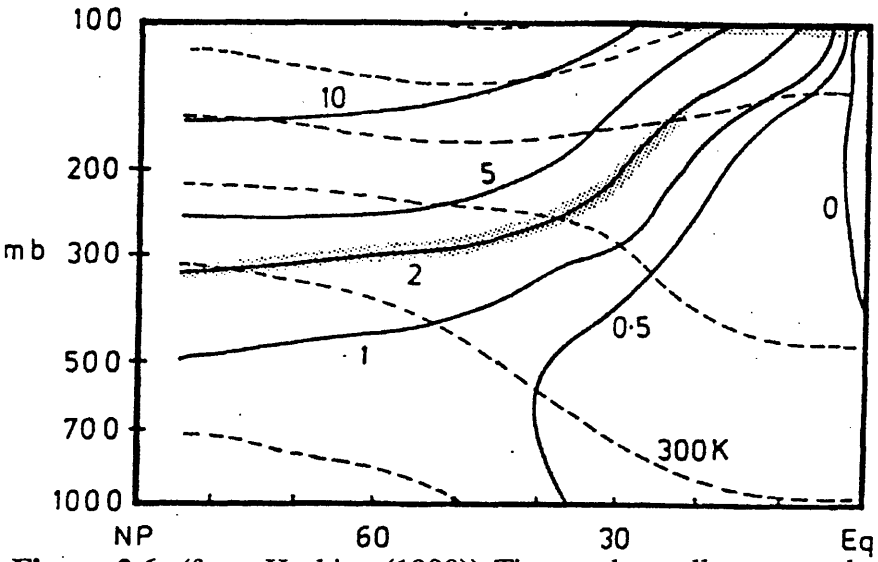

Figure 2.6: (from Hoskins (1990)) Time and zonally averaged PV, and isentropes for the Northern Hemisphere. Contour interval of PV as shown, contour interval for potential temperature, 30K.

2.2.6 *Geostrophic scatter diagrams*

Given that, as noted in Section 2.2.1, the wind is nearly parallel to isopleths of Q, it is anticipated that the isopleths of Q and the streamfunction for the non-divergent wind (or the Montgomery potential) should also be aligned. Figure 2.7a shows the contours of Q and M for 0000 UTC 1 January 1991. The Q field on this date is indeed nearly parallel to the contours of M. A compact way of representing this information is the construction of a "geostrophic scatter diagram" in which the Q values calculated at each grid point are plotted against the corresponding M value (Figure 2.7b).

In this scatter diagram three distinct regions may be identified - a region corresponding to tropospheric values of PV, a "near jet region" composed of those points sloping upward and to the left, and a region corresponding to stratospheric values of PV of about 5PVU. The characteristic features seen on the isentropic surfaces - the near homogenization of

a)

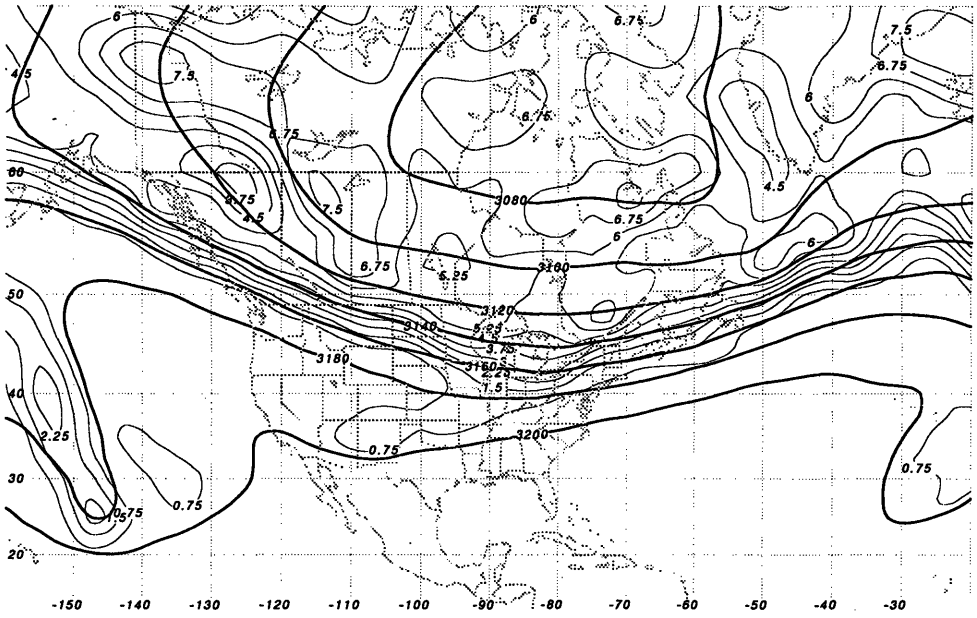

b)

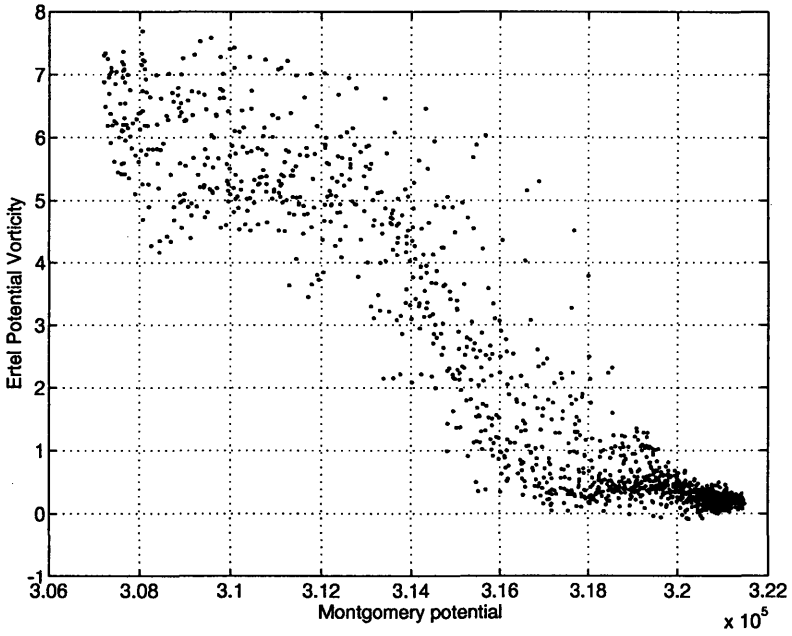

Figure 2.7: (a) 0000 UTC 1 January 1991 Montgomery potential (contour interval 20 x 10^2 J kg^{-1}) and Ertel PV (contour interval .75 PVU); (b) Geostrophic scatter diagram for M and Q. (c) and (d) as for (a) and (b), except for 1200 UTC 14 January 1991.

PV gradients for tropospheric and stratospheric values of PV are then easily seen in this diagram, although the geographical information about Q and M is lost. In the corresponding regions of Q-M space, the scatter is largest and the points appear to be scattered about

c)

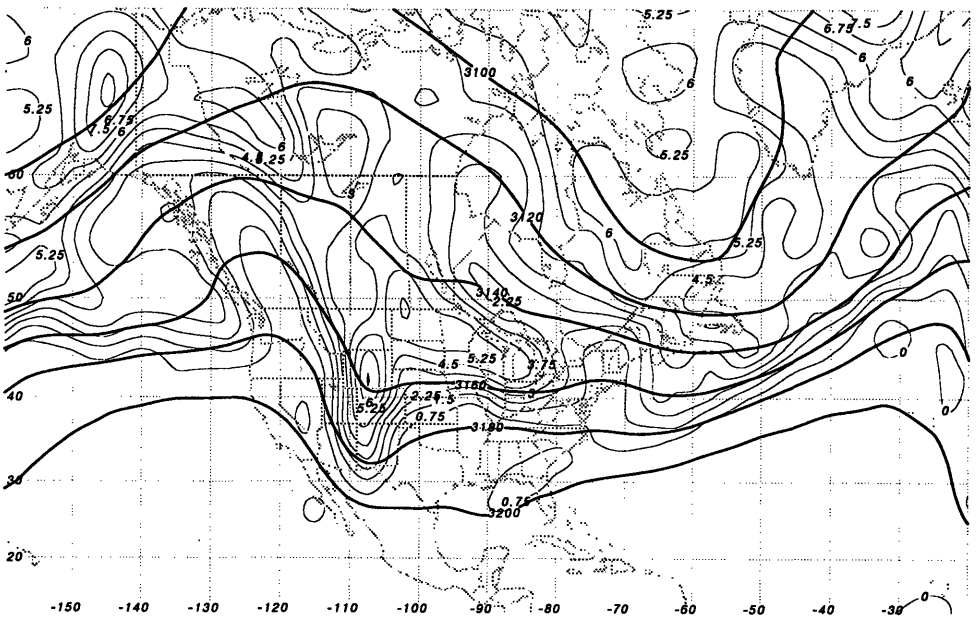

d)

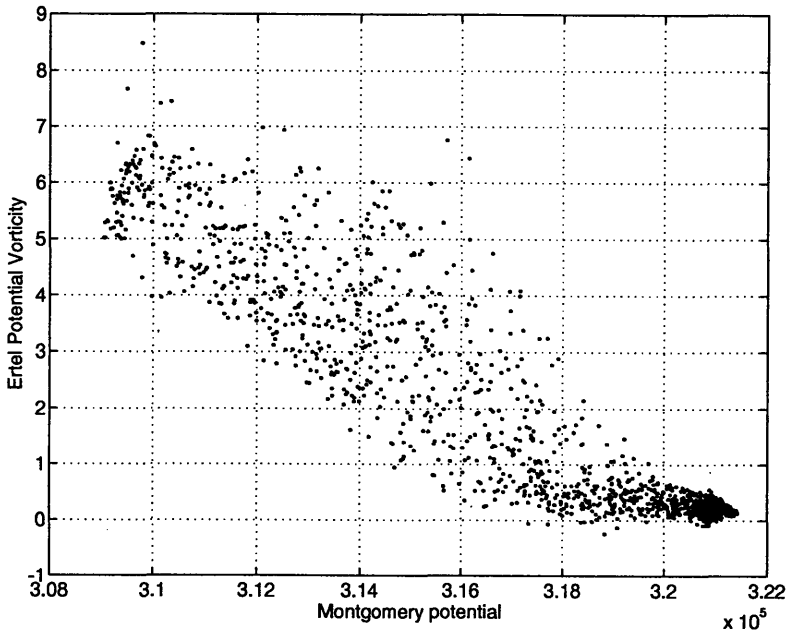

nearly horizontal lines (constant Q) in the diagram while the points clustered about the jet are typically characterized by smaller scatter.

If the points were to collapse onto a single curve in Q-M space, the flow at that level, would be steady, as a functional relationship, $Q = Q(M)$ could be identified. Under these circumstances, the flow is said to be of "free mode form", Read *et al.* (1986). A free mode, as used in this text, will be defined as a steady, unforced solution to the equations of

motion. The scatter in these diagrams is an indication of the deviation from free mode form. Read *et al.*, suggest a more meaningful way to construct and interpret these diagrams if the points which make up the scatter diagram are selected from points chosen to lie along a closed curve in physical space. The area enclosed on the resulting scatter diagram is equal to the net geostrophic advective flux of Q across the curve in physical space.

Figure 2.7c shows the Q and M fields for another time (1200 14 January 1991). The near parallelism of the isopleths of Q and M is not as apparent on this date. The prominent regions of geostrophic advection seen on the chart are associated with considerable scatter on the geostrophic scatter diagram (Figure 2.7d).

2.3 Factors which determine the observed potential vorticity distribution

2.3.1 *Physical processes affecting the distribution of PV*

A natural question to ask is, "Why is the observed distribution of PV (nearly) isentropically uniform away from the jets?" Rhines and Young (1982) show that homogenization of pseudo-potential vorticity (or PPV), q_p, given by

$$q_p = \nabla^2\Psi + \beta y + \frac{f_0^2}{\rho_s}\frac{\partial}{\partial z}\left(\frac{\rho_s}{N^2}\frac{\partial \Psi}{\partial z}\right) \tag{2.6}$$

(where Ψ is the streamfunction for the geostrophic flow, ρ_s is the basic state density, N^2 is the basic state stratification.), may occur within closed mean streamlines provided that the forcing of the PPV is negligible within that streamline. The physical processes which affect the distribution of potential vorticity are isentropic mixing, horizontal diffusion, baroclinic instability, radiation, latent heating, and diffusion of vertical momentum. The actions of most of these processes tend to drive the potential vorticity to be isentropically uniform and vertically non-uniform. Each of these process will be briefly considered:

Let q be a conserved quantity along an isentropic surface. Then q obeys the relation:

$$\frac{\partial q}{\partial t} + \boldsymbol{v} \cdot \nabla q = S, \tag{2.7}$$

where $\boldsymbol{v}$, is the horizontal velocity along the isentropic surface, and S represents sources and sinks of the q. Define an averaging process, "$\bar{}$", which may be either a time or spatial average, and denote " $'$ " as a deviation from that average, then the mean equation for the variance in q, q'^2,may be derived

$$(\frac{\partial}{\partial t} + \bar{\boldsymbol{v}} \cdot \nabla) \frac{\overline{(q')^2}}{2} = \overline{S'q'} - \overline{\boldsymbol{v}'q'} \cdot \nabla \bar{q} \tag{2.8}$$

Under circumstances in which q'^2 is increasing following the flow, and the forcing of q is negligible, (2.7) shows that the eddy flux of q may be down gradient. The eddies act to mix the q (potential vorticity as an example) so as to decrease the mean gradient of q. Thus isentropic mixing may act to horizontally homogenize potential vorticity.

By relating (2.8) to the dispersion of fluid parcels from a reference latitude, Bretherton (1966) demonstrates that baroclinically unstable waves act to destroy gradients of potential vorticity at the steering level of the unstable wave, as there must be an unbalanced down gradient flux of PPV at that level.

Both radiation and latent heating act to redistribute potential vorticity in the vertical. Radiation effects this redistribution by locally adjusting the lapse rates. Radiative effects are most effective near boundaries - cloud tops (or bottoms) or near the earth's surface. Latent heating is often observed to redistribute potential vorticity from the upper troposphere to the lower troposphere in regions of large scale stable ascent. Observational studies have noted the development of upper tropospheric ridges downstream of large scale precipitation areas coincident with an increase in lower level cyclonic vorticity. Eliassen and Kleinschmidt (1959) and Davis (1990) suggest that diabatic processes along warm fronts lead to the production of a "high level" anticyclone (low PV) ahead of a developing

surface cyclone. This production is attributed to the redistribution of PV. Diagnostic potential vorticity tendency calculations performed by Davis (1990) for the local generation of PV by condensation in saturated, stably stratified ascent lend support to this interpretation. Recent modeling studies of moist cyclogenesis and moist frontogenesis (Emanuel et al. (1987) and Montgomery and Farrell (1991)) have produced results whose dynamics appear to be consistent with the above observations.

Rhines and Young demonstrate that in flows in which the eddy fluxes of PPV are of "intermediate strength"

$$J(\overline{\Psi}, \overline{q_p}) \gg \nabla \cdot \overline{v'q'_p} \gg \text{"}dissipation\text{"}$$

then the pseudo - potential vorticity within closed mean streamlines of a fluid, $\overline{\Psi}$, may become homogenized.

One can infer some of the characteristics of the forcing of statistically steady flows by consideration of the slope of the curve on a geostrophic scatter diagram (Read *et al.)*. Following the development of Read *et al.*, the time averaged equation for a flow in which the eddy transport of PPV is approximated by a down - gradient diffusion, and the source of PPV is represented by S, is given by

$$J(\overline{\Psi}, \overline{q_p}) = S + K\nabla^2 q_p \tag{2.9}$$

where K, is the Peclet number of the flow. For sufficiently weak sources, (2.10) has a solution $q_p = q_p(\Psi)$. An integral over the area enclosed by a mean streamline gives

$$-K\int \nabla q_p \cdot \mathbf{n} dl = -K\int \frac{dq_p}{d\Psi} \nabla \Psi \cdot \mathbf{n} dl = \int S dx dy$$

or,

$$\frac{dq_p}{d\Psi} = \frac{\int S dx dy}{-K \int \mathbf{v} \cdot d\mathbf{l}} . \tag{2.10}$$

Observations and modelling studies suggest that there is a positive correlation between the sign of the areal averages source of PPV (numerator of (2.11) and the circulation integral taken around the mean stream line (Read *et al.*), thus from this relationship one can see that the tendency for the scatter diagrams to have a negative slope (*i.e.* $dQ/d\Psi < 0$), follows. Furthermore, homogenization of Q is consistent with there being only weak sources and sinks of PPV (Rhines and Holland).

A simple catalog of the processes which redistribute PV is not enough to determine why the distribution of PV is as observed. Processes which act over the shortest time scales will have a much greater influence on the instantaneous PV distribution than those processes which act over much longer time scales. For simplicity, consider the free troposphere (i.e., that part of the atmosphere above the planetary boundary layer). The principal processes that determine the time rate of change of PV in this region are the advection across the intense tropopause PV gradient and diabatic processes associated with radiation and latent heat release. HMR estimate the typical time scale for the modification of PV by 1 PVU by radiation to be O(5 days to a week), while modification by a similar amount by latent heating (in their example, latent heating due to convection beneath a cold tropopause anomaly) occurs on a shorter time scale 0(1 to 2 days). Time series of observed distributions of PV suggest that latent heating associated with large scale condensational heating my change PV by 1 PVU on a time scale of about a day. Advection of PV at jet level may change the PV by 1 PVU on time scales less than 1 day (Shutts, 1987). Despite the fact that advections of PV can compete with diabatic changes due to latent heating, the latent heating is localized in the ascent regions of cyclones. Hence, in a areal averaged sense, the dominant process which determines the PV distribution at jet level is horizontal

advection. Shutts (1987) demonstrates that "to zeroth order, isentropic wind vectors point along the isopleths of Q." It must be stressed however that away from the jets, the forcing of the PV distribution is determined by a balancing of the various mechanisms discussed earlier.

2.4 Theory

The concept of a basic state is at the heart of the theoretical understanding of the dynamics of wave systems. The basic states themselves can be characterized in terms of the distributions of PV associated with them. Motivated by the observed PV distribution, the dynamical implications that such a distribution has on perturbations to basic states in which the PV gradients are concentrated is addressed.

2.4.1 *Wave Propagation and Structure*

The early work of Rossby (1939), which introduced the theory of long waves (waves with wavelengths of several thousand kilometers manifested as large undulations in the polar jet on synoptic charts), has proven useful in providing a qualitative picture of the propagation of both the long waves of concern to Rossby and the shorter wavelength features referred to as "short waves" or "mobile troughs."

Rossby waves owe their existence and propagation to lateral gradients in the potential vorticity. In the simplest framework to consider their basic dynamics - that of horizontally nondivergent flow on a β plane, with a constant zonal wind $\overline{U}$ the existence of the waves is due solely to the variation in the planetary vorticity. Their dynamics is governed by the conservation and invertibility of absolute vorticity. The dispersion relation for these waves is obtained by linearizing the equation for conservation of vorticity about the basic state zonal flow, assuming a plane wave perturbation, $\psi = exp\,(i\,(kx + ly - \omega t))$ (where k

and l are the zonal and meridional wave numbers respectively, and ω the wave frequency) to obtain

$$\omega = \bar{U}k - \frac{\beta k}{k^2 + l^2} \ . \tag{2.11}$$

The phase speed of the wave, c, is given by $c = \omega k^{-1}$. From (2.10), it is apparent that waves are dispersive - with long wavelengths waves travelling westward relative to the basic state zonal wind faster than those with shorter wavelengths waves. Furthermore, it is seen that for a fixed zonal wave number, and wave frequency, the mean flow determines whether or not lateral propagation of the wave is allowed. This is demonstrated by rewriting (2.2) as

$$l^2 = \frac{\beta}{\bar{U} - c} - k^2 \ .$$

The meridional wave number must be real for there to be lateral propagation of Rossby waves. The "tilt" of the phases line of the wave on the β plane is determined by the basic state winds and vorticity gradient, β.

That the structure of Rossby waves is intimately related to the structure of the mean flow can be seen in the following example. Consider steady, non-divergent, barotropic flow,

$$J(\Psi, q) = 0 \ .$$

Divide the total flow into basic state and a perturbation

$$\Psi = \bar{\Psi} + \Psi' \quad \text{and} \quad q = \bar{q} + q'$$

then,

$$J(\Psi, q) = J(\overline{\Psi}, q') + J(\Psi', \overline{q}) + J(\Psi', q') = 0$$

If one considers "weakly" nonlinear waves then,

$$J(\Psi, q) \approx J(\overline{\Psi}, q' - \Lambda_0 \Psi') = 0$$

which has a solution

$$q' - \Lambda_0 \Psi' = 0 \ ,$$

where

$$\Lambda_0 = -\frac{1}{U_0}\frac{dq}{dy} \ . \tag{2.12}$$

Λ_0 is known as the *trapping potential* (Butchart *et al.*, 1989). It is a function of the basic state gradient of vorticity and the basic state wind. If the trapping potential has a minimum, there is the potential for locally meridionally trapping a perturbation to the basic state. As there are basic state variations in the y direction, the assumed form of the solution is

$$\Psi = exp(ikx)\,\phi(y)$$

then

$$\phi_{yy} + (-k^2 - \Lambda_0)\,\phi = 0$$

Waves are meridionally confined if

$$k^2 > -\Lambda_0 = \frac{1}{U_0}\frac{dq}{dy}$$

From this relationship, it is seen that the basic state may confine perturbations provided that the trapping potential has a local minimum and provided that the zonal scale of

the disturbance is sufficiently small. Ioannou and Lindzen (1986) emphasize the importance of meridional shear in meridionally confining instabilities.

If one assumes that the vorticity gradient in the atmosphere is piecewise constant on an f - plane (as a crude model of the tropopause potential vorticity distribution) (Figure 2.8), with the discontinuity at some latitude $y = y_0$, and then solves the linearized relation for conservation of vorticity about this basic state, one finds that the waves in this simple model have a streamfunction, Ψ, given by

$$\Psi = exp\,(i\,(kx - \omega t))\,exp\,(-k|y - y_0|)\,. \tag{2.13}$$

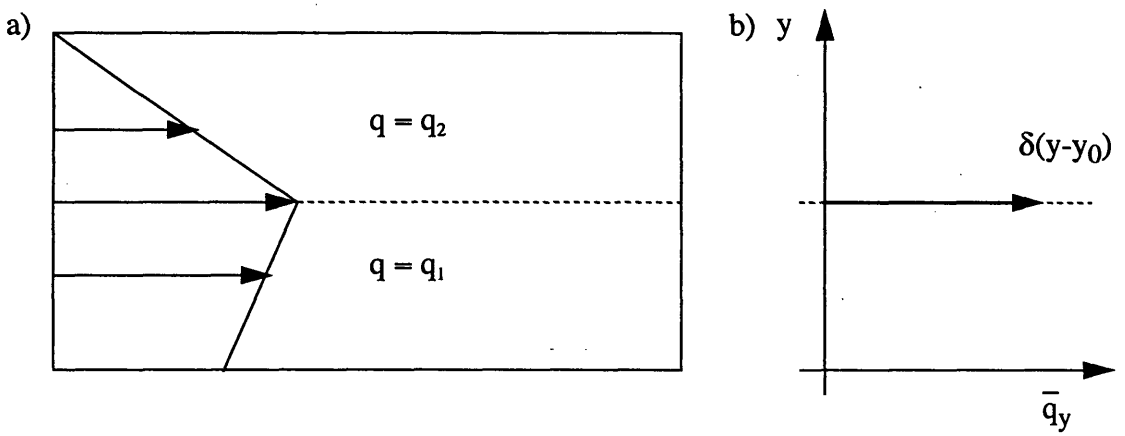

Figure 2.8: (a) An idealized flow in which the vorticity is piecewise constant, (b) the gradient of vorticity for this flow.

The waves are seen to be trapped at the discontinuity and evanescent away from the latitude $y = y_0$. The dispersion relationship for the waves (considering the case $k > 0$) is

$$\omega = U(y_0)\,k - \frac{\Delta q}{2}. \tag{2.14}$$

where Δq is the jump in vorticity in the domain. The waves are seen to be dispersive, but their energy (*i.e.* group velocity), $c_{gx} = \frac{\partial \omega}{\partial k} = U(y_0)$ propagates with the wind at the discontinuity.

It is reasonable to question whether the nature of the solution of the barotropic vortic-

ity equation on a beta plane (2.10) smoothly transitions into the solution (2.13) in the limit in which the width of the region having a gradient in the planetary vorticity shrinks to zero and the vorticity gradient, β, increases. To address this question, solutions are sought to the following problem

$$\left[\left(\frac{\partial}{\partial t} + \overline{U}\frac{\partial}{\partial x}\right) \nabla^2 + \beta \left(H(y+Y) - H(y-Y)\right) \frac{\partial}{\partial x} \right] \psi = 0$$

where H(y) it the Heaviside function. Assume solutions of the form $\Psi = \psi(y)\,(exp\,(i\,(kx - \omega t)))$

and get

$$\psi(y) = \begin{cases} \text{For } y > Y,\ \psi(y) = Ae^{-ky} \\ \text{For } -Y < y < Y,\ \psi(y) = Be^{-ily} + Ce^{ily},\ \text{where } \left(l^2 = \frac{\beta}{\overline{U} - c} - k^2\right) \\ \text{For } y < Y,\ \psi(y) = De^{ky} \end{cases}$$

Requiring continuity of the streamfunction and velocity fields at -*Y* and +*Y*, gives the dispersion relation for the problem,

$$\tan 2lY = -\frac{2lk}{k^2 - l^2} \quad . \tag{2.15}$$

For small $l << (2Y)^{-1}$,

$$\tan 2lY \cong 2lY \quad .$$

Substituting for l^2 into (2.5) and simplifying gives

$$c = \overline{U} - \frac{\beta Y}{2k^2 Y + k} \quad .$$

Now let $\beta Y = \frac{\Delta q}{2}$, which gives

$$c = \overline{U} - \frac{\frac{\Delta q}{2}}{2k^2 Y + k} \quad .$$

Now keeping Δq constant and letting the width of the propagation region go to zero

results in

$$\lim_{Y \to 0} c = \overline{U} - \frac{\Delta q}{2k} \ .$$

which is the result previously derived (2.13).

The preceding suggests that as the width of the region supporting wave propagation becomes smaller, the propagation characteristics of waves in the region supporting wave propagation will change.

The distribution of potential vorticity plays a role in the vertical propagation of stationary waves as well. Charney and Drazin (1961) determine criterion for the propagation of stationary waves from the troposphere into the stratosphere. They find that waves are trapped in a mean easterly flow, or in flows in which the vertically averaged westerlies exceed a critical value determined by the magnitude of the PPV gradient, the total horizontal wave number, and the mean stratification. Lindzen (1994) has expanded upon the work of Charney and Drazin in his examination of the effect of concentrated PPV gradients on the dynamics of stationary waves. Linzden (1994) finds that the concentration of the PPV gradients at the tropopause leads to a significant enhancement of the stationary wave response at the tropopause due to forcing at the surface. Lindzen interprets this amplified response to a partial reflection of waves tunneling between the surface and the tropopause.

2.4.2 *Instability of zonal flows*

In addition to its significance in wave propagation, the structure of the PV gradient is important in terms of the assessment of stability of atmospheric flows. Just as one can view the stability of unstratified sheared flows as the mutual intensification of counter-propagating vorticity waves (Lighthill, 1963), one can view the stability of quasi-geo-

strophic flows as the mutual interaction and intensification of counter propagating Rossby waves (HMR). For a quasi-geostrophic fluid, the stability criterion for perturbations about a zonal flow can be phrased in terms of the PPV gradient (Charney and Stern (1962)): *Stability is assured if the meridional gradient of the generalized pseudo - potential vorticity (q_p) is of single sign.* The generalized PPV is given by:

$$q_p = \nabla^2\Psi + \beta y + \frac{f_0^2}{\rho_s}\frac{\partial}{\partial z}\left(\frac{\rho_s}{N^2}\frac{\partial \Psi}{\partial z}\right) + f_0^2\left(N^{-2}\frac{\partial \Psi}{\partial z}\right)\left(\delta(z) - \delta(z - z_t)\right) \qquad (2.16)$$

where z_t represents an upper boundary (the tropopause perhaps) in some previously defined domain. The delta function contributions at the boundaries represent the inclusion of boundary thermal contributions to the definition of the PPV. Bretherton (1966) demonstrated that horizontal variations in potential temperature along a horizontal boundary may be incorporated into the definition of PPV as a delta function sheet of PPV located near the boundary. For a flat lower boundary, Bretherton showed that positive potential temperature perturbations are associated with cyclonic circulations and negative potential temperature perturbations are associated with anticyclonic circulations. Conversely, on an upper boundary, cold perturbations are associated with cyclonic circulations and warm perturbations with anticyclonic circulations.

A relatively simple analytical model of baroclinic instability, in which the basic state is a crude representation of the atmosphere, is the Eady model (Eady, 1949). Eady considered the stability of a vertically confined rotating Boussinesq fluid on an f - plane with no internal gradient in the basic state PPV. The basic state consisted of a zonal wind U = U(z). Normal mode solutions to the Eady system (Eady modes) exhibit exponential growth for wavenumbers less than a critical value. The most unstable mode has its phase tilting westward with height and a propagation speed equal to the mean speed of the current in which

it is imbedded. For shorter wavelengths, the solutions consist of two independent "edge waves" - each of which propagates along the vertical boundaries of the domain as a Rossby edge wave. The characteristic horizontal scale of the disturbances is the Rossby deformation radius (L_d), typically about 1000 km in the atmosphere. The characteristic e - folding time of the most unstable mode is a few days. Rivest (1990) solved simple Eady like models to study the dynamics of the maintenance and excitation of upper waves. Using simple basic states typical of the troposphere and lower stratosphere, Rivest showed that the Eady modes share many of the characteristics of upper mobile troughs discussed in the observational studies of Sanders (1988) and Davis (1990). The maximum stream-function for the modes is found at the tropopause and the magnitude of the deformation of a flexible tropopause was of a magnitude comparable to observations.

The dynamical implications of an interior meridional gradient of PPV on instability has been addressed by Charney (1947), Bretherton (1966), and Hyun (1981) who found that an internal $q_{p,y}$ of a given sign destabilizes a boundary having a $q_{p,y}$ of opposite sign. Rivest (1990) showed the existence of slowly decaying short wave disturbances (referred to as "quasimodes") in basic states possessing potential vorticity gradients in the interior and at boundaries. These disturbances, which are superpositions of the singular modes of the Eady (1949) problem, appear as a sharply peaked distribution when viewed in the phase speed domain. Quasimodes were found to erase midtropospheric PV gradients and enhance tropopause potential temperature gradients through their downgradient fluxes of PV and heat. The rate of decay of the "quasimodes" was found to increase with the latitu-dinal gradient in the planetary vorticity distribution.

The lack of gradients of PV on isentropic surfaces in the interior of the atmosphere can be exploited to determine a condition for the baroclinic neutrality of the atmosphere. Con-straining the meridional wavenumber by the width of the subtropical jet, Lindzen (1993)

uses the Eady model's total wavenumber cutoff to determine a maximum tropopause height below which instability can occur. Lindzen suggests that since the calculated tropopause height is close to the observed, this suggests that the atmosphere tends toward baroclinic neutrality.

2.4.3 *Arnol'd's theorems*

As the Charney - Stern criterion is only a necessary condition for instability, there are cases in which the Charney - Stern criterion is violated, and yet the observed flow is stable. A set of stability theorems was developed by Arnol'd (1965) and has been recently applied in the study of planetary atmospheres (Dowling, 1993). These theorems, known as Arnol'd's first and second stability theorems (hereafter referred to as *A1* and *A2*, respectively), provide additional necessary conditions for (for linear and non-linear) stability of zonal and non-zonal flows (McIntyre and Shepherd, 1987). These theorems are stated below:

Arnol'd's First Theorem:

For a steady, unifunctional flow in which $Q = Q(\Psi)$, if

$$0 < c < \frac{d\Psi}{dQ} \leq C < \infty ,$$

where c and C are constants, then the flow is stable. This theorem may be interpreted for flows in which $\frac{d\Psi}{dQ} > 0$ (*i.e.* Rossby wave propagation is in the same direction as the basic flow in which they are embedded). Under these circumstances, Rossby waves cannot be "held in step" and consequently may not phase lock - instability is prevented. A1 is essentially a restatement of Fjortoft's Theorem.

Arnol'd's Second Theorem:

For a flow in which $Q = Q(\Psi)$, if

$$0 < c < -\frac{d\Psi}{dQ} \leq C < \infty \tag{2.17}$$

where $cK_0^2 > 1$ and where K_0^2 is the smallest eigenvalue to the problem,

$$\nabla^2\Psi + K^2\Psi = 0$$

with appropriate boundary conditions, then the flow is stable. The upper bound on $\frac{d\Psi}{dQ}$, C, simply requires that $\frac{d\Psi}{dQ}$ be finite.

In our atmosphere, because $\frac{d\Psi}{dQ} < 0$, *A2* is the appropriate stability criterion to apply. $\frac{d\Psi}{dQ} < 0$ corresponds to the well known phenomena of Rossby wave propagation westward relative to the basic flow. In these situations, Rossby waves may propagate against the basic current and consequently there exists the possibility that the waves may be held stationary with respect to one another. The interaction time between the two counterpropagating waves under such circumstances would then be essentially infinite and an exponential growth due to their mutual interaction could occur. McIntyre and Shepherd note that boundary constraints (used in the solution to the eigenvalue problem mentioned above) can reduce the intrinsic phase speed of the upstream propagating waves and thereby suppress the instability.

Stamp and Dowling (1993) observe that stationary waves play a key role in the stability of the Jovian atmosphere which has been determined to be neutrally stable (Dowling, 1993). Stamp and Dowling conclude that slow moving waves are expected for systems near neutral stability with respect to *A2*. This result would seem to naturally follow directly from the stability criterion. For a finite $\frac{d\Psi}{dQ}$, neutrality would correspond to $\frac{d\Psi}{dQ} \cong \frac{1}{K_0^2}$. For a zonal flow, $\frac{d\Psi}{dQ}$ is the reciprocal of the square of the total wavenumber (i.e., the wavenumber of the stationary wave, K_s):

$$-\frac{d\Psi}{dQ} = \frac{-\frac{d\Psi}{dy}}{\frac{dQ}{dy}} = \frac{\bar{U}}{\frac{dQ}{dy}} = \left(k^2 + l^2 + \left(\frac{m}{L_d}\right)^2\right)^{-1} = (K_s^2)^{-1} \tag{2.18}$$

K_s corresponds to the wave number gravest mode for this domain, and would consequently be expected to be the slowest eastward propagating mode - thus, in an atmosphere near neutral stability, slow moving westward waves are anticipated.

2.5 An illustrative example

The chapter is concluded with an illustrative example which demonstrates that time and space means of potential vorticity (or vorticity in the barotropic case) are not suitable as basic states for the study of synoptic scale waves.

We reconsider horizontally nondivergent barotropic flow on an f plane with piecewise constant vorticity. If we consider a purely sinusoidal displacement of amplitude $2Y$ of the dividing contour between the two PV region, the resulting disturbance will propagate westward relative to the flow as a sinusoidal oscillation, of amplitude $2Y$ (Figure 2.9a).

If one were to live on a world in which this were the vorticity distribution, the time mean distribution of vorticity as a function of latitude would be given by:

$$\bar{q}(y) = \begin{cases} q_1 \text{ for } y \geq Y \\ (q_1 T_1 + q_2 T_2)/(T_1 + T_2) \text{ for } -Y \geq y \geq Y \\ q_2 \text{ for } y \leq -Y \end{cases}$$

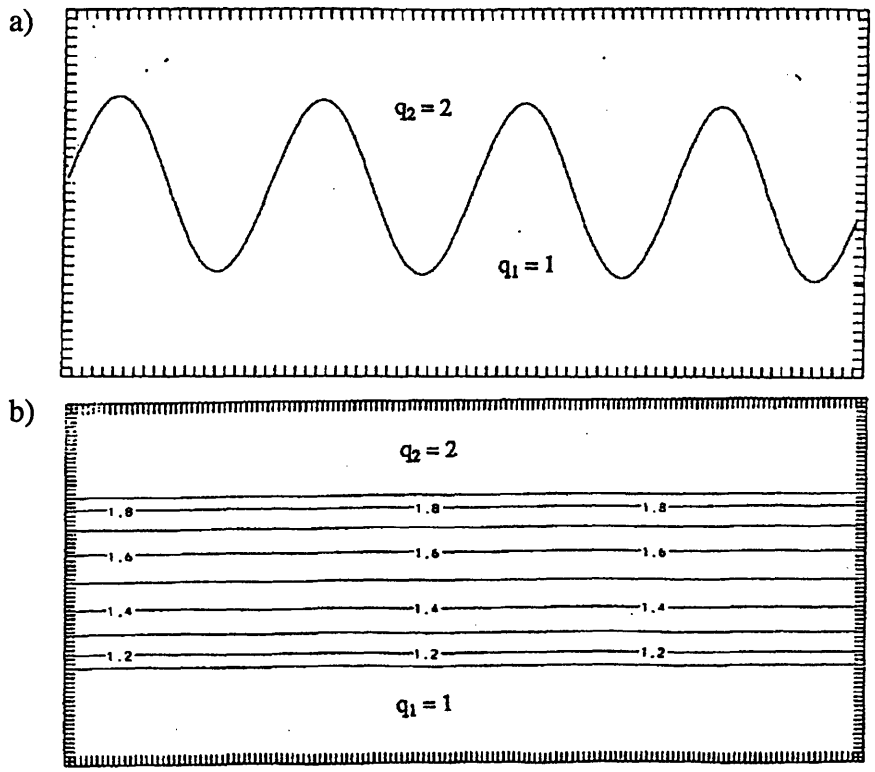

Figure 2.9: (a) Wave propagating along vorticity discontinuity with $q_2 = 2$ to the north and $q_1 = 1$ to the south of the discontinuity, (b) time averaged vorticity for the situation depicted in (a)

where T_1 and T_1 represent the amount of time a given location 'observes' a value of vorticity equal to q_1 and q_1 respectively. This distribution is shown in Figure 2.9b. The time mean distribution of q for $y > |Y|$ is constant at either q_1 or q_2, while the distribution for $y < |Y|$ smoothly varies between q_1 and q_1. Based on the discussion of the previous section, it is apparent that if one were to define a basic state as the time averaged vorticity, the spectrum of waves supported on this basic state is much greater - non-zero meridional wave numbers and hence meridional propagation of waves is allowed. The time averaged flow (for this example) ***is not*** representative of the basic state upon which the wave we were considering propagated. While the atmosphere does not possess a delta function gradient in potential vorticity at the jet, this example serves to illustrate the inherent problems in using time averaged flows as basic states. In the next chapter, we develop a technique

which would allow one to recover the basic state for the above example and for observed atmospheric flows.

2.6 Summary

In this chapter, analyses of the PV distribution in the troposphere and lower stratosphere as well as the dynamical implications of these observations were presented as a foundation for work in the succeeding chapters. A clear example of why it is inappropriate to use a time mean or zonal mean flow as a basic state has been presented. In this section we present a synthesis of the observations and dynamics.

The key observations:

- Potential vorticity is nearly homogeneous along isentropic surfaces away from the surface of the earth, and away from the polar and subtropical jets.
- The gradients of PV away from the jets are smaller than, or at most comparable to, the gradients in PV associated with the latitudinal gradient of the Coriolis parameter, β.
- Near the polar and subtropical jets, the PV gradients are several (4 to 6) times those associated with β, and are concentrated within approximately 8^{o} latitude of the jets.
- The observed wind and streamfunction fields are nearly aligned with the isopleths of PV in regions in which the flow is strong.
- Near jets, time and zonal means of gradients of Ertel PV are weaker and much more widely distributed in space than are instantaneous distributions of these fields.

The factors that influence the time mean distribution (eddy fluxes and non-conservative effects) tend to render the PV isentropically uniform (away from the jets) and vertically non-uniform with a local minimum in the mid-troposphere. A comparison of the

time scales of the varying processes which determine the time mean PV distribution suggests that the "advective control" of the PV dominates near the jets, while non-conservative effects such as latent heat release, radiative effects, and frictional forcing balance in regions away from the jets.

The dynamical implications of these observations:

- The tight gradients of PV near the jets suggest that the polar and subtropical jets may trap propagating wave disturbances in the vicinity of the jets.
- The concentrated gradients of PV along the tropopause influence both the structure of surface forced stationary waves (Lindzen, 1994), as well as the structure of synoptic scale transients.
- The negative slope on the Q - M scatter diagrams suggests that Arnol'd's second stability theorem may be relevant to the atmosphere.
- Despite the significant eddy and viscous transports of PV and the non-conservative forcing of PV, consideration of idealized conservative flows may be more relevant to the atmosphere (Read, 1986).

The dynamical / diagnostic quantity that links many of the above ideas is the relationship between Q and Ψ or M. This relationship, which is in large measure determined by the eddies and the forcing of PV, appears to be fundamental in characterizing the observed flow. In subsequent chapters, this relationship is used in the determination of a basic state and a refractive index.

Chapter 3

Determining a Basic State

In the previous chapter, a description of the instantaneous distribution of Ertel PV was presented. The key features of the observed distribution were the near homogenization of PV along isentropic surfaces away from the polar and subtropical jets and the coincidence of strong winds with the strongest PV gradients. At the conclusion of Chapter 2, it was demonstrated that the time mean of an idealized distribution of vorticity (with all the gradient at the jet axis) could lead to an unrealistic basic state - the nonhomogeneous nature of the observed vorticity and wind distribution prevents one from determining a basic state from time (or space) averaging.

One of the earliest attempts at defining realistic basic states for studying synoptic scales waves based on the observations that the PV gradients are concentrated at the jets was by Platzman (1949). Motivated by the observational work of Palmén (1948) and collaborators, Platzman modeled the upper tropospheric flow as barotropic with a piecewise constant vorticity distribution (as described in Section 2.2, except in physical coordinates). Platzman's results are essentially those described in Section 2.4.1 - that the waves are dispersive while the energy of the waves moves at the speed of the wind at the vorticity discontinuity.

Verkley (1994) attempts to simplify the description of the dynamics of the atmosphere by assuming equivalent barotropic dynamics and that the description of the atmosphere might be limited to a single isentropic surface which intersects the tropopause. As with Platzman, Verkley considers a piecewise constant vorticity distribution, with the higher values poleward of the tropopause. The work of Verkley differed from that of Platzman in

that Verkley sought to obtain nonlinear waves by applying contour dynamic techniques. Verkley found that the assumption of a single line of discontinuously leads to sharp zonal velocity profiles peaked at the tropopause. The waves that are supported in Verkley's basic state are neutral and resemble Rossby-Haurwitz waves.

There are two problems with Verkley's work: the neglect of the underlying surface baroclinity that may interact with the wave motions along the tropopause, and the neglect of the second jump in potential vorticity on higher isentropic surfaces (associated with the subtropical jet) along which another set of waves may propagate.

The basic state that will be determined should be characteristic of the flow through which synoptic scale eddies propagate. As both the observed instantaneous and time mean flows are nearly balanced (Davis, 1990), the basic flow should be balanced as well. Two balance assumptions that are most relevant to consider for synoptic scales are geostrophic balance and non-linear balance (Charney, 1955). A final requirement is that the basic state flow be steady. This last requirement is chosen because we have observed that the instantaneous flow has an underlying robust tendency to be nearly steady and because this allows the resulting state to be used for linear stability analyses. We return to this idea in Section 3.2.

In this chapter, a technique used in the determination of a three dimensional basic state is presented. In Section 3.1 we continue our motivation for the method to be presented later in this chapter by first demonstrating a technique to obtain a basic state for the piecewise constant problem discussed in Section 2.5. The method requires that a frame of reference be found in which the wave field is steady. As we are seeking a steady basic state, in Section 3.2 previous techniques used to determine steady flows are discussed. In Section 3.3 a description of the data set used is presented, followed by a discussion of the methodology developed to determine a steady, balanced, basic state.

3.1 Determining a basic state for the "model problem"

3.1.1 *Returning to the Illustrative Example*

The first model problem to be considered was first discussed in Section 2.5 where it was found that the time mean flow was not a suitable choice to describe the basic state for the propagation of waves on a piecewise constant potential vorticity flow on an f - plane. The observations of the near parallelism of PV contours with streamfunction contours suggests that a significant portion of the observed flow is slowly evolving or, in fact, steady.

This one observation allows a functional relationship between q and Ψ to be defined. For the present problem, viewed in a frame of reference moving at speed $c = U - \frac{\Delta q}{2k}$, the wave of Figure 2.9 is stationary. The streamfunction contours and the isopleths of vorticity then are (by definition) aligned - the flow, in this frame of reference, has been rendered steady. A geostrophic scatter diagram for the flow is schematically shown in Figure 3.1. The relationship between vorticity and streamfunction takes on a step function distribution

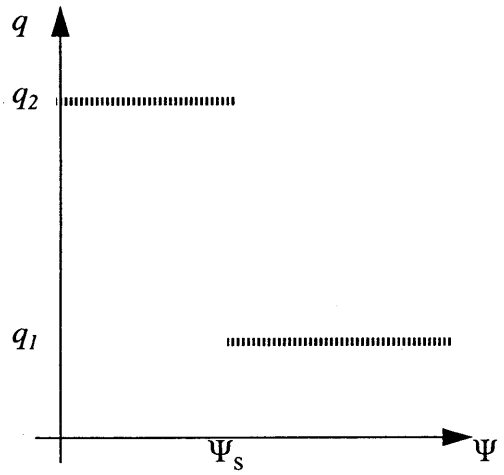

Figure 3.1: Geostrophic scatter diagram for the piecewise constant vorticity distribution seen in the frame of reference of the wave (shown in Figure 2.9a). Ψ_s represents that value of streamfunction at which the vorticity jumps for a value of vorticity q_2 north of the vorticity discontinuity to a value q_1 south of the discontinuity.

$$q(\Psi) = \begin{matrix} q_1 \text{ for } \Psi \geq \Psi_s \\ q_2 \text{ for } \Psi \leq \Psi_s \end{matrix}$$

- with high values of vorticity (q_2) north of some dividing streamfunction contour, Ψ_S, and low values (q_1) south of the contour. We also recall that from the simple time averaging, there exist two latitudes - one north and one south of the contour $\Psi = \Psi_S$, at which the vorticity field is undisturbed, at $y = \pm Y$. With this information, the basic flow vorticity field may now be reconstructed.

The reconstruction of the two-dimensional basic state vorticity field involves "mapping" (affixing geography to) the scatter diagram of Figure 3.1. This task is accomplished by solving the equation

$$\nabla^2 \Psi = q(\Psi) \quad , \tag{3.1}$$

subject to the boundary conditions $\Psi(-Y) = \Psi_B$ and $\Psi(Y) = \Psi_T$. This *nonlinear* equation is rather simple, and may be solved analytically for the streamfunction. Equation 3.1 maybe written as

$$\nabla^2 \Psi = \frac{d^2\Psi}{dy^2} = q(\Psi). \tag{3.2}$$

We solve the problem separately in the two regions in which q is uniform and then apply boundary conditions at $\pm Y$, as well as matching conditions at the interfaces of the two regions.

The solution in both regions may be written as

$$\begin{aligned} \Psi_1 &= \frac{q_1}{2} y^2 + C_1 y + C_2 \\ \Psi_2 &= \frac{q_2}{2} y^2 + C_3 y + C_4 \end{aligned} \tag{3.3}$$

The boundary and matching conditions are

$$\begin{aligned} \Psi_1(-Y_B) &= \Psi_B \\ \Psi_2(Y_T) &= \Psi_T \\ \Psi_1 = \Psi_2 \quad &\text{at } y = y_s \\ u_1 = u_2 = u_s \quad &\text{at } y = y_s \end{aligned} \quad , \tag{3.4}$$

The solution to this system (3.2) - (3.4) is given in Appendix A. This problem may also be solved numerically using an iterative procedure.

3.1.2 *Uniqueness of solutions*

In this subsection, the uniqueness of solutions of (3.2) with boundary conditions is addressed by means of another model problem. We consider a flow characterized by a linear q - Ψ relation:

$$q(\Psi) = -a^2\Psi + b \, , \tag{3.5}$$

where the relationship was chosen to have a negative slope to mimic observed geophysical flows. We solve for the flow in a region bounded by $y = \pm\frac{L}{2}$. The solution to (3.1) with q as given in (3.5) is

$$\Psi = A\sin(ay) + B\cos(ay) + \frac{b}{a^2} \, , \tag{3.6}$$

where A and B are arbitrary constants. The boundary conditions

$$\begin{aligned} \Psi(-\frac{L}{2}) = \Psi_1 &= A\sin(-a\frac{L}{2}) + B\cos(-a\frac{L}{2}) + \frac{b}{a^2} \\ \Psi(\frac{L}{2}) = \Psi_2 &= A\sin(a\frac{L}{2}) + B\cos(a\frac{L}{2}) + \frac{b}{a^2} \end{aligned} \tag{3.7}$$

are used to fix the constants.

The solutions to the system (3.7) are not unique if the determinate of the matrix of coefficients for the variables A and B is zero. That condition is

$$\sin(a\frac{L}{2})\cos(a\frac{L}{2}) = 0$$

or

$$a = \frac{2\pi n}{L}, \frac{(2n+1)\pi}{L} \tag{3.8}$$

where n is an integer, greater than or equal to zero. The smallest value of a for which the solution is unique is $a^2 < \frac{\pi^2}{L}$. This condition may be rewritten in the form

$$0 < \left(\frac{L}{\pi}\right)^2 < \frac{1}{a^2} = -\frac{d\Psi}{dq} < \infty. \tag{3.9}$$

This form is identical to that of (2.16) (Arnol'd's Second Stability Theorem). This result suggests that those flows which are unique solutions to (3.1) with the q - Ψ relation (3.5) and satisfying the boundary conditions (3.7) are stable. Pedlosky (1987) suggests that the instability of a flow is related to the ability of the flow to find more than one solution to $q = q(\Psi)$ while simultaneously conserving PV and satisfying the boundary conditions.

The essential elements of the procedure to be outlined in section 3.3 have been presented. In order to determine a steady, balanced basic state we require a relationship between q and Ψ (to ensure steadiness and to produce a flow which is dynamically similar to the observed flow), a balance assumption, and boundary conditions which ensure the spatial distribution of the PV is consistent with the observed distribution.

3.2 Determining steady flows

As was first noted in Section 2.2, and reiterated in subsequent sections, the observed flow tends to be characterized by contours of q and Ψ being nearly parallel - a situation which implies an approximate functional relationship between q and Ψ, in other words a nearly *steady flow*. The existence of steady flows or stationary states in the atmosphere has been shown to influence the dynamical response of modeled atmospheric flows to weak forcing (*e.g.* Charney and Devore (1979), Pierrehumbert and Malguzzi (1984), and Branstator and Opsteegh (1989)). In situations in which an unforced, steady solution could be

obtained for barotropic flow on an f or β plane, Pierrehumbert and Malguzzi demonstrate the existence of local multiple equilibrium states - both a high zonal index (low amplitude) steady flow and a low zonal index (high amplitude) steady flow when the flow was subjected to weak Ekman damping.

Given the importance of steady flows, many attempts have been made to determine the structure and conditions for the existence of these steady flows both analytically and observationally. Most extant studies have sought steady solutions to the barotropic vorticity equation, as this equation has been assumed to capture the essential "slow dynamics" of the atmosphere (Branstator and Opsteegh, hereafter BO).

Analytical solutions of the barotropic vorticity equation on a sphere fall into two classes - the Rossby - Haurwitz waves and modons. Rossby - Haurwitz waves are exact analytic solutions of the barotropic vorticity equation on a sphere in the case that the streamfunction is a single spherical harmonic mode. BO note that the existence of Rossby - Haurwitz waves of the same total wavenumber would be characterized by a linear relationship between q and Ψ. Modons, on the other hand, may be analytically constructed by allowing the trapping potential to change discontinuously on moving from closed to open Q or Ψ contours (Butchart *et al.*, 1989). On a geostrophic scatter diagram the signature of a modon structure would be the existence of two distinct linear relationships between Q and Ψ.

Attempts at identifying free or steady solutions in atmospheric data have relied on either diagnostic techniques in which a qualitative comparison between the observed distribution of points on scatter diagrams to the signatures of the known free mode solutions is made (Butchart et al., Illari (1984), Ek and Swaters (1994)) or by attempting to quantitatively find the solutions to the unforced barotropic vorticity equation (BO, Anderson (1992)).

BO and Anderson sought solutions, Ψ_S to

$$J(\Psi_S, f + \nabla^2 \Psi_S) = 0$$

by seeking to minimize a functional $F(\Psi_S)$

$$F(\Psi_S) = \sum_i (J(\Psi_S, f + \nabla^2 \Psi_S))_i^2 \tag{3.10}$$

(where 'i' is an index for the sum over complex spectral coefficients of the Jacobian) with respect to Ψ_S. F represents the degree to which the observed flow departs from free mode form.

Using observed instantaneous flows at 500 hPa as an initial guess, BO were able to find minima to (3.10) which closely resembled their initial guess. The relationship between absolute vorticity and streamfunction was observed to be nonlinear or piecewise linear and therefore not characteristic of the known analytic solutions discussed above. The solutions BO find were characterized by a decrease in variance of relative vorticity at relatively high wave numbers (approximately greater than 10) generally associated with synoptic scales. BO argue that the distribution of free modes is not uniform. BO suggest that the part of phase space in which the atmosphere resides (determined from the initial guesses) is highly populated with the distinct states they found being a comparable distance apart as individual observed flows.

Anderson also obtains minima to (3.10) for 300 hPa flow which have characteristics similar to those found by BO. Figure 3.1a (taken from Anderson) shows the distribution of 300 hPa streamfunction averaged over 0000 and 1200 UTC for 14 January 1987. The corresponding scatter diagram is shown in Figure 3.1c This distribution was used as the initial field in the solution to (3.10). The solution to (3.10), (Figure 3.1b), which Anderson refers to as a nearly steady state (NSS), and its corresponding scatter diagram are shown in Fig-

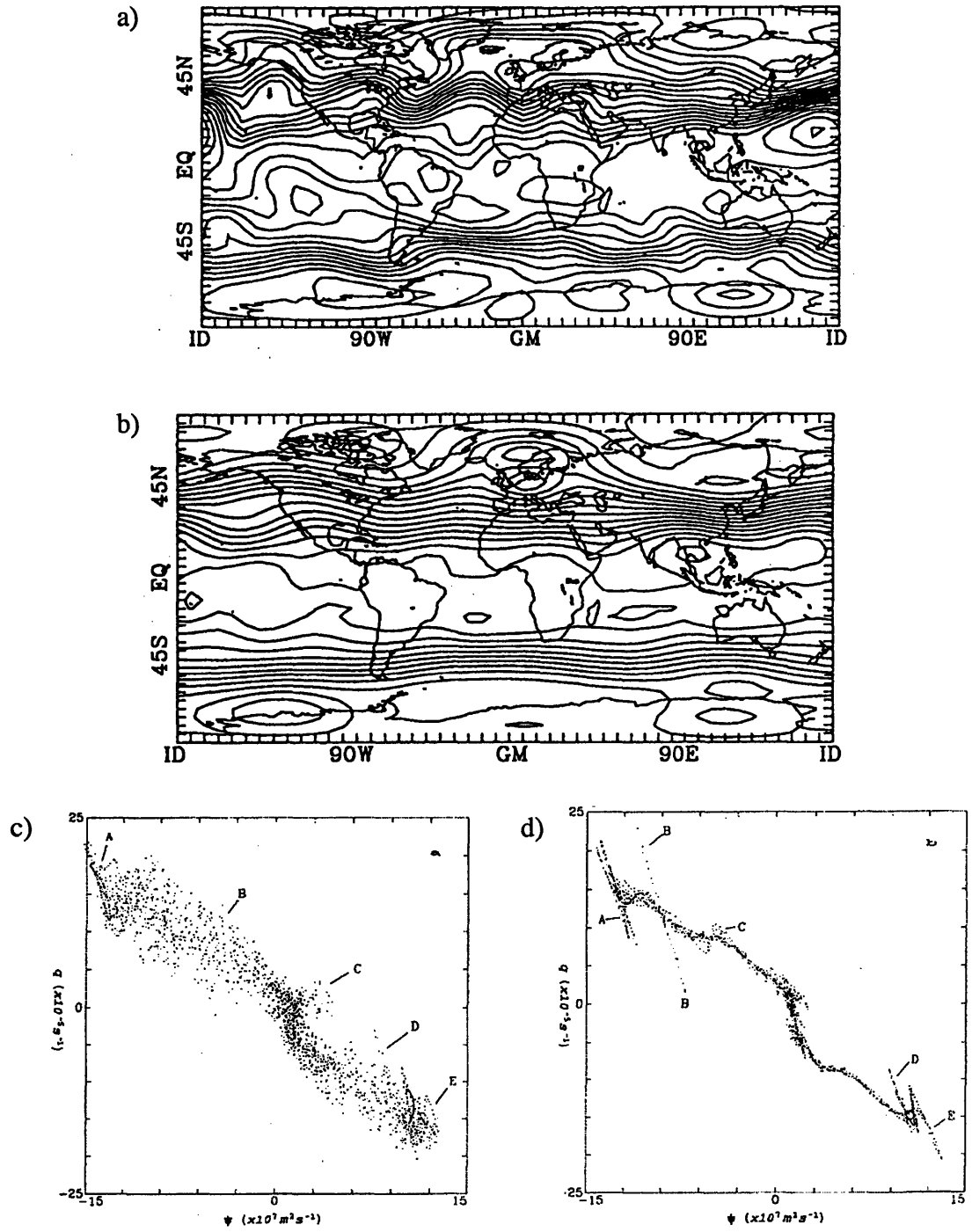

Figure 3.2: (a) Average of 0000 and 1200 UTC observed 300 hPa streamfunction for 14 January 1987 (contour interval 10^7 m^2s^{-1}), (b) Streamfunction of the NSS corresponding to time in (a), (c) and (d) geostrophic scatter diagrams for (a) and (b) respectively with ordinate absolute vorticity (units s^{-1}). (from Anderson (1992))

ure 3.1d. Note the similarities in both the streamfunction fields, the apparent "filtering" of smaller scale structures in the streamfunction fields, and more importantly the q - Ψ scatter plots (although the scatter has been considerably reduced in (Figure 3.1d). The labels identify on the scatter plots Figures 5.1 (c and d) various flow regimes. The labels A, B, D, and E point out regions in which blocking flows are observed. The differing functional relationships between q and Ψ found in the blocked flow regimes have a signature characteristic of a modon-like flow. Anderson additionally finds that all identified nearly stationary states found are barotropically unstable.

The work of BO and Anderson, coupled with the observations presented in the Section 2.2 lend credence to the idea that the instantaneous observed flow is dominated by a low wavenumber, nearly steady component. That the flow is dominated by such a component supports the primacy of the relationship between q and Ψ.

Finally it should be noted that while the barotropic solutions obtained by BO and Anderson are steady (or nearly so), they would not necessarily be appropriate as basic states as they may not be balanced.

3.3 Data set and methodology

In this section, the data set and methodology used to determine a steady, balanced, basic state from observed data are described. The order of the discussion is as follows: first a description of the data set used is provided, second a description of how the Q and Ψ relation is determined from the data is presented, and finally a discussion of the balance and boundary conditions that are employed in the solution is provided.

3.3.1 *Data set and isentropic analysis*

The data used in this work were from the NMC Global Analyses available from NCAR on 145 x 37, 2.5 degree grids. The analyses are based on synoptic observations (surface reports, aircraft observations, soundings, and satellite derived fields) taken at or near 0000 UTC and 1200 UTC and run through the Global Data Assimilation System as part of the analysis and forecast cycle for NMC's global spectral model. The particular fields used include the surface temperature, geopotential height, temperature, and wind (u- and v-components) at mandatory levels from 1000 hPa to 100 hPa. Except where otherwise noted, in the presentation to follow the data used were taken for the month of January 1991.

Isentropic analyses of wind, pressure, and Montgomery potential was performed on the data by linearly interpolating mandatory level data to the desired isentropic level. Stability, used in the calculation of PV, is calculated using a vertical finite difference of pressure over a 10 K thick layer.

Two points must be made with regard to this data set: while this data set is suitable for studying the evolution of synoptic scale disturbances, its vertical and horizontal resolution may be too coarse to resolve the concentrated vertical and horizontal gradients of potential vorticity in the atmosphere. This is not a severe limitation - the data set is of sufficient resolution to capture many of the features seen in isentropic analyses constructed from radiosonde observations. The second point is of more concern - Davis and Emanuel (1991) note that in the NMC analyses, the temperature at the surface is based on a downward extrapolation of stability just above the surface, while heights are extrapolated downward based on a standard atmosphere profile. The resulting distribution of mass and temperature are not in hydrostatic balance.

3.3.2 *Obtaining a unifunctional Q and Ψ (or M) relationship*

As has been discussed in previous sections, the relationship between the potential vorticity and the streamfunction (or the Montgomery potential) will be of fundamental dynamical importance in determining and characterizing the basic state. The observations and diagnostic tools discussed in previous sections provide some hints at how such a relationship might be determined.

As this study is primarily concerned with the propagation of synoptic scale waves, the wavy part of the flow (i.e. that part of the flow in the vicinity of the jets and their concomitant concentrated PV gradients) is of particular interest. Typically the weak flow surrounding the subtropical gyres and the lower stratospheric circulations is not wave-like and we can therefore assume that the PV in these regions is homogenized. For the flow to be truly steady and continuous, the Q -Ψ relationship must be global. To determine such a Q - Ψ relationship, for each 12 hour period in the data set, we average Q along those Ψ (or M) contours which are continuous around the globe. The average values of Q values from each day are then averaged over a time period longer than the periods of the wave motions of interest (the averaging is performed over a month). The resulting set of points, M *vs.* $\overline{Q}^M$ (where the overbar followed by 'M' indicates an average of a quantity along a corresponding contour of M), are then fit with either a first, fourth, or fifth degree polynomial. The scatter diagrams of this averaged data is shown are given in Appendix B. For isentropic surfaces which intersect the earth's surface in middle and high latitudes, no suitable set of M contours could be found to perform the aforementioned averaging. For these surfaces, a linear fit to the scatter diagram of the data was performed.

3.3.3 *Balance Assumptions*

In this section two balance approximations which may be used in the determination of the basic state are presented - geostrophic balance and non-linear balance.

Geostrophic Balance

Geostrophic balance is derived from balance between the Coriolis force and the horizontal pressure gradient forces. On an isentropic surface, this balance may be expressed in terms of the Montgomery potential

$$\boldsymbol{u}_g = \frac{1}{f_0}\boldsymbol{k}\times\nabla M \ ,$$

where $\boldsymbol{u}_g$ is the geostrophic wind, and $\boldsymbol{k}$ is the local unit upward normal. An expression relating the potential vorticity to the streamfunction is required. To determine this expression, (2.1) is written in terms of M. The absolute vorticity on an isentropic surface, $\zeta_{a\theta}$, may be written as

$$\zeta_{a\theta} = f + \frac{1}{f_0}\nabla^2 M \ .$$

The pseudodensity, σ, may be written as

$$\sigma = -\frac{\partial p}{\partial \theta} = -\frac{dp}{d\pi}\cdot\frac{\partial \pi}{\partial \theta} \ .$$

Recognizing that

$$M = \theta\pi + gz \ , \text{and} \ \ \frac{\partial M}{\partial \pi} = \theta .$$

and with some further manipulation, (2.1) may be rewritten as

$$Q_g = \frac{f + \frac{1}{f_0}\nabla^2 M}{\left(\frac{p_0}{\kappa g c_p^{\frac{1}{\kappa}}}\right)\left(\frac{\partial M}{\partial \theta}\right)^{\frac{1}{(\gamma-1)}} M_{\theta\theta}} . \qquad (3.11)$$

where $p_0 = 1000$ hPa, $\kappa = 2/7$, $c_p = 1004.7$ J kg K^{-1}, and $\gamma = .287$.

(3.11), which may be rewritten as

$$\frac{1}{f_0}\nabla^2 M - \left(\frac{p_0}{\kappa g c_p^{\frac{1}{\kappa}}}\right) Q_g \left(\frac{\partial M}{\partial \theta}\right)^{\frac{1}{(\gamma-1)}} M_{\theta\theta} = f, \tag{3.12}$$

is the "definition" of Q_g (the geostrophic potential vorticity). Given the distribution $Q_g = Q_g(x,y,\theta)$ in some domain, together with boundary conditions, (3.12) may be solved to determine the three dimensional geostrophically balanced flow within that domain. In this problem, rather than knowing $Q_g = Q_g(x,y,\theta)$, $Q_g = Q_g(M;\theta)$ is known, and so a typical inversion of PV cannot be undertaken. Solutions to this problem are determined by starting with an initial guess for M, evaluating Q_g, inverting in the "normal" fashion to solve for M. This new value of M is then used to start the process again. The cycle continues until a value of M satisfying (3.11) and the $Q_g = Q_g(M)$ relationship is found. Appendix D contains a brief description of the numerics of the solution.

Nonlinear Balance

To derive the nonlinear balance relation, the horizontal velocity field, $\boldsymbol{u}$, is partitioned into a nondivergent ($\boldsymbol{u}_\Psi = \boldsymbol{k} \times \nabla \Psi$) and an irrotational component ($\boldsymbol{u}_\chi = \nabla \chi$) (i.e. $\boldsymbol{u} = \boldsymbol{u}_\Psi + \boldsymbol{u}_x$). The horizontal momentum equations are then scaled such that terms of order a Rossby number determined by the irrotational part of the velocity field are neglected compared with terms of order Rossby number determined by the nondivergent part of the velocity field. The divergence of the scaled horizontal momentum equation may then be written

$$\nabla \cdot (\boldsymbol{u}_\Psi \cdot \nabla \boldsymbol{u}_\Psi) + \nabla^2 M - f\nabla^2 \Psi - \hat{k} \times \nabla f \cdot \boldsymbol{u}_\Psi = 0$$

or as,

$$\nabla \cdot \left(\nabla M + \nabla \frac{\boldsymbol{u}_\Psi^{\,2}}{2} \right) = -(\nabla \cdot (\hat{k} \times \boldsymbol{u}_\Psi (f + \nabla^2 \Psi))) \tag{3.13}$$

Using the Bernoulli energy, B, $B = M + \frac{\boldsymbol{u}_\Psi^{\,2}}{2}$, (3.13) may be rewritten as

$$\nabla^2 B = -(\nabla \cdot ((f + \nabla^2 \Psi) \nabla \Psi)) . \tag{3.14}$$

The potential vorticity scaled in a similar manner is given by

$$Q \cong \frac{-(f + \nabla^2 \Psi)}{\left(\frac{p_0}{\kappa g c_p^{\frac{1}{\kappa}}} \right) \left(\frac{\partial M}{\partial \theta} \right)^{\frac{1}{(\gamma - 1)}} M_{\theta\theta}} \tag{3.15}$$

Steadiness in the system (3.13) and (3.14) requires that $Q = Q(\Psi)$ ***and*** $Q = Q(B)$. Given the relationships between Q, Ψ, and B, the system (with appropriate boundary conditions) may be solved in an iterative manner to determine Ψ.

In this work a solution scheme assuming geostrophic balance is presented. In the next section the boundary conditions are discussed.

3.3.4 *Boundary Conditions*

The boundary conditions for this inversion are chosen to satisfy two assumptions: that the basic state be steady and that the shape of the basic flow pattern be characteristic of the flow for the time period over which the basic state is deemed relevant. As with the standard three dimensional inversion problem, (3.11) requires lateral and vertical boundary conditions. The solution will be determined on a hemisphere, consequently no zonal boundary conditions are required. While no northern boundary conditions are required, for the convenience of a solution on a rectangular grid, the northern boundary is chosen to be at 87.5 N, where the *time mean* Montgomery potential is specified. The southern boundary

condition is determined by first finding the mean position (for a given longitude, the mean latitude), on each isentropic surface, of a Q contour. Given the Q value, the M value for this contour is known. For each isentropic surface, this M value is then set at the mean position of its corresponding Q contour and these values of M are used as boundary conditions.

The lower boundary is taken to be at the lowest level of the data set, 1000 hPa. Recalling that the surface thermal distribution is dynamically equivalent to a delta function of PV near the surface, in order that there be a truly steady flow, we must require that the advection of potential temperature be zero at the lower boundary. This may be accomplished by either requiring the surface geostrophic wind to be wind be zero (*i.e.* requiring the 1000 hPa geopotential height to be a constant) *or* requiring the Montgomery potential to be parallel to the isentropes at the lower boundary (i.e. $M = M(\theta)$ at 1000 hPa.). The latter requirement is utilized in this work. The relationship between M and θ is shown in Figure 3.3 below.

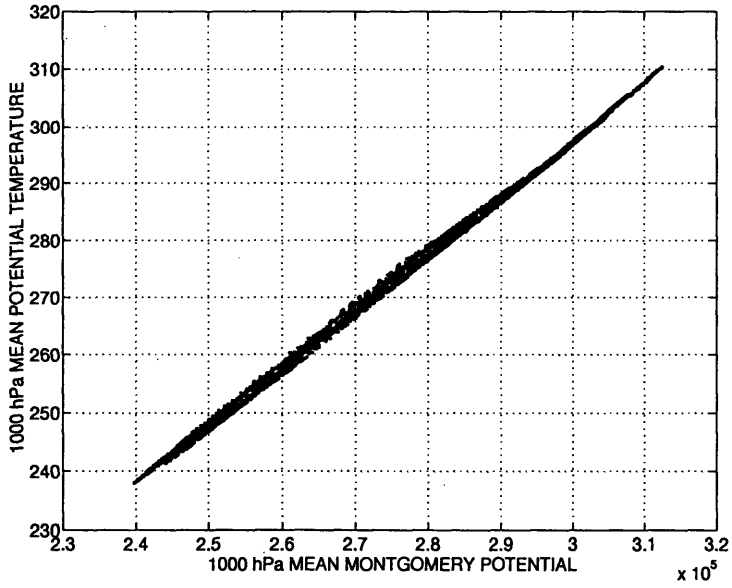

Figure 3.3: Relationship between Montgomery potential and potential temperature at the lower boundary (1000 hPa).

While a more appropriate upper boundary condition would be one analogous to the boundary condition chosen for the lower boundary, the upper boundary condition is chosen to be the time mean M on the 365K isentropic surface. The choice of a time mean field would seem to contradict the basic idea of this work - that time means of quantities characterized by inhomogeneous distributions will have less concentrated gradients than instantaneous realizations of the quantity.

At the 365K level, the sharp gradients of PV are concentrated along the subtropical jet. Because observations reveal that the "subtropical jet is characterized by great steadiness, both in wind direction and in geographical location" (Palmén and Newton, 1969), it is anticipated that the time mean flow and PV in the lower stratosphere would serve as a satisfactory surrogate for the basic state flow in that region.

Chapter 4

Application of the Technique

In this chapter, the results of a determination of a basic state through the application of the technique outlined in the previous chapter is presented for the month of January 1991. Section 1 contains a description of the basic state. For the purposes of comparison, the *time mean* fields of Montgomery potential, potential vorticity, and wind are presented and discussed in Section 2. In Section 3, a comparison of both the basic state and time mean vorticity flux fields is presented.

4.1 Basic state

As discussed in the previous chapter, the basic state for January 1991 is determined by solving the system

$$\frac{1}{f_0}\nabla^2 M - \left(\frac{p_0}{\kappa g c_p^{\frac{1}{\kappa}}} \right) Q_g \left(\frac{\partial M}{\partial \theta}\right)^{\frac{1}{(\gamma-1)}} M_{\theta\theta} = f,$$

with

$$Q_g = Q_g(M;\theta),$$

determined from observations and

$$\theta = \theta(M) \text{ at } 1000\ hPa,$$

at the lower boundary (Figure 4.1). The January 1991 *time mean M* is specified at 365 K (Figure 4.2), the time mean M at the northern lateral boundary at 87.5 N, and

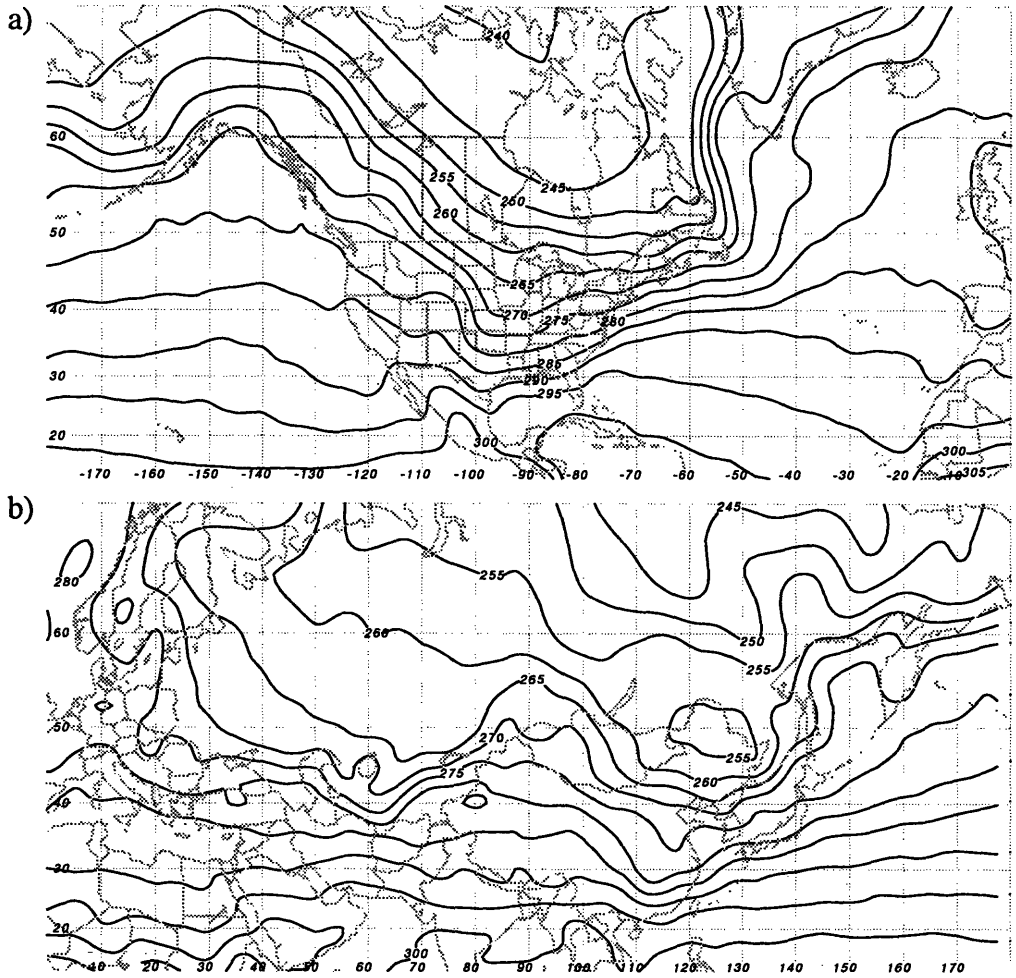

Figure 4.1: Lower boundary condition: Potential temperature at 1000 hPa. a) (western half of Northern Hemisphere), b) eastern half of Northern Hemisphere. Contour interval 5K.

$$M = M(\theta)$$

is specified along the January 1991 time mean *position* of a set of Q contours (for a list of the contours, see Appendix B, Table 2).

Rather than discuss the results of the calculation on each isentropic level, three representative levels have been selected for discussion. Except where otherwise noted, the results to follow are displayed in the following format - the upper chart (a) corresponds to results for the western half of the Northern Hemisphere (12.5^0 N to 70^0 N, 180^0 W to 0^0

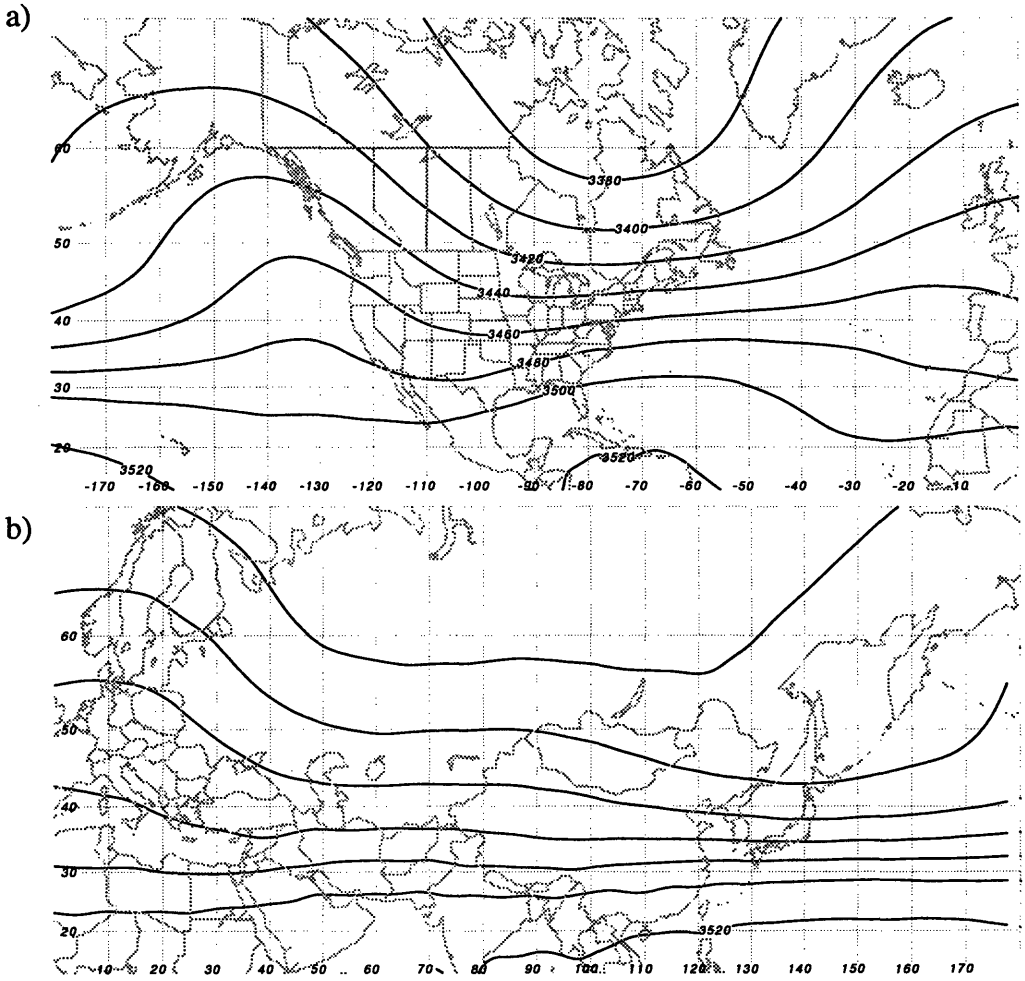

Figure 4.2: Upper boundary condition: Time mean 365K Montgomery potential. Contour interval 20 x 10^2 J kg^{-1}. (a) western half of Northern Hemisphere, (b) eastern half of Northern Hemisphere.

W), while the lower diagram (b) corresponds to the eastern half of the Northern Hemisphere (12.5^0 N to 70^0 N, 0^0 E to 180^0 E).

The irregular structure in the Montgomery potential fields is related to the discretization of the mean location of the mean Q contour which defines the southern boundary of the domain of the solution.

4.1.1 *Basic state flow on the 350K surface*

Figure 4.3a shows the Montgomery potential and isotachs for the geostrophic wind on the 350K isentropic surface for the basic state. The strongest jets at this level are found along and to the east of the east coast of North America and eastern Asia and the western

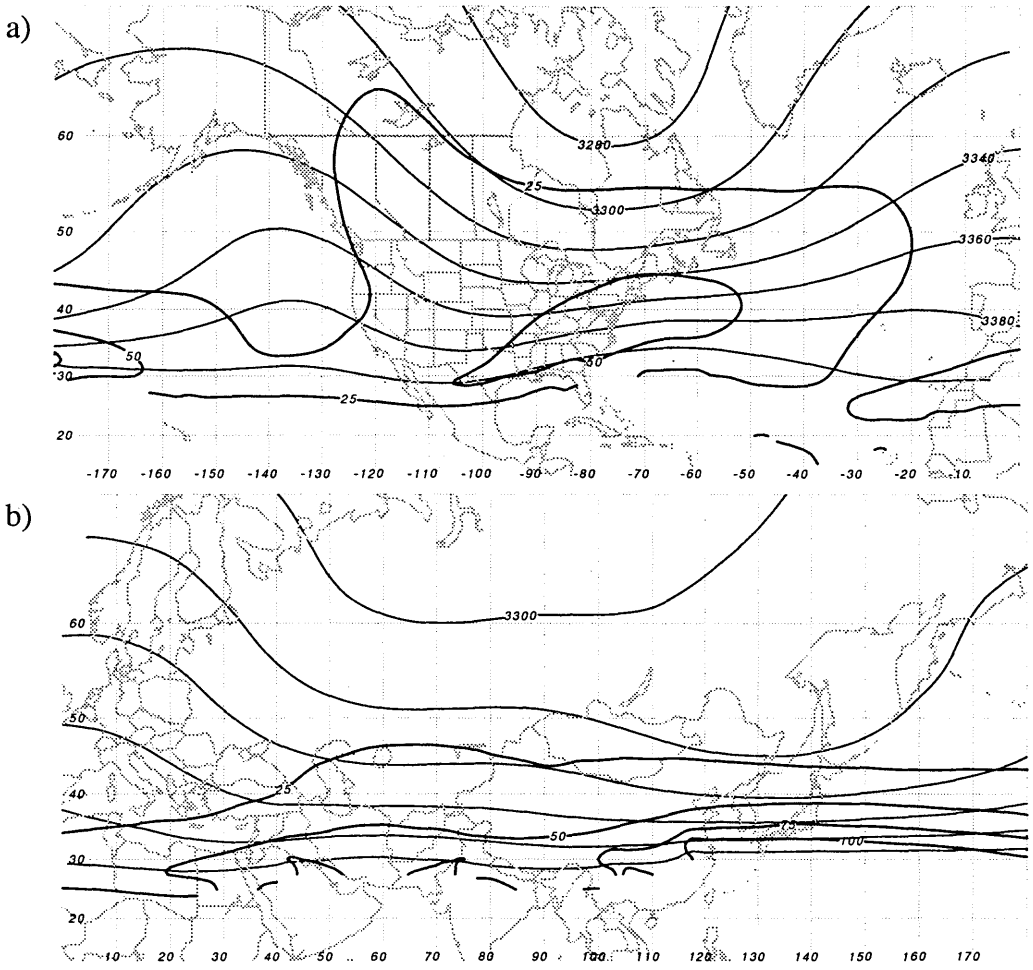

Figure 4.3: Basic state Montgomery potential (thin contours, contour interval 20 x 10^2 J kg^{-1}) and isotachs of geostrophic wind (heavy contours, contour interval 25 ms^{-1}) at 350 K.

Pacific with maxima in excess of 50 ms^{-1} and 100 ms^{-1} respectively. The flow is nonzonal, with ridge axes located at the basic state jet entrance regions over the eastern Pacific at approximately 140^0 W and over western Europe along the Greenwich meridian. The flow becomes diffluent as it moves into the ridges. The basic flow over the western portion of the Northern Hemisphere at high latitudes is dominated by a large cyclonic gyre centered near 75^0 W 75^0 N. Over the eastern half of the Northern Hemisphere, (Figure 4.3b) with the exceptions of the ridge over Europe and a trough over the east central Asia, the flow is markedly zonal.

The geostrophic PV and the geostrophic winds are shown in Figures 4.4a and 4.4b. As with the instantaneous fields, the PV gradients are concentrated near the jets, and by construction the winds are seen to blow parallel to the isopleths of PV. North of the subtropical jet, in regions in which the basic state winds are light, the PV gradients are weak.

Further evidence of the steadiness of the solution is found in the scatter diagram (constructed by using all of the points in the domain of the solution) in which we see the points collapsing towards a curve (Figure 4.4c).

4.1.2 *Basic state flow on the 320K surface*

The 320 K basic flow Figure (4.5a, b) resembles the flow described on the 350K surface. As with the 350 K surface, the ridges axes are found near 140^0 W and the Greenwich meridian, a large cyclonic gyre is located over northern Canada, and an nearly zonal flow lies over much of southern Asia along 30^0 N). The jet maximum along the East coast of North America at this level is in excess of 75 ms^{-1}, while the maximum south of Japan is weaker - at about 55 ms^{-1}. There is some indication of a ridge in the Montgomery potential over eastern Mongolia.

The PV and wind fields for this level are plotted in Figure 4.6 (a,b). The gradients are seen to be concentrated near the jet cores and are weaker elsewhere. Regions in which the magnitude of the PV gradients is small correspond to the weak cyclonic flow in the circulation centers over northern Canada and Russia. The geostrophic scatter diagram for the flow, Figure 4.6 (c), shows that the flow is essentially steady at this level.

4.1.3 *Basic state flow on the 290K surface*

The 290K surface intersects the 1000 hPa surface in the subtropical part of the domain. North of this intersection, the gradients of the Montgomery potential are weak compared with the rest of the domain (Figure 4.7 (a,b)). The maximum in geostrophic wind found on this level is in association with the jet observed at higher isentropic layers along the east

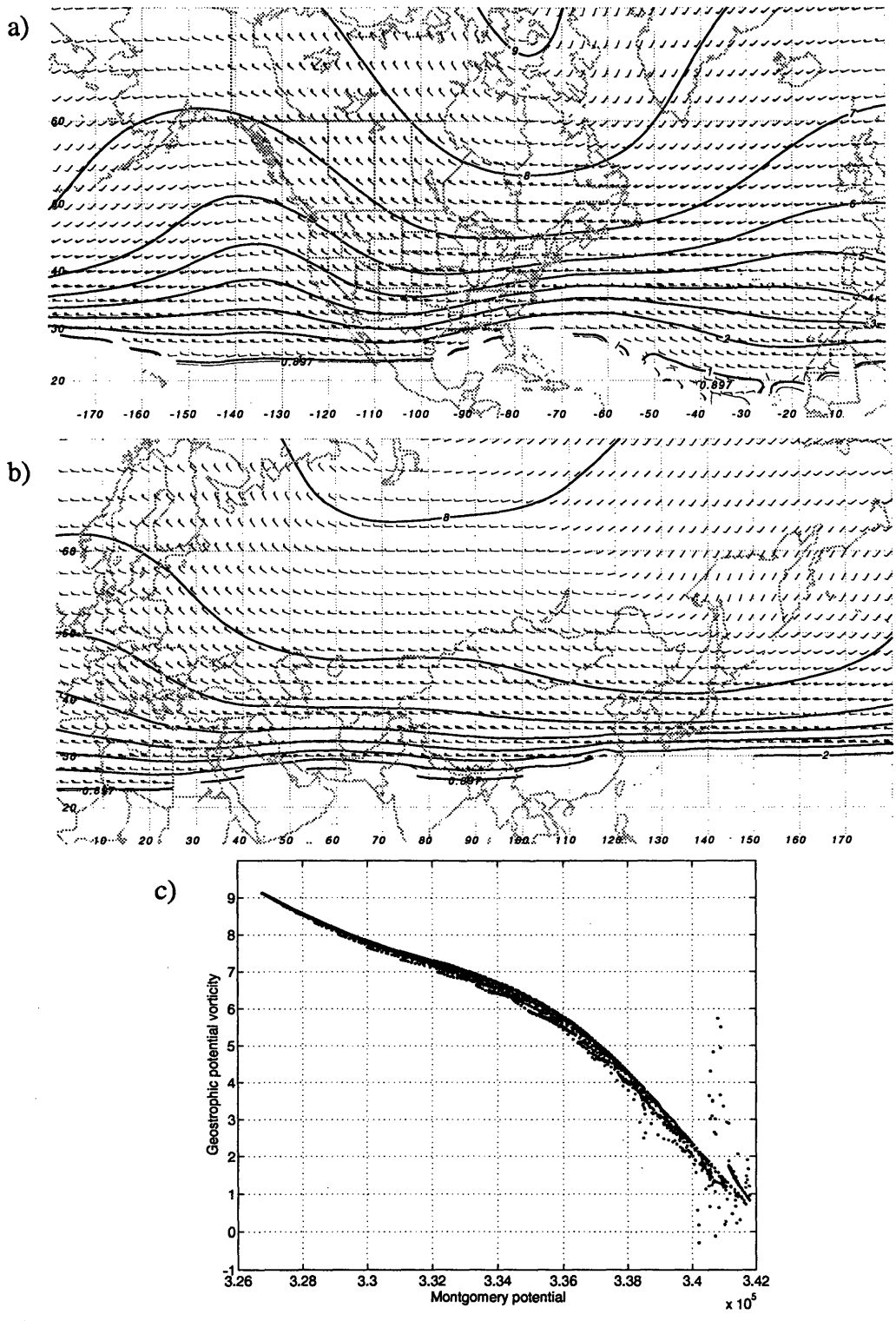

Figure 4.4: (a) and (b) Basic state Ertel potential vorticity and geostrophic winds on the 350K surface; contour interval 1 PVU. Winds in ms^{-1}, short barb 5 ms^{-1}, long barb 10 ms^{-1}. (c) 350K Basic state geostrophic scatter diagram

a)

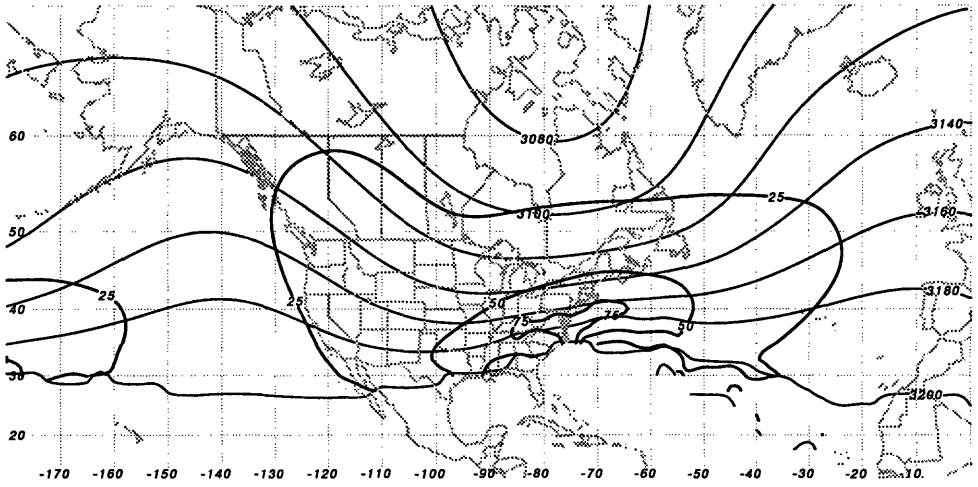

b)

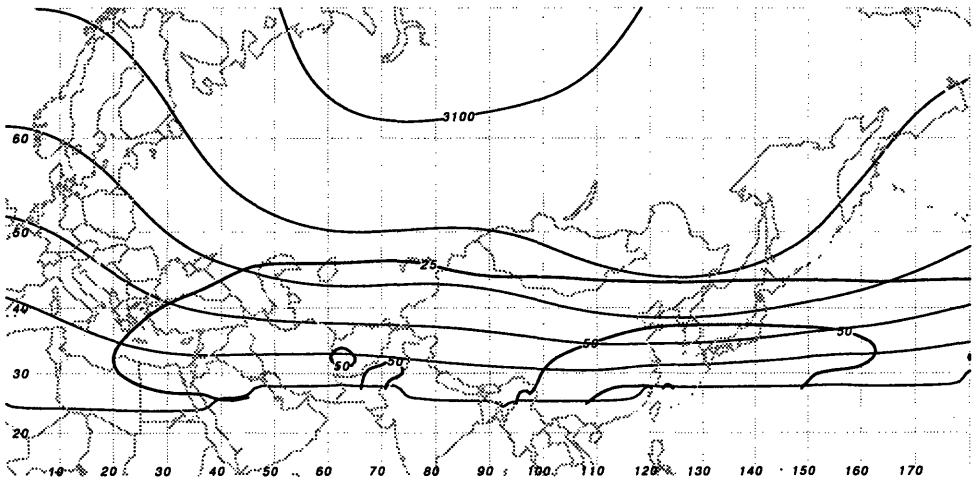

Figure 4.5: As in Figure 4.3, except for the 320K surface

coast of North America (speed of nearly 30 ms^{-1}). The "shape" of the flow is quite similar to the flow seen at higher levels - with ridging found over the ocean basins and low Montgomery potential (troughs) found over the continents. The flow over the eastern part of the solution domain is wavier than at higher levels - with the suggestion of a trough elongated northeast - southwest over western Russia, a small amplitude ridge over Mongolia, and a trough oriented northwest - southeast over the eastern Asia.

The PV distribution (Figure 4.8 (a,b)) at the 290K level is much "flatter" than the PV distributions at high levels. The gradients are weaker, and the winds are lighter. The tropo-

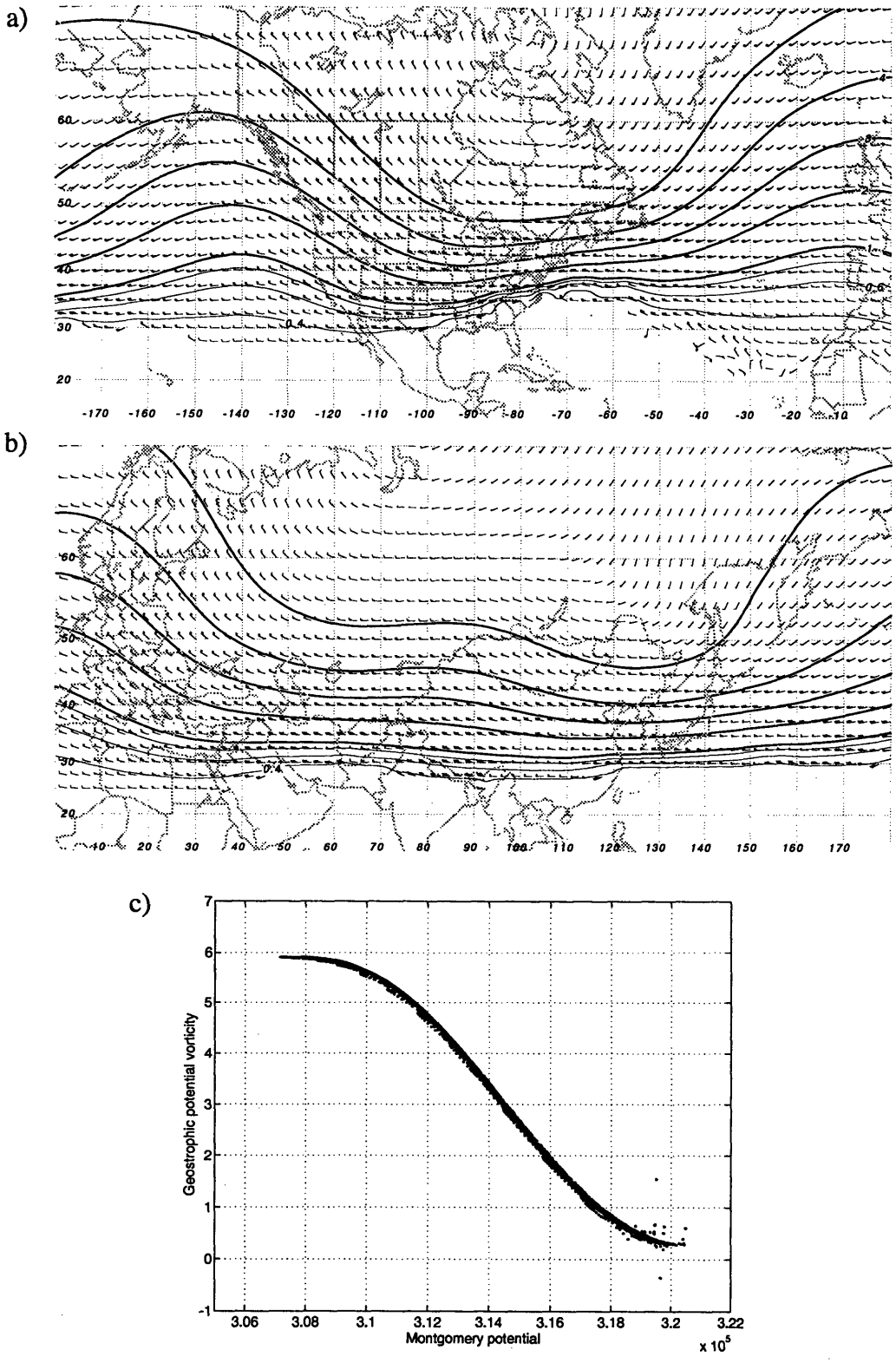

Figure 4.6: As in Figure 4.4, except for 320K surface.

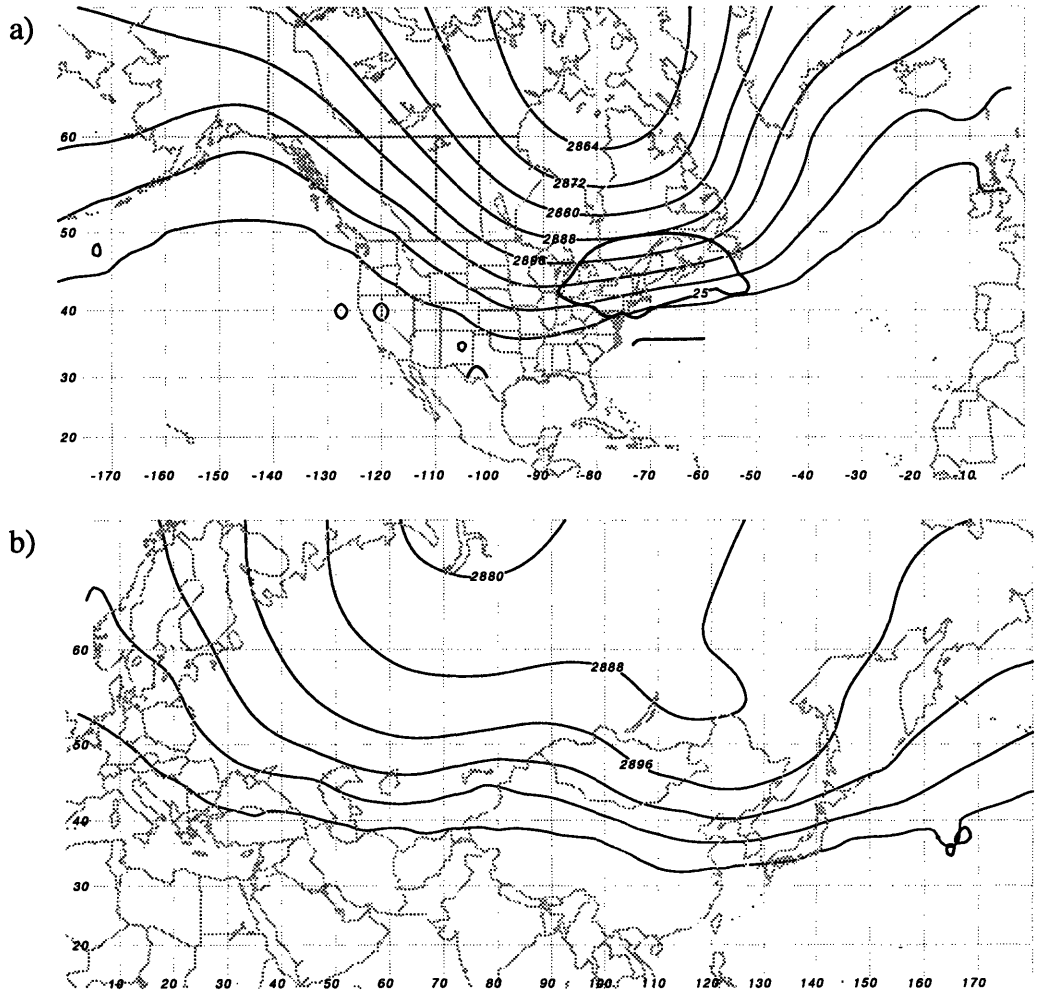

Figure 4.7: As in Figure 4.5, except for the 290K surface

spheric values of PV are seen to be well mixed in the ridges over the ocean basins. The geostrophic wind field for the solution is also seen to be lighter - particularly nearest that portion of the domain that intersects the 1000 hPa surface.

In summary, the basic state flow is characterized by equivalent barotropic structure - with the large-scale flow ridges and troughs of the flow being identifiable in the vertical on each of the isentropic surfaces and with the low level PV and Montgomery potential in phase with the 1000 hPa temperature field. The equivalent barotropic structure is anticipated, as tilting of the trough or ridge axes with height, could lead to thermal advections at

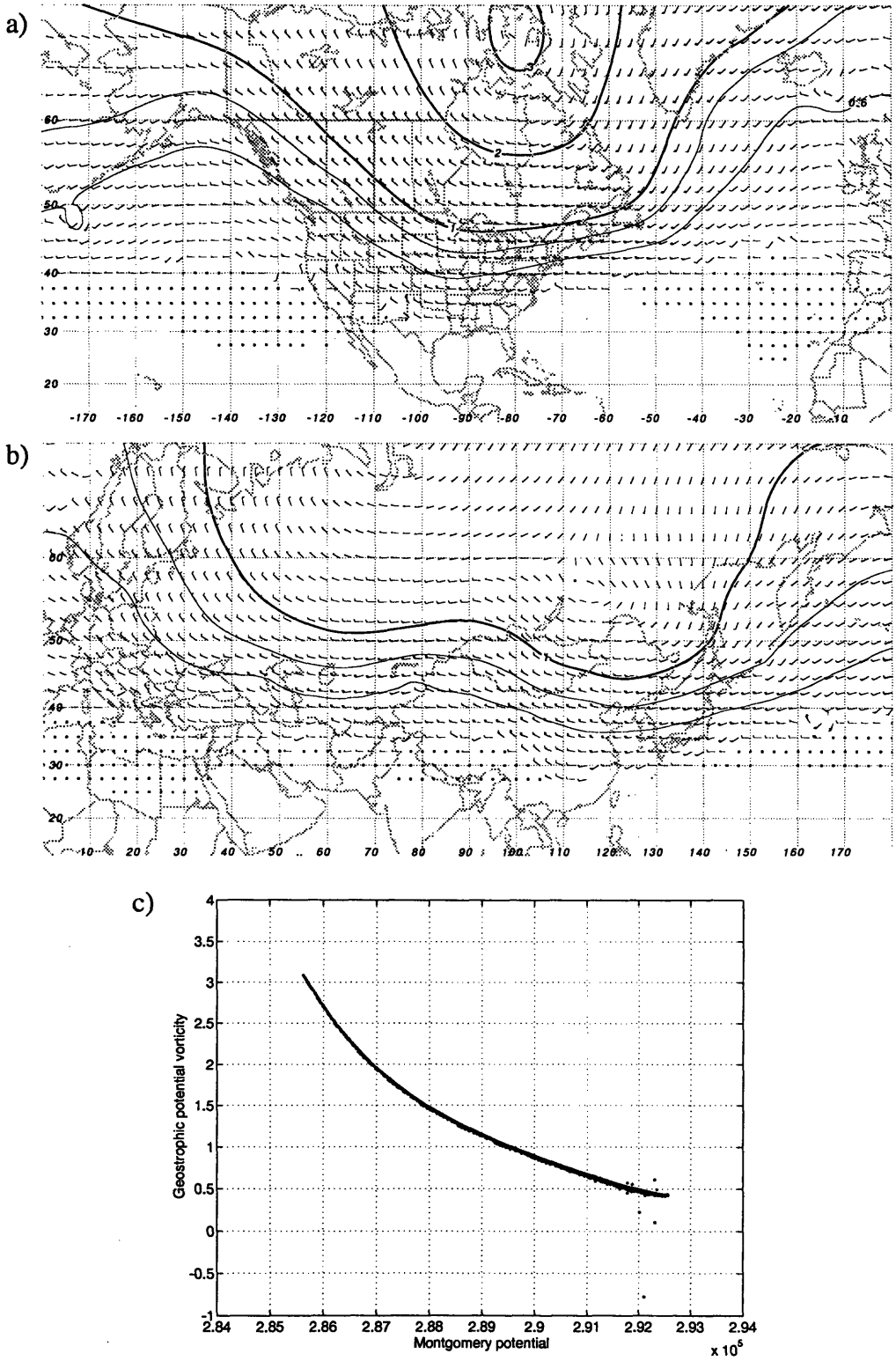

Figure 4.8: As in 4.4, except for the 290K surface.

the surface or PV advections in the interior, either of which could result in an unsteady flow.

It has been demonstrated that there is a distinction between a basic state and a time mean state. In order to distinguish the results of this basic state calculation from the time mean flow, a discussion of the time mean Montgomery potential, PV, and winds is presented in the following section.

4.2 Time mean flow

The time mean flow for January 1991 is described in this section. The time mean flow is defined as the flow derived from time averages of the height, wind, and temperature fields on isobaric surfaces. Thus when the term "time mean PV" is used, it is taken to mean the PV calculated from the time averaged wind and temperature. The mean flow will be discussed for the 350K, 320K, and 290K surfaces.

4.2.1 *350K surface time mean M*

A comparison of the Montgomery potential fields for the basic state and the time mean fields at 350K shows that there are in fact many similarities between these two fields in terms of their large scale structure. In the time mean (Figure 4.9 (a,b)), ridges are located near the over the central and eastern basins of the oceans, which there are troughs located over central and eastern North America, eastern Asia and Eastern Europe/western Russia. The time mean subtropical jet extends along 30^0 N from northern Africa to the Central Pacific with a jet maximum southeast of Japan. A second, though weaker maximum, is associated with this jet located over the southeastern U.S., extending east-northeast into the Atlantic. Finally two areas of diffluence in the flow are seen in the central Pacific and the central Atlantic.

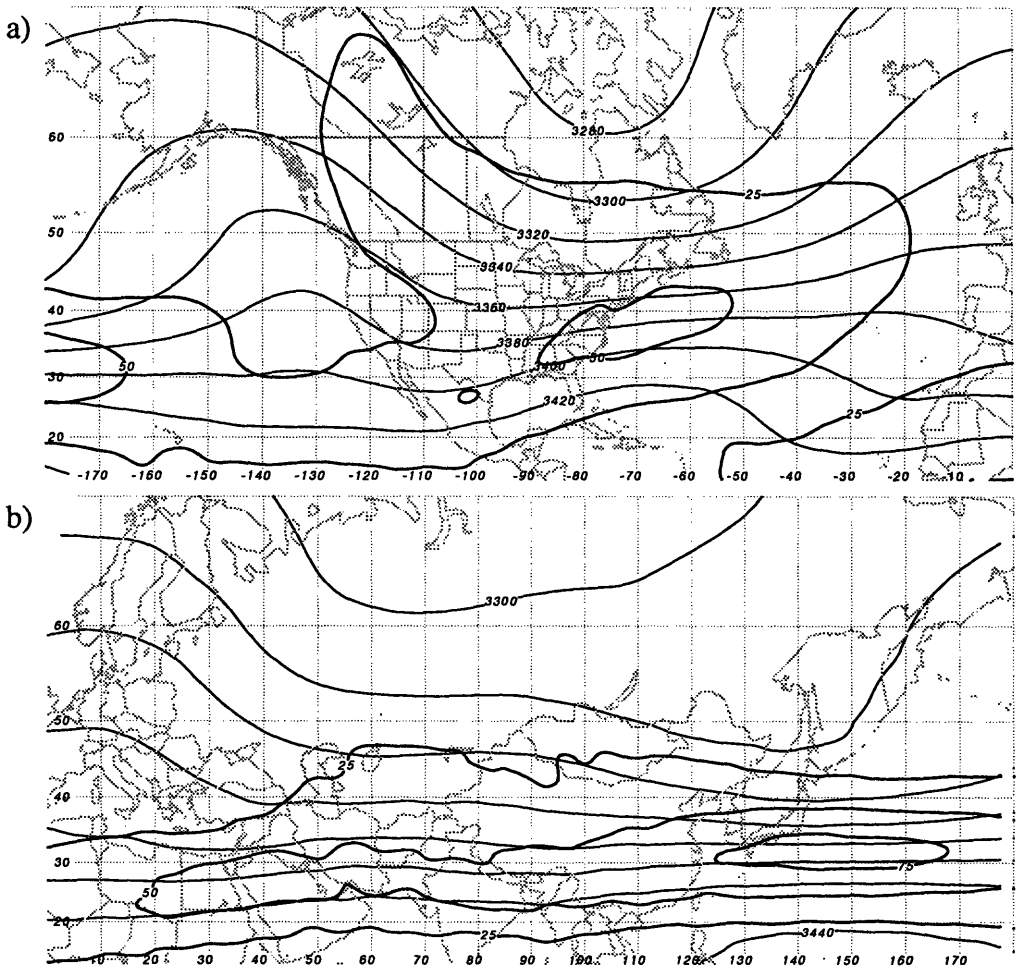

Figure 4.9: As in Figure 4.3, except for the time mean flow on the 350K surface.

The differences between the basic state and time mean flow fields (*i.e.* basic state - time mean) as well as the implied geostrophic wind are presented in Figure 4.10. On the 350K surface (figure 4.10 a and b), the biggest difference in the geostrophic wind is found along the southern periphery of the domain where the subtropical jets lies. For all of the surfaces, over the continents (oceans), the sense of the circulation implied by the difference in geostrophic winds between the two states is cyclonic (anticyclonic).

While the wind field for the time mean averaged flow (Figure 4.11) is quite similar to the wind field for the basic state geostrophic flow, the PV fields are noticeably different. The time averaged PV field is quite noisy - particularly over the eastern Northern Hemi-

sphere where there are several closed contours of PV. The wind barbs are most nearly aligned with the contours of the time mean PV, where the flow is strongest. North of the subtropical jet, in the lower stratosphere, the wind blows across the PV contours.

The non-steady nature of this flow is best depicted in the geostrophic scatter diagram constructed for this level (Figure 4.11c). A comparison of the scatter diagram for the basic state flow (Figure 4.6c) indicates that the slopes of the curve suggested by the points in the time mean flow is shallower than of the slope of the cluster of points composing the basic state curve.

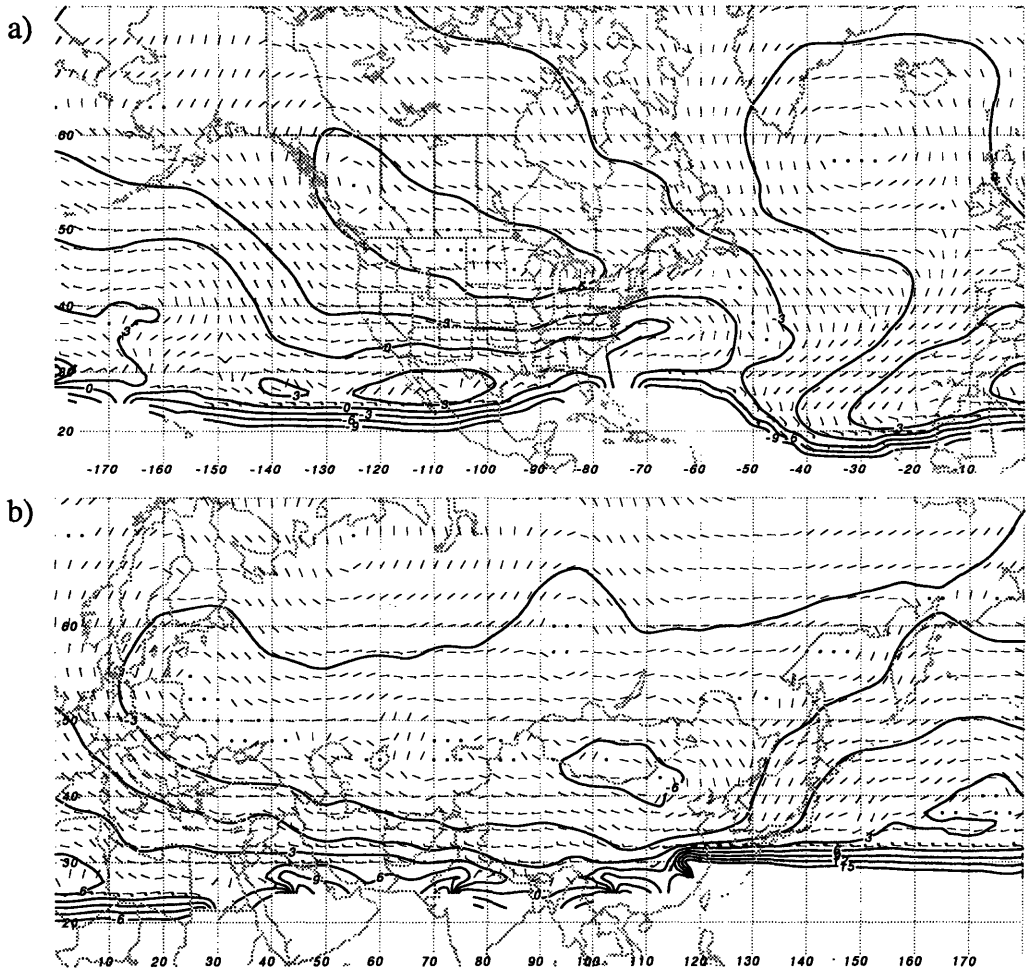

Figure 4.10: Difference field (basic state less time mean) for 350K Montgomery potential (contour interval 3 J kg^{-1}) and implied geostrophic winds associated with the differences in Montgomery potential, in ms^{-1}.

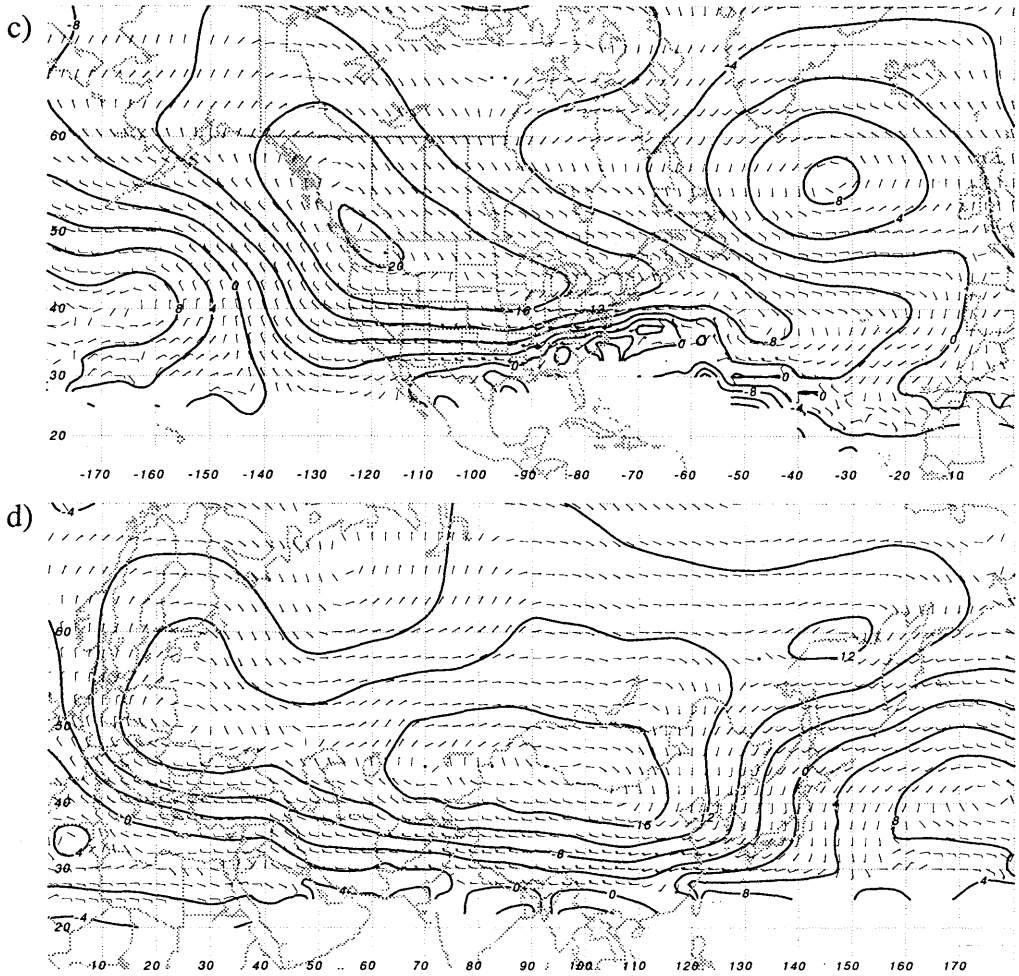

Figure 4.10 continued (c) and (d) for 320 K surface

The time mean 320K Montgomery potential (Figure 4.12) differs from the basic state in a few regions. The time mean ridge in the Pacific is slightly further to the west of the ridge in the basic state, the mean geostrophic winds are weaker in the jet cores, the mean (analyzed and geostrophic) winds at high latitudes (north of the subtropical jet) are stronger than the corresponding geostrophic winds, and the mean jets are found at higher latitudes than the basic state jets.

Gradients in the time mean PV (figure 4.13) away from the jets are weaker than at the location of the jets. Horizontal gradients of time mean tropospheric PV are not nearly as small as those of the instantaneous distributions described in Section 2.2. The scatter dia-

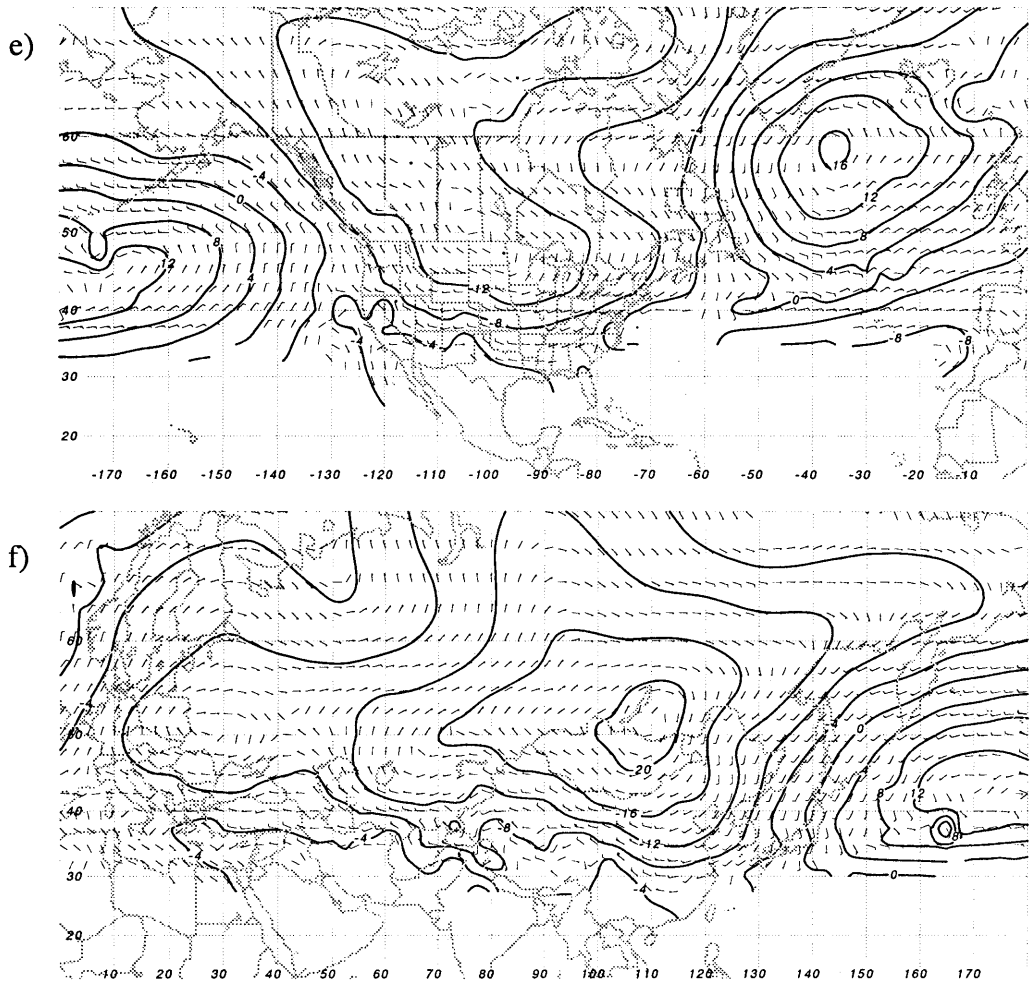

Figure 4.10 continued: (e) and (f) for the 290K surface

gram for the time mean flow is less steep in the jet region that the scatter diagram for the basic state - suggestive of a "smearing out" of the gradient in the time mean.

On the 290K surface (Figure 4.14), the basic patterns described above appear to be shifted somewhat to the east of the patterns at higher levels, the eastern Atlantic ridge, is now decidedly centered over western Europe, and the trough over eastern Asia seen on the 350K and 320K surfaces is extends out into the western Pacific. The maximum time mean geostrophic winds are found at the base of the trough over eastern North America - to the northwest of their corresponding location in the basic state.

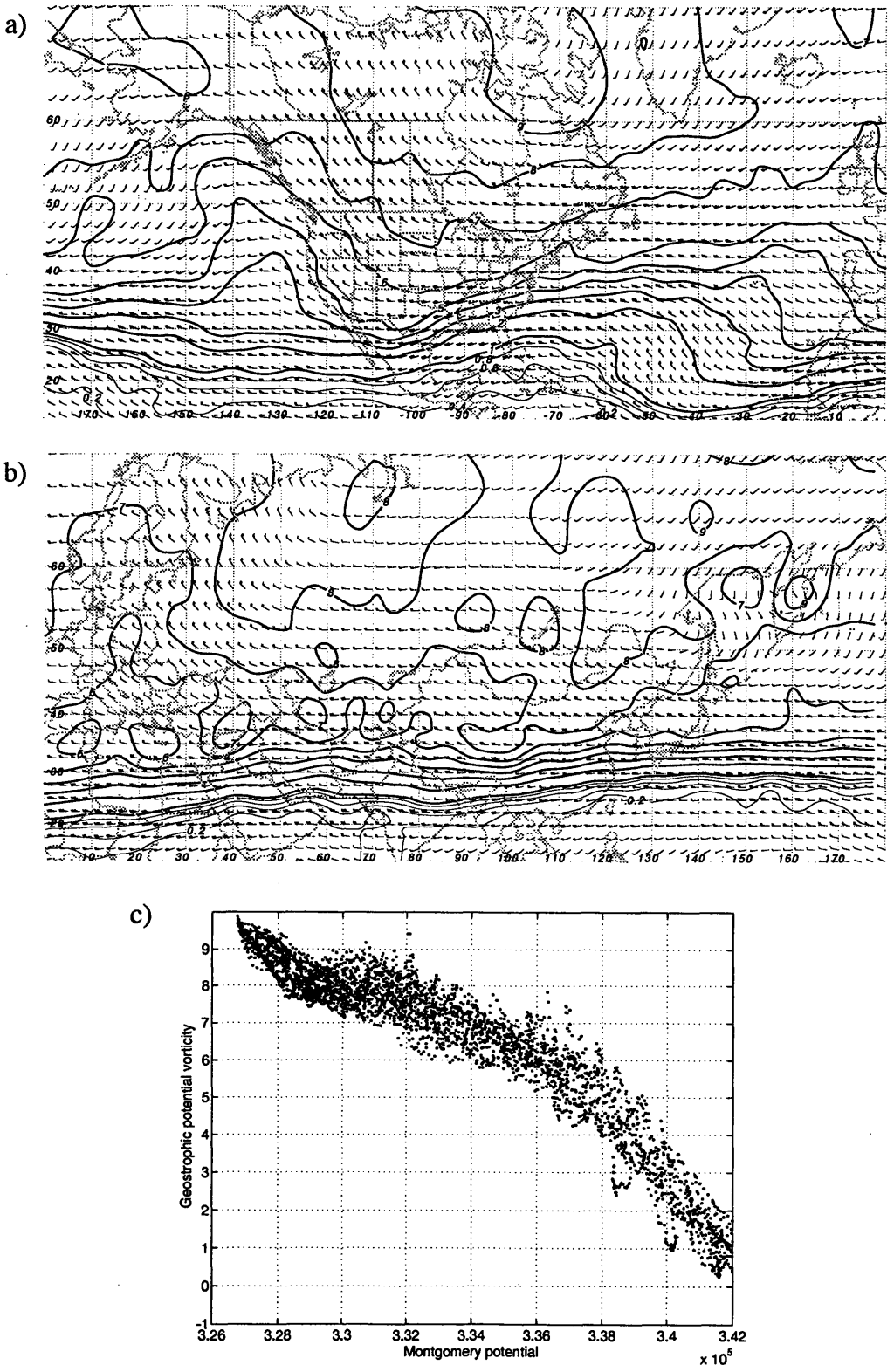

Figure 4.11: As in Figure 4.4, except for the time mean flow at 350K

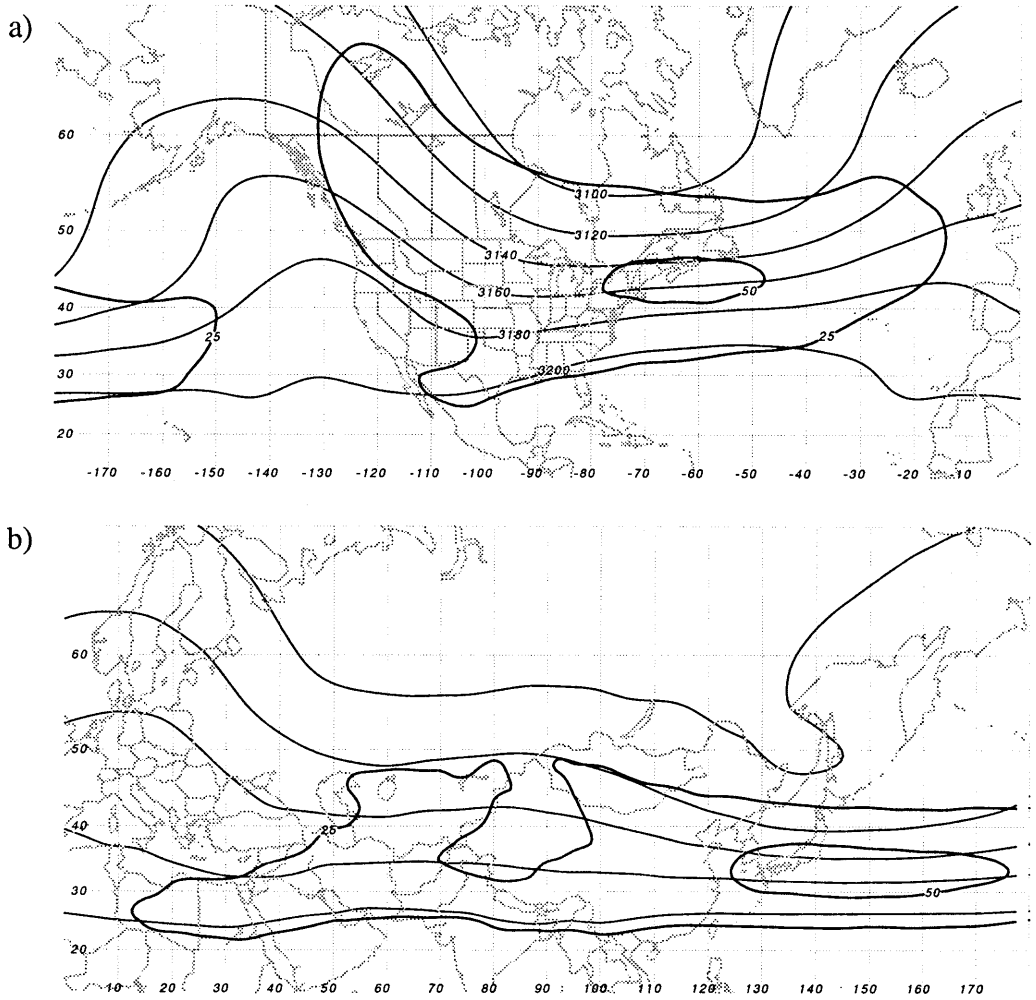

Figure 4.12: As in Figure 4.9, except for the 320K surface

Over the domain, the time mean wind fields are comparable in both magnitude and direction with the geostrophic winds of the basic state with the notable exception being the wind field associated with the east Asian trough. Because the trough is almost "cut-off" in the time mean, the associated cyclonic wind field produces easterlies south of the Kamchatka Peninsula (north of the time mean cyclonic circulation center). The areal domain averaged PV for this surface is smaller in the time mean compared with the basic state.

On the 290K surface the PV is nearly uniform in the eastern part of the Northern Hemisphere, while there do appear to be systematic gradients of PV colocated with the

a)

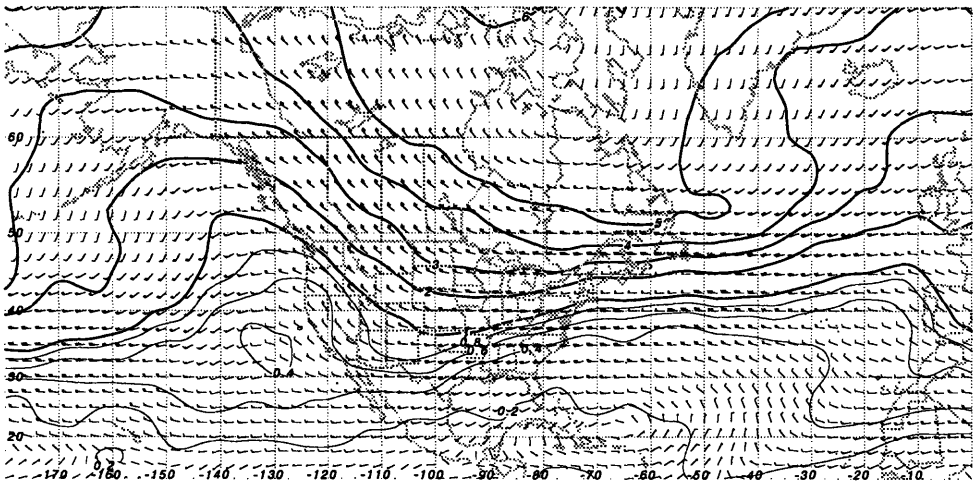

b)

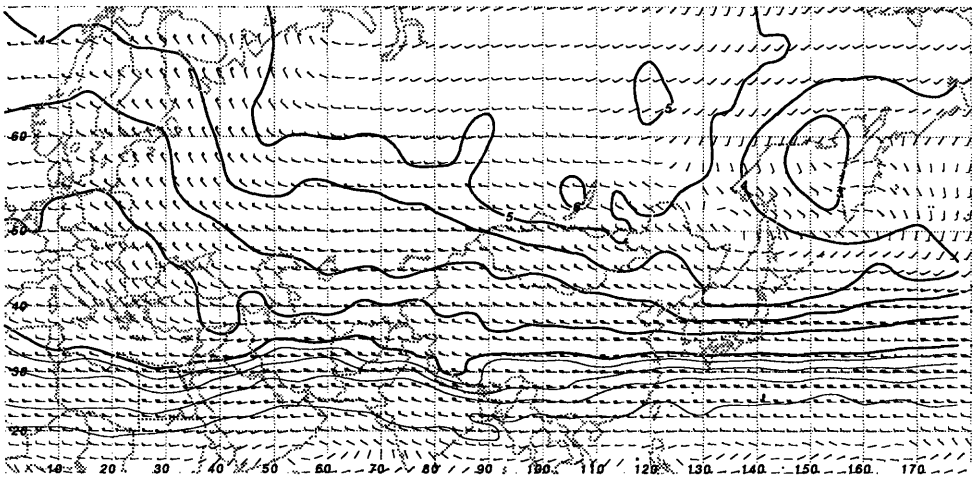

c)

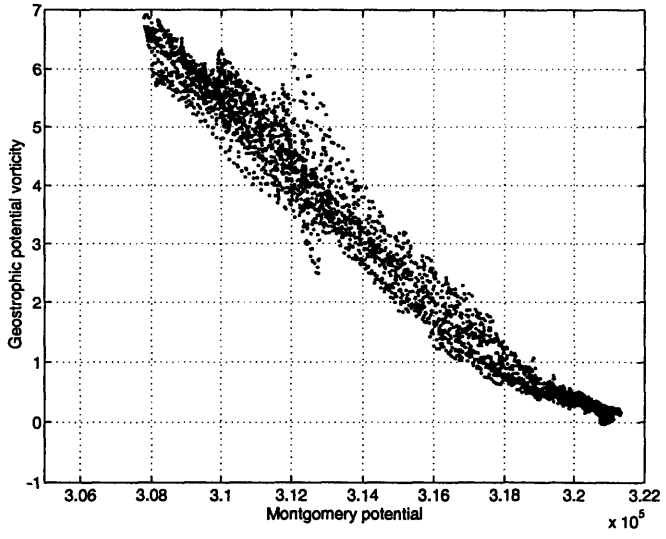

Figure 4.13: As in Figure 4.4, except for the time mean flow on the 320 K surface.

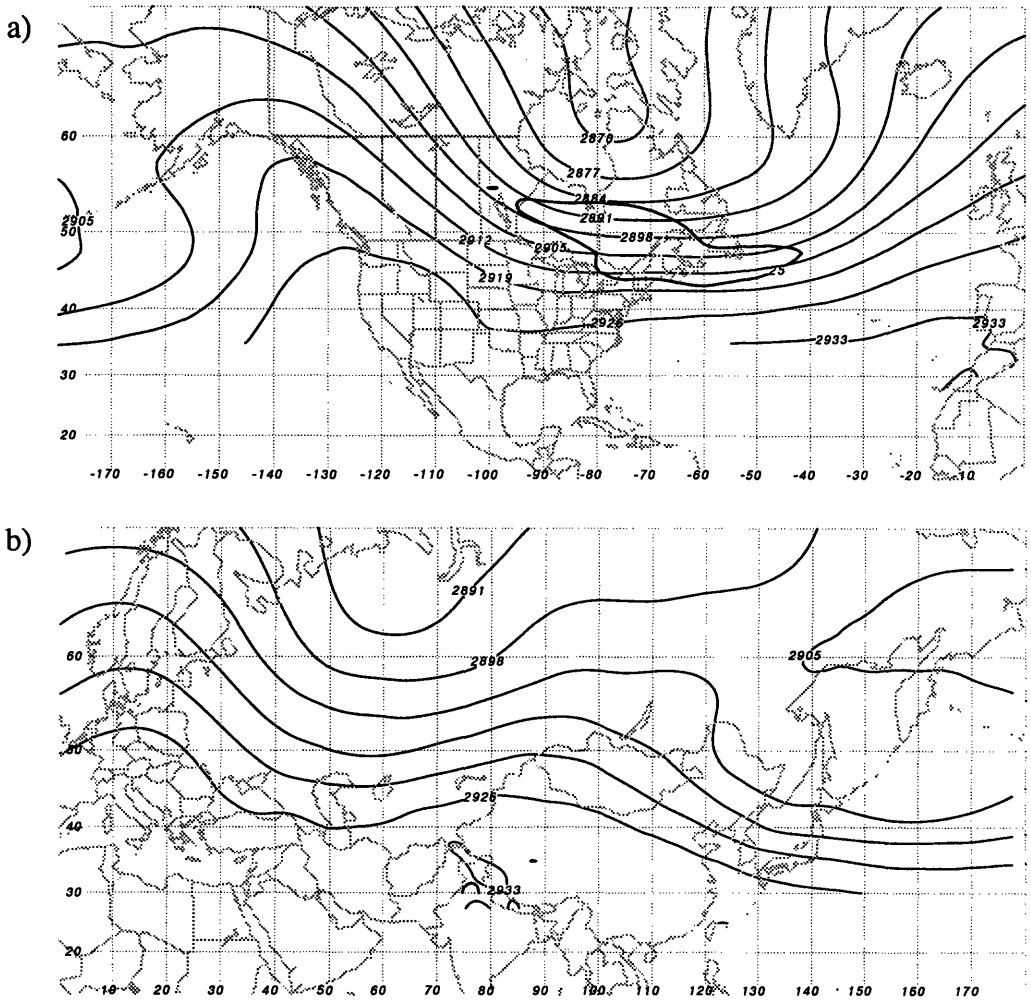

Figure 4.14: As in Figure 4.3, except for time mean flow on the 290K surface. Contour interval is 7 x 10^2 J kg^{-1}.

polar jet (or a reflection of the polar jet at that surface) over the western hemisphere (Figure 4.15a).

In summary, the gross characteristics of the time mean flow are similar in structure to the basic state flow, with the exception of the subtle shift westward with height of the zonal nonhomogeneities (ridges and troughs) of the flow in the time mean flow. The time mean PV distribution is rather noisy, with several maxima and minima in regions in which the flow is weak. The gradients of PV distribution in the time mean are not as intense as those of the instantaneous flows, nor is the PV distribution away from the jets nearly as

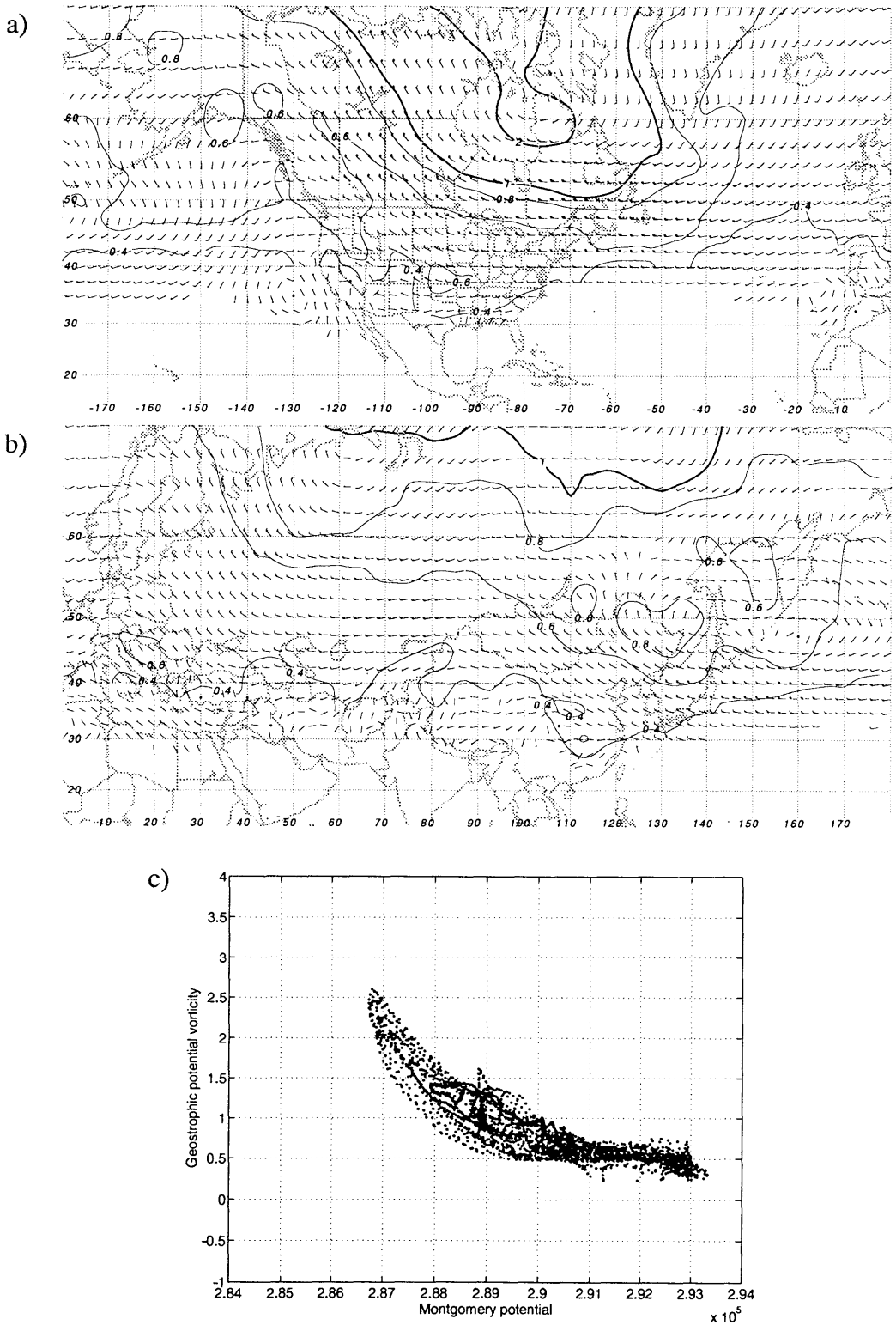

Figure 4.15: As in Figure 4.4, except for the time mean flow on the 290K surface.

uniform. The strongest gradients in the time mean are located along and just east of North America and eastern Asia. Despite the fact that the winds and temperatures have been averaged, the PV distribution in the time mean is rather "noisy". This noisy field may be due, in part, to the fact that PV is calculated as the product of differentiated quantities - resulting in an amplification of small scale structure in the data. Another reason may be attributed to the fact that the averaging has not been over a sufficiently long period of time so as to phase average over all of the transient eddies. North of the subtropical and polar jets (particularly over eastern Asia (Figures 4.3b and 4.5b), there are several local maxima and minima in the PV distribution. These extrema in the PV are not dynamically significant (in terms of their contribution if this time mean distribution were inverted) as they are generally much smaller than a typical Rossby deformation radius. While the flow is nearly parallel to the isopleths of PV, there are regions of significant advection (not shown) near the jets - even for this time mean flow.

4.3 Bernoulli's theorem and the total flux of potential vorticity

In this section, a further distinction is made between the basic state flow and the time mean flow. In anticipation of the discussion to follow in the next chapter, a set of diagnostic calculations is presented which may be used to characterize both flows.

The calculations rely on a generalization of Bernoulli's theorem developed by Schär (1993). Bernoulli's Theorem states that for a steady, inviscid, and adiabatic flow

$$\frac{dB}{dt} = 0$$

(i.e. the Bernoulli energy, B, is constant along streamlines of the flow). In isentropic coordinates, the Bernoulli function is given by

$$B = c_p T + gz + \frac{1}{2}\boldsymbol{u}\cdot\boldsymbol{u} = M + \frac{1}{2}\boldsymbol{u}\cdot\boldsymbol{u}.$$

For an adiabatic flow, the flow is by definition along an isentropic surface, if the flow is also steady and inviscid, Bernoulli's Theorem applies and the flow must also lie along a surface of constant Bernoulli energy. Thus, a streamline for steady flow is defined as the intersection of an isentropic surface with a surface of constant Bernoulli energy (Figure 4.16 (a)).

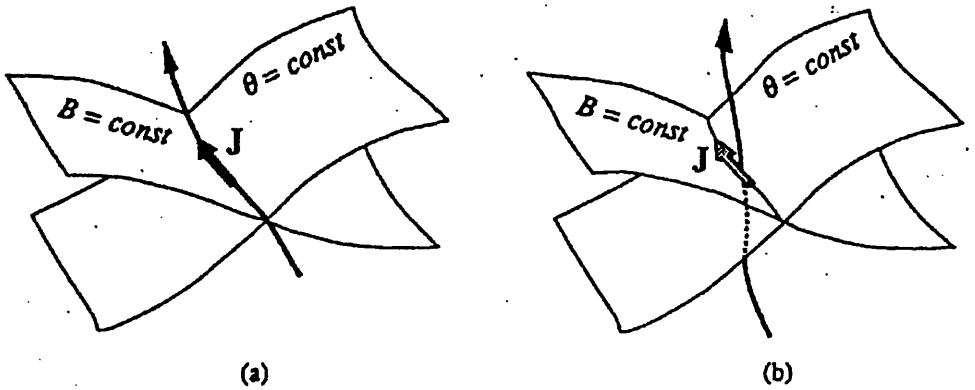

Figure 4.16: (taken from Schär (1993)). (a) For steady, inviscid, and adiabatic flow, Bernoulli's theorem requires that the Bernoulli energy, B, be constant along streamlines. The flow must also lie along an isentropic surface, θ. A streamline of the flow is then defined as the intersection of the B and θ surfaces. The total flux of PV is indicated by the dark vector. (b) For statistically steady flow, with diabatic and frictional effects present, the total flux of PV (grey arrow) is still aligned along the intersection of B and θ surfaces, however the mean streamline of the flow is no longer necessarily aligned with the θ or B surfaces.

Schär has derived a relationship between the total flux of vorticity within an isentropic layer and the Bernoulli function. The derivation of this relationship proceeds as follows:

The equation of motion in isentropic coordinates,

$$\frac{d\boldsymbol{u}}{dt} + \dot{\theta}\frac{\partial \boldsymbol{u}}{\partial \theta} + f\boldsymbol{k}\times\boldsymbol{u} = -\nabla M + \boldsymbol{F} \tag{4.1}$$

may be rewritten as

$$\left(\frac{\partial}{\partial t} + \dot{\theta}\frac{\partial}{\partial \theta}\right)\boldsymbol{u} + \boldsymbol{k}\times\boldsymbol{u}\zeta_{a\theta} = -\nabla B + \boldsymbol{F}$$

or

$$\frac{\partial \boldsymbol{u}}{\partial t} + \boldsymbol{k} \times \boldsymbol{J} = -\nabla B \,, \tag{4.2}$$

where $\boldsymbol{J}$ is the total flux of vorticity defined in (2.5). (4.2) may finally be rewritten as

$$\boldsymbol{J} = \boldsymbol{k} \times (\nabla B + \frac{\partial \boldsymbol{v}}{\partial t}) \,. \tag{4.3}$$

For a steady flow, (4.3) may be interpreted as saying that the Bernoulli energy is the streamfunction of the total flux of PV on isentropic surfaces. Further, the total flux of PV (now with advective and non-advective contributions included) is still aligned with both the B and θ surfaces - even for flows in which diabatic and frictional effects are still present (Figure 4.16b).

Figure 4.17 shows isopleths of M on the 320K surface overlaid with the total PV flux evaluated from (4.3) for the western part of the Northern Hemisphere. The degree to which the advective flux of potential vorticity dominates the total PV flux is apparent, as the flux vectors are nearly parallel with the M contours. A close inspection of Figure 4.17 reveals that there is a component of $\boldsymbol{J}$ normal to the isopleths of M for *both* the basic state and time mean flows. In order to isolate this non-advective component of the flux, the component of $\boldsymbol{J}$ normal to the M contours, *i.e.*

$$\boldsymbol{J}_{normal} = \frac{\boldsymbol{J} \cdot \nabla M}{|\nabla M|^2} \nabla M,$$

is plotted (Figures 4.18). The component of the flux normal to the M contours is dominated by a rotational component. Schär and Wernli (1994) relates this rotational component to a local maximum in the kinetic energy of the flow. As anticipated, the component of the flux is non-divergent (not shown) for the basic state flow - implying that the basic state flow is unforced. For the time mean flow however; the flux of PV away from the

local maximum in kinetic energy, is divergent. This indicates that the time mean flow is in fact forced..

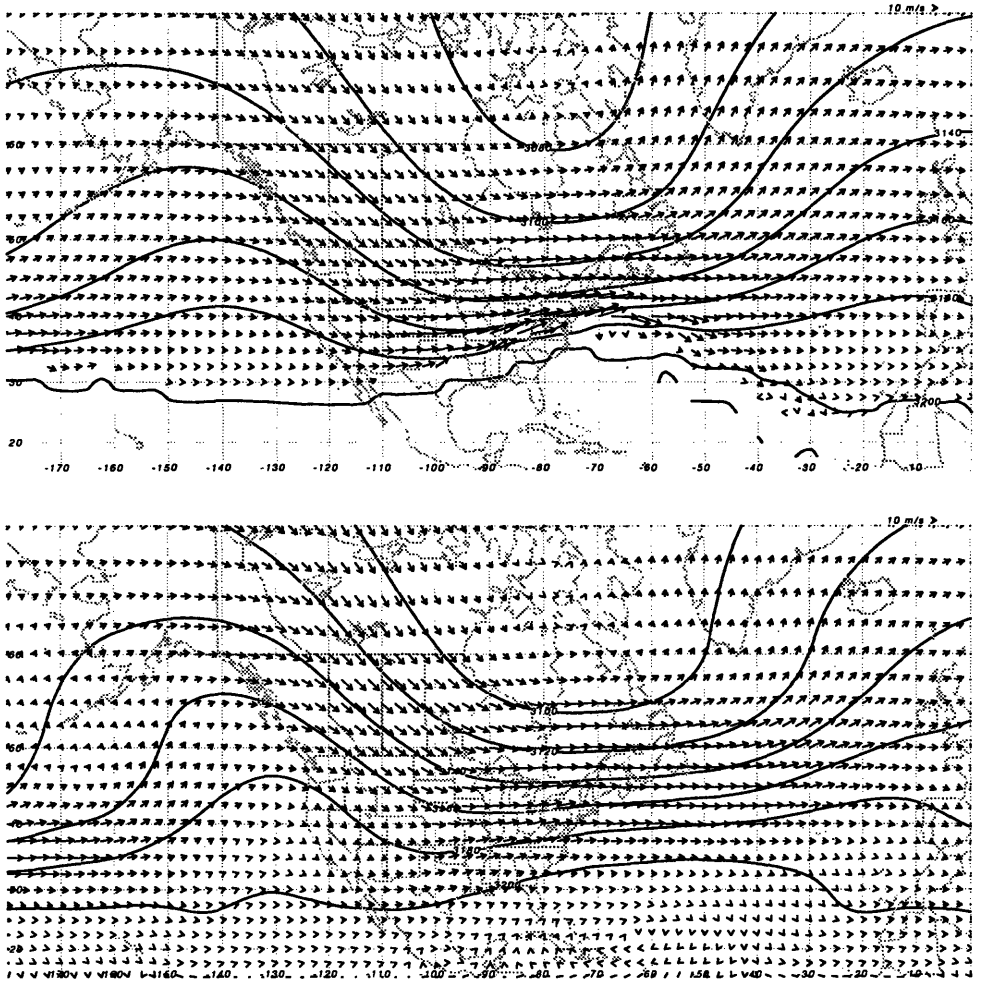

Figure 4.17: 320 K Montgomery potential (contour interval 20 x 10^2 J kg^{-1}) and PV fluxes (for scale of vector, see upper right of figure, scale 10^{-4} m^{-2} s^{-1}) for (a) basic state and (b) time mean flow.

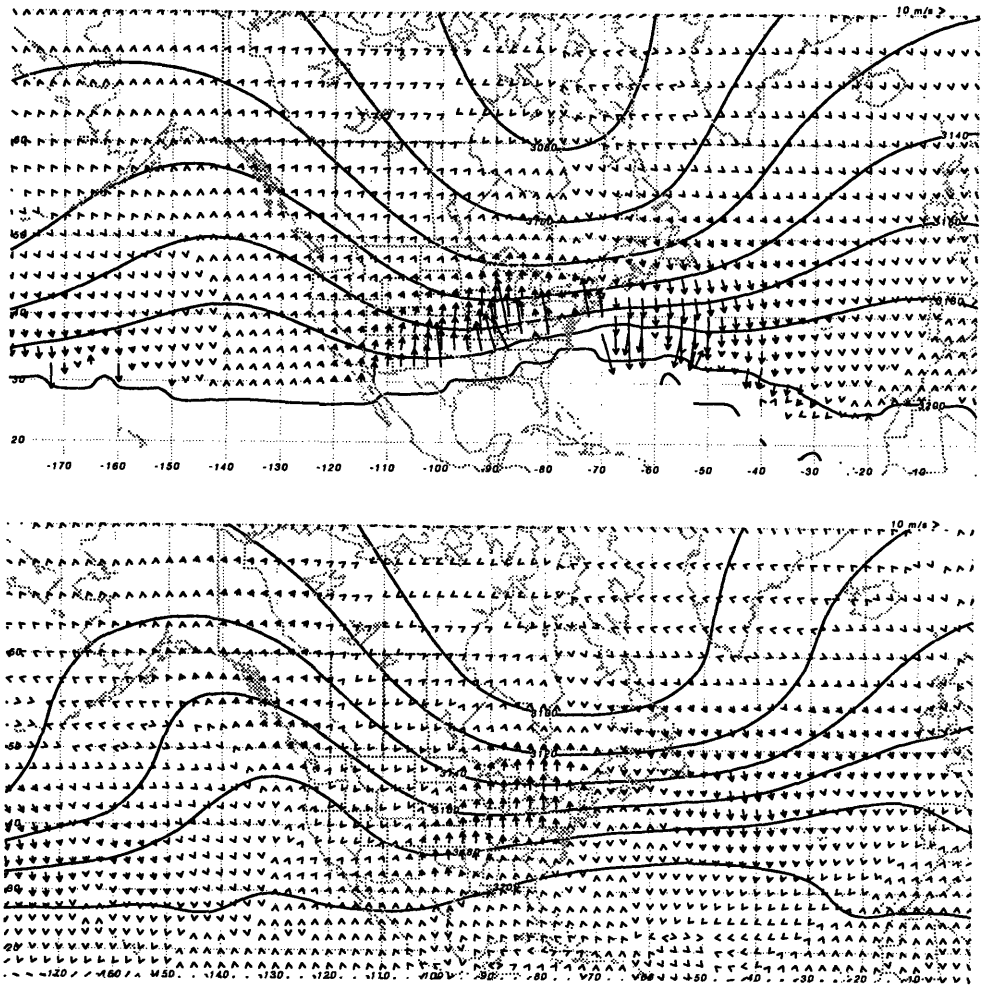

Figure 4.18: 320 K Montgomery potential (as in Figure 4.17) and nonadvective flux of potential vorticity (for scale of vector, see upper right of figure, scale 10^{-5} m^{-2} s^{-1}) for (a) basic state and (b) time mean flow.

Chapter 5

Refractive Index

A complete description of the wave propagation characteristics of the atmosphere is necessary, as wave motions constitute an important means of "communication" between remote locations within the atmosphere. The concept of wave motions forced in one region influencing the atmospheric flow in another has long been a topic of interest in synoptic and dynamic meteorology. Vertical wave propagation from stationary sources has been used to explain the structure of the observed upper tropospheric and stratospheric large scale wave structure (*e.g.* Charney and Drazin, Matsuno, 1970). Attempts at linking the dynamics of the tropical atmosphere with middle latitude responses have focused on the lateral propagation of Rossby waves from a source in the tropics into higher latitudes. The ability of waves to propagate from one region to another depends on the structure of the medium through which the waves propagate. The present chapter begins with a brief review of the theory of the propagation of waves in a nonhomogeneous medium. One diagnostic quantity that may be used to study the wave propagation in such a medium is the refractive index. A refractive index in isentropic coordinates is derived and then applied to describe the basic state determined in Chapter 4.

5.1 Theory and interpretation

5.1.1 *Wave propagation in an nonhomogeneous medium*

That the propagation of waves will be affected by nonhomogeneities of the medium through which the waves pass has been understood for some time. Analytical analyses of the propagation characteristics of waves in inhomogeneous medium rely on the assumption that the properties of the medium vary slowly over the length scale of the waves. This

assumption will be rather loosely termed the "WKB" assumption in the discussion to follow.

A rather general analysis of the effects of variations in a medium's character on the propagation of waves has been provided by Lighthill (1987) based upon the earlier work of Whitham (1960). Lighthill considers a wave packet described by

$$\psi = \Psi(x_1, x_2, x_3, t)\, exp\,(i\phi(x_1, x_2, x_3, t))$$

where Ψ is the streamfunction amplitude, and ϕ is the phase of the wave. The phase satisfies

$$\frac{\partial \phi}{\partial x_i} = k_i, \quad \frac{\partial \phi}{\partial t} = -\omega \tag{5.1}$$

where ω, the wave frequency (a function of position), is related to the wavenumber vector $\mathbf{k} = (k_1, k_2, k_3)$, through the dispersion relation

$$\omega = \omega(k_1, k_2, k_3, x_1, x_2, x_3) \quad .$$

The group velocity of these waves is given by

$$c_{g_i}(k_1, k_2, k_3, x_1, x_2, x_3) = \frac{\partial \omega}{\partial k_i}. \tag{5.2}$$

Taking a spatial derivative $\frac{\partial}{\partial x_i}$ of the second relation in (5.1) yields

$$\frac{\partial}{\partial x_i}\left(\frac{\partial \phi}{\partial t}\right) = -\frac{\partial \omega}{\partial k_j} \cdot \frac{\partial k_j}{\partial x_i} - \frac{\partial \omega}{\partial x_i} \quad \text{or,} \tag{5.3}$$

$$\frac{\partial k_i}{\partial t} + c_{g_j} \frac{\partial k_i}{\partial x_j} = -\frac{\partial \omega}{\partial x_i}. \tag{5.4}$$

The left side of (5.4) is the time rate of change of the wavenumber component k_i moving with the group velocity of the wave packet; that is

$$\frac{dk_i}{dt} = -\frac{\partial \omega}{\partial x_i}. \tag{5.5}$$

The above system of equations, (5.6) and (5.3) describe the *refraction* of the wave packet (the rate of change of wavenumber along a ray path (defined as the local direction of the group velocity vector of the wave packet under consideration)). Given a description of the basic state, the initial values for the position and composition (wave vector) of the wave packet, the system may be integrated forward to study the evolution of the wave packet.

Using relationships (5.3) and (5.6), one may further show that

$$\frac{d\omega}{dt} = 0 . \tag{5.6}$$

(5.6) indicates that ω is constant along a ray path. If the basic flow is homogeneous in a direction, x_i, the wavenumber component in that direction, k_i, is also constant.

5.1.2 *The concept of a refractive index*

In a study of the vertical propagation of tropospheric disturbances into the stratosphere, Matsuno (1970) introduced the notion of a refractive index for the propagation of planetary waves. Recognizing that the conservation of PPV equation linearized about a zonal flow $U = U(y,z)$ could be written in the canonical form of a wave equation

$$\Psi_{yy} + \frac{f_0^2}{N_0^2}\Psi_{zz} + \left(\frac{\beta}{U-c} - k^2\right) = 0 ,$$

Matsuno identified the term in parentheses, as being the equivalent of a refractive index squared for the lateral and vertical propagation. In numerical solutions of the linearized wave propagation equation, Matsuno observed that minima in the distribution of this refractive index acted as a barrier to wave propagation.

Karoly and Hoskins (1982) (hereafter KH) relate the concepts of ray tracing to the index of refraction for vertical planetary wave propagation. Using the ray equations, (5.2) and (5.5), KH demonstrate, for WKB conditions, that waves are refracted towards gradients in the total wave number, $\mathbf{K}_\omega$. KH show that regions of local maxima of $\mathbf{K}_\omega$ focus the paths of rays and act as a wave guide and demonstrate the importance of the curvature of the flow in determining the structure of the refractive index. KH further suggest that, at least for their study, the applicability of WKB techniques in realistic basic states may still be valid.

The form of the quasi-geostrophic refractive index, n^2_{QG}, is approximately,

$$n^2_{QG} = \frac{\beta_{eff}}{U - c}$$

where β_{eff} is the effective PPV gradient - including horizontal and vertical shears of the basic wind, suggests that the refractive index may be maximized near jets where the contribution to the horizontal shears to the PPV gradient can be large due to the large curvature in the jet profile in the vicinity of the jets. The index wouldn't necessarily be large at the jet axis as the wind contributes inversely to the refractive index. As noted in Chapter 2, jets may act as wave guides for waves with sufficiently small zonal wavelengths. Branstator (1983) demonstrates that wave energy emanating from wave sources placed within or near regions of the atmosphere in which the refractive index is maximized about a jet, may be ducted. The proximity of a critical line near the wave guide may also lead to over-reflection of waves within the guide.

5.2 Derivation of a refractive index

In this section, a refractive index is derived for the study of waves propagating along a zonal flow in thermal wind balance with a basic state meridional temperature distribution. The quasi-geostrophic assumption that the static stability be only a function of height does not apply to flows such as the one shown in Figure (2.3). Rather than utilizing the quasi-geostrophic refractive index to study the derived basic state, higher order balance relations (which make no assumptions on the lateral variation of stability, or the relative sizes of relative vorticity to the Coriolis parameter) are used to derive an index of refraction. The index is derived making use of the geostrophic momentum approximation in pseudo-height coordinates (Hoskins and Bretherton 1972) as well as in isentropic coordinates.

5.2.1 *Semi-geostrophic refractive index*

The derivation begins with the definition of potential vorticity within the semi-geostrophic equations for a Boussinesq fluid (Hoskins, 1972). The form of the PV in this system, the *geostrophic potential vorticity* (GPV), is simply the potential vorticity evaluated using the geostrophic wind, Q_g. Q_g satisfies,

$$\frac{1}{f_0^2}\nabla_X^2\Phi + \frac{f_0\theta_0}{gQ_g}\Phi_{ZZ} = 1, \tag{5.7}$$

where Φ is the geopotential height in geostrophic coordinates, all capital letter express the fact the horizontal derivative are taken along a surface of constant height in geostrophic coordinates.

For convenience, redefine Q_g

$$Q_0 = \frac{gQ_g}{f_0\theta_0} \Rightarrow \frac{1}{f_0^2}\nabla^2\Phi + \frac{1}{Q_0}\Phi_{ZZ} = 1.$$

Separate the flow into basic state and perturbations

$$\Phi = \overline{\Phi} + \Phi' = \overline{\Phi}(Y,Z) + \Phi'(X,Y,Z,T), \text{ and} \tag{5.8}$$

$$Q_0 = \overline{Q}_0(Y,Z) + Q'(X,Y,Z,T). \tag{5.9}$$

The overbar terms satisfy

$$\frac{\overline{Q_0}\nabla^2\overline{\Phi}}{f_0^2} + \overline{\Phi}_{ZZ} = \overline{Q_0}, \tag{5.10}$$

so that

$$Q' = \frac{\overline{Q_0}}{\overline{\Phi}_{ZZ}}\left(\frac{\overline{Q_0}\nabla^2\Phi'}{f_0^2} + \Phi'_{ZZ}\right). \tag{5.11}$$

At this point we derive the dispersion relationship for the Rossby waves. The linearized conservation equation for GPV about a zonal flow is

$$\left(\frac{\partial}{\partial T} + \overline{U}\frac{\partial}{\partial X}\right)Q' + v'\frac{\partial\overline{Q}_0}{\partial Y} + w'\frac{\partial}{\partial Z}\overline{Q_0} = 0. \tag{5.12}$$

Assuming that the perturbations are geostrophic,

$$v' = \frac{1}{f_0}\frac{\partial\Phi'}{\partial X}. \tag{5.13}$$

An expression is needed to relate w' to the geopotential perturbation. That expression is the thermodynamic equation which may be solved for w' to get

$$w' = -\frac{1}{\frac{g}{\theta_0}\overline{\theta}_Z}\left(\left(\frac{\partial}{\partial T} + \overline{U}\frac{\partial}{\partial X}\right)\Phi'_Z + \frac{g}{\theta_0 f_0}\overline{\theta}_Y\frac{\partial\Phi'}{\partial X}\right). \tag{5.14}$$

Substituting (5.13), (5.15), and (5.16) into (5.14), regrouping terms and noting that

$$\frac{g}{\theta_0}\overline{\theta}_Z = \Phi_{ZZ}, \tag{5.15}$$

gives

$$\left(\frac{\partial}{\partial T}+\bar{U}\frac{\partial}{\partial X}\right)\left(\frac{\overline{Q_0}}{\frac{g}{\theta_0}\bar{\theta}_Z}\left(\frac{Q_0\nabla^2\Phi'}{f_0^2}+\Phi'_{ZZ}\right)-\frac{\frac{\partial}{\partial Z}\overline{Q_0}}{\frac{g}{\theta_0}\bar{\theta}_Z}\Phi'_Z\right)=-\frac{1}{f_0}\frac{\partial\Phi'}{\partial X}\left(\overline{Q_{0Y}}-\frac{\bar{\theta}_Y}{\bar{\theta}_Z}\overline{Q_{0Z}}\right). \quad (5.16)$$

Hoskins (1976) recognizes the term in parenthesis on the right hand side of (5.18) as just the meridional gradient of GPV along an isentropic surface

$$\overline{Q_{0Y}}-\frac{\bar{\theta}_Y}{\bar{\theta}_Z}\overline{Q_{0Z}}=\left(\frac{d}{dY}\overline{Q_0}\right)_{\theta=const}.$$

Hence,

$$\left(\frac{\partial}{\partial T}+\bar{U}\frac{\partial}{\partial X}\right)\left(\left(\frac{\nabla^2\Phi'}{f_0^2}+\Phi'_{ZZ}\right)-\frac{\frac{\partial Q_0}{\partial Z}}{\overline{Q_0}^2}\Phi'_Z\right)=-\frac{\frac{g}{\theta_0}\bar{\theta}_Z}{Q_0 f_0}\frac{\partial\Phi'}{\partial X}\left(\frac{d}{dY}\overline{Q_0}\right)_{\theta=const}. \quad (5.17)$$

Simplifying gives

$$\left(\frac{\partial}{\partial T}+\bar{U}\frac{\partial}{\partial X}\right)\left(\nabla^2\Phi'+f_0^2\left(\frac{\Phi'_Z}{\overline{Q_0}}\right)_Z\right)=-\frac{f_0\frac{g}{\theta_0}\bar{\theta}_Z}{\overline{Q_0}^2}\frac{\partial\Phi'}{\partial X}\left(\frac{d}{dY}\overline{Q_0}\right)_{\theta=const}. \quad (5.18)$$

Rewriting the above expression in terms of Q_g, and identifying the term on the right hand side multiplying the meridional velocity, as an "effective β", β_{eff}, obtain

$$\beta_{eff}=\frac{f_0^2}{\zeta_g\overline{Q}_g}\left(\frac{d\overline{Q}_g}{dY}\right)_{\theta=const}. \quad (5.19)$$

The above result indicates that, unlike in the QG system, the important gradients of PV are those along isentropic surfaces, and that the gradient is not of GPV itself, but rather the GPV gradient weighted by its reciprocal.

5.2.2 *A refractive index in isentropic coordinates*

Given that β_{eff} may be expressed in terms of a gradient of GPV on an isentropic surface, it would seem natural to re-express the refractive index in isentropic coordinates. To

that end, the derivation for this form starts from the a development of a set of equations attributed to Eliassen (1983).

Eliassen considers an adiabatic, inviscid, zonal flow on a β plane. Let $\Pi = \Pi(p)$, be the Exner function, then the equations for the geostrophic and hydrostatic relations in isentropic coordinates for the flow are

$$\frac{\partial M}{\partial y} = -fU \text{ and } \frac{\partial M}{\partial \theta} = \Pi(p) .$$

The basic state density, ρ, is

$$\rho(y,\theta) = (\theta \frac{d\Pi}{dP})^{-1} = (\theta\Gamma)^{-1} . \tag{5.20}$$

The equations of motion linearized about such a basic state flow are

$$D_t u' - \zeta_{a\theta} v' + M'_x = 0 \tag{5.21}$$

$$D_t v' + fu' + M'_y = 0 \tag{5.22}$$

where

$$D_t = \frac{\partial}{\partial t} + U\frac{\partial}{\partial x}$$

The equation of continuity in isentropic coordinates is

$$\frac{d}{dt}(ln(\frac{\partial p}{\partial \theta})) + \nabla \cdot \boldsymbol{u} = 0$$

Linearized about the basic flow, this equation becomes

$$D_t(p'_\theta) + p_\theta u'_x + (v' p_\theta)_y = 0 \tag{5.23}$$

where

$$p' = \rho_0 \theta M'_\theta$$

If the geostrophic momentum approximation (Hoskins, 1975) is made (wherein the advected momentum is replaced with the geostrophic momentum). (5.22) and (5.23) become

$$D_t u'_g - \zeta_{a\theta} v' + M'_x = 0 \tag{5.24}$$

$$D_t v'_g + f u' + M'_y = 0 \tag{5.25}$$

(5.25) and (5.26) may then combined into a single expression for the conservation of the inverse of potential vorticity (Eliassen).

$$D_t \mu(m') = \left(\frac{1}{Q}\right)_y \frac{M'_x}{f} \tag{5.26}$$

where the operator μ is given by

$$\mu(m') = \frac{1}{f}\left(\frac{\zeta_{a\theta}}{f}\frac{M'_{xx}}{fQ_g} + \left(\frac{M'_y}{fQ_g}\right)_y + \left(\frac{M'_\theta}{g\Gamma}\right)_\theta\right), \tag{5.27}$$

and Q_g is the potential vorticity, $Q_g = g\zeta_{a\theta}/\sigma$.

Assuming a sinusoidal perturbation of the form

$$M' = M'(y,\theta)\exp(i(kx + ly + m\theta - \omega t)), \tag{5.28}$$

substituting (5.28) into (5.27), and making the WKB assumption that the variations in the basic state are much slower than that of the perturbation, yields the following dispersion relation

$$\omega(y,\theta) \cong Uk - \frac{\frac{f^2}{\zeta_{a\theta}Q_g}\frac{\partial Q_g}{\partial y}k}{k^2 + \frac{f}{\zeta_{a\theta}}l^2 + \frac{f^2}{g\sigma\Gamma}m^2}. \tag{5.29}$$

Here, the effective β is very similar to that derived within the semigeostrophic framework. Now a refractive index, n^2 is derived

$$n^2 = k^2 + \frac{f}{Z}l^2 + \frac{f^2}{g\sigma\Gamma}m^2 = \frac{\frac{f^2}{\zeta_{a\theta}Q}\frac{\partial Q}{\partial y}}{U-c} = \frac{f^2\frac{\partial}{\partial y}lnQ}{\zeta_{a\theta}(U-c)}. \tag{5.30}$$

The expression for the total wave number (or refractive index) may be written in a more compact form. The key step in rewriting this expression relies on Schär's generalization of the Bernoulli Theorem. Recall that for steady flow, the Bernoulli energy is the streamfunction for the total flux of vorticity in an isentropic layer. For a zonal flow, this expression is

$$-\frac{\partial B}{\partial y} = U\zeta_{a\theta} \tag{5.31}$$

If one were to perform a Galilean transformation to a frame of reference moving with the wave at a phase speed **c**, then above relation may be written as

$$-\frac{\partial B_c}{\partial y} = (U-c)\zeta_{a\theta} \tag{5.32}$$

where B_c satisfies.

$$\nabla^2 B_c = \nabla\cdot((U-c)\zeta_{a\theta}) \tag{5.33}$$

Substituting (5.34) into (5.32) results in

$$n^2 = -f^2\frac{\partial}{\partial B_c}lnQ_g \tag{5.34}$$

The elegance of this expression is that it relates the refractive index to two conserved quantities for steady, inviscid, adiabatic flows. Additional calculation is involved, in order to evaluate (5.33) for different phase speeds, c. (5.34) may be applied to conventional analyses by making use of the following approximation

$$n^2 \cong -f^2\frac{\nabla lnQ_g\cdot\nabla B_c}{\nabla lnB_c\cdot\nabla B_c} \tag{5.35}$$

5.3 Evaluation and interpretation of basic state refractive index

The refractive index is evaluated for phase speeds c = 0 ms^{-1} and c = 10 ms^{-1}. The results are presented on the 305K surface for the basic state flow. The expression (5.30) is approximated by

$$n^2 \cong f^2 \frac{\nabla lnQ_g \cdot \nabla M}{\zeta_{a\theta}(U-c)|\nabla M|} = f^2 \frac{\nabla lnQ_g \cdot \boldsymbol{n}}{\zeta_{a\theta}(U-c)} \tag{5.36}$$

where the vector $\boldsymbol{n}$, is locally normal to the isopleths of the Montgomery potential.

To demonstrate the utility of the approximation (5.35), we compare a calculation of the refractive index for ($c = 0$) using both (5.35) and (5.36). Figure 5.1 shows the calculation using (5.35) while Figure 5.2 show the corresponding calculation using 5.36). Following Thorncroft et al. (1993). the quantity plotted is

$$K_c = an \tag{5.37}$$

where a is the radius of the earth. The advantage of plotting K allows one to apply the charts for more than one value of k (the zonal wavenumber).

The similarities of Figure 5.1 and Figure 5.2 provides a partial verification of the expression (5.35). The figures show a band of maximum nondimensional wave number (refractive index) for waves of phase speed $c = 0$ ms^{-1}, located just to the north of the sub-tropical jet of the basic state. The largest maxima in K are located in regions characterized by ridges in the Montgomery potential. The large scale minima in this quantity correspond to the cyclonic gyres in the M distribution.

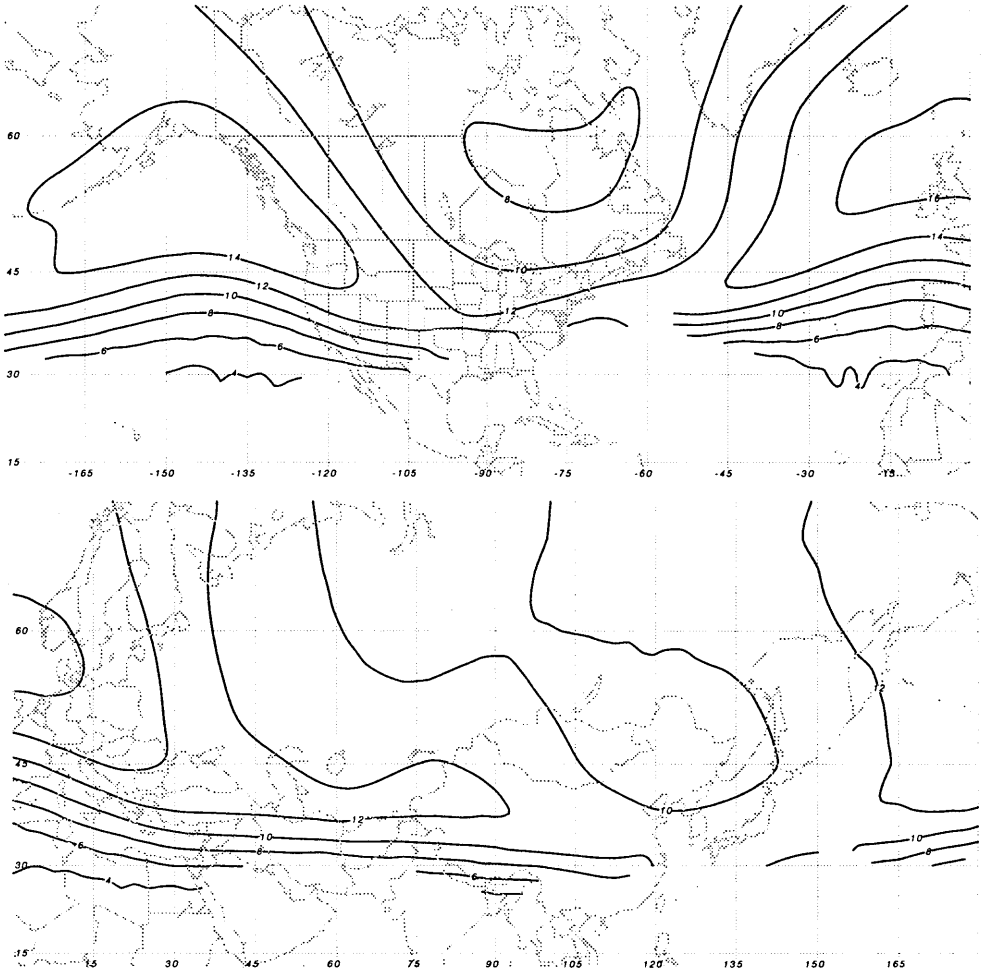

Figure 5.1: Nondimensional wave number, K=an), see text. Contour interval 2. (top) western hemisphere, (bottom) eastern hemisphere.Evaluated using (5.35)

The distribution of $K_{c=0}$ suggests that stationary waves generated in regions where $K_{c=0}$ is a maximum (over the eastern Atlantic and over Central and eastern Pacific) may be trapped. The response to the forcing over northern Canada and northern Russia might tend to propagate away from the regions of forcing.

Figure 5.3 shows the total wave number for c = 10 ms^{-1}. The refractive index for this value of c is a maximum over the major oceans, and Hudson's Bay. There is also a local maximum just north of the subtropical jet, that extends from the Pacific northwest of the United States southeastward to the southeast United States coast. Over Asia, there is a

Figure 5.2: As in 5.1, except calculated from expression (5.36)

local minimum in the refractive index over middle latitudes. The maximum values to the north and south of this region are associated with critical lines of the waves.

Over North America, The distribution $K_{c=10}$ suggests that mobile troughs of phase speed c = 10 ms^{-1}, would be tend to be trapped meridionally through the waveguide-like region extending over the United States.

Over Asia, the interpretation of these plots is complicated by the existence of critical lines on either side of channel of minimum values in K.

Due to the rather complex structure of K for non-zero phase speeds, a more complete set of diagnostic calculations, such as ray tracing or wave activity diagnostics (Plumb,

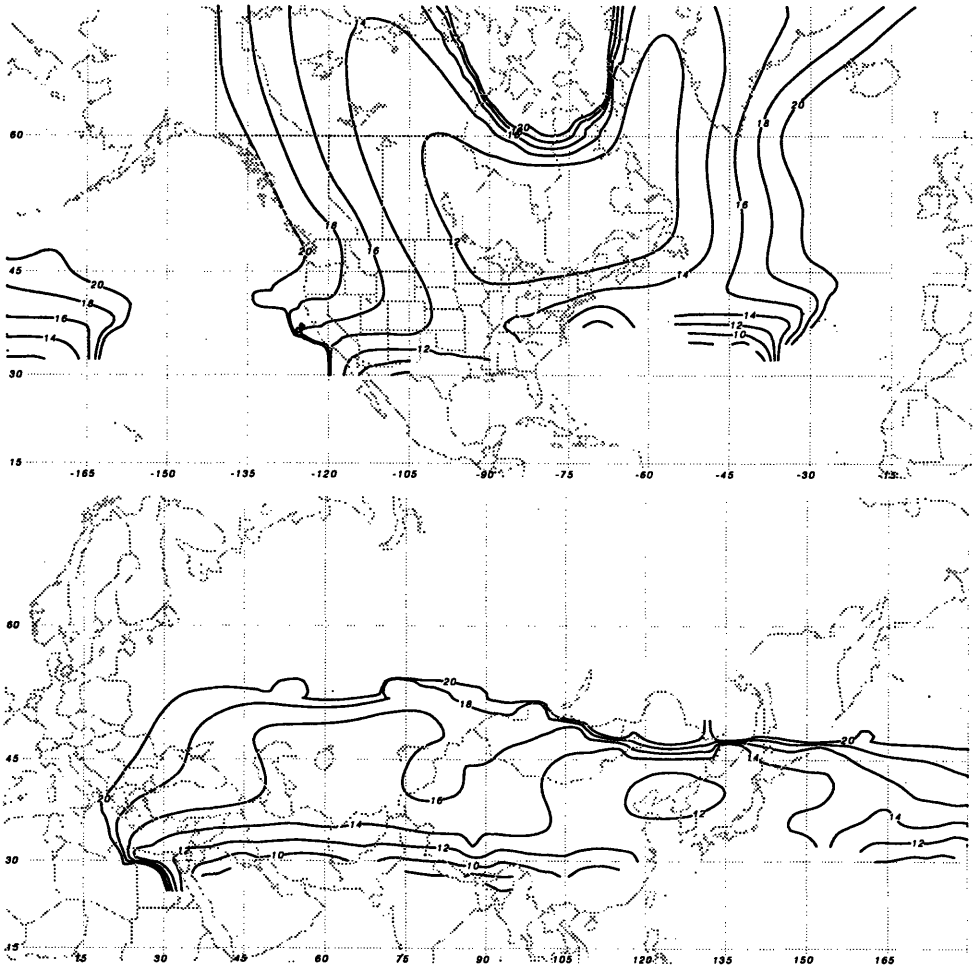

Figure 5.3: 305K nondimensional total wavenumber for c=10, contour interval 2

1986) should be performed to quantitatively understand the characteristics of waves in this basic state.

Chapter 6

Conclusions and Summary

6.1 Summary of principal results

The primary goal of this thesis was the development of a set of diagnostic tools to be used to further the current understanding of the dynamics of synoptic scale systems in middle latitudes. The tools that have been developed are a new definition of a basic state - based on observations of the instantaneous flow, and constrained by dynamical principles, and a new expression for the refractive index of waves that may be used to characterize the propagation of waves.

Basic states are the fundamental tools used to understand various phenomena including wave propagation, the instability of flows, and the initial value development of perturbations. The traditional definitions of basic states, which have relied on the space or time averages of a flow, have been shown to be inappropriate given the highly nonhomogeneous distribution of potential vorticity in the atmosphere. Furthermore, simple time mean flows may not in fact be steady - if the period over which the averaging takes place is not sufficiently long enough to remove transient features. The presence of non-steady components of the flow may allow for interactions between the components. The interaction of these nonsteady components of the time mean flow with the phenomena being studied may obscure the results.

The key observations used to determine the basic state are that potential vorticity is nearly uniform in the troposphere and lower stratosphere away from the polar and subtropical jet streams and that analyses of Ertel potential vorticity and Montgomery potential show a tendency for the isopleths of Q to be aligned with the isopleths of M in regions in

which the flow is strong. Geostrophic scatter diagrams of Q and M constructed for individual isentropic surfaces suggest that a functional relationship between Q and M (i.e. $Q = Q(M;\theta)$) may be defined for each isentropic surface. Within the limitations of the data, scatter diagrams of M and θ at 1000 hPa suggests that there is a tendency for the geostrophic wind at the surface (in the time mean) to be along isentropes.

The technique used to determine the steady, balanced basic state essentially involves inverting the potential vorticity field subject to a geostrophic balance condition, constraining the solution to obey $Q = Q(M)$, and satisfying certain boundary conditions (including the constraint on M and θ) at the lower boundary. The resulting nonlinear problem is solved iteratively.

The basic state that is found should be regarded as the balanced mass and wind fields of a steady flow in which synoptic scale waves and other transient features have been removed while certain dynamically important features of the observed potential vorticity distribution have been retained. That the flow in any way resembles a time mean field, while being more than coincidental, is unimportant. The basic state is that state characteristic of the one in which synoptic scale waves propagate.

The technique is demonstrated by solving for a basic state flow for January 1991. The basic state that is determined is, by construction, characterized by an equivalent barotropic structure with ridges over the oceans and troughs over the continents. Surface winds are light. These features appear to be related to what is known as a "thermally equilibrated" response. (Marshall and So, 1990).

If the thermal forcing, H, in the atmosphere is of a Newtonian form, $H = \gamma(T - T^*)$ (where γ represents a thermal relaxation time scale and T^* is a three-dimensional equilibrium temperature distribution), and the spectrum of T^* projects onto free stationary Rossby-Haurwitz waves, then the possibility exists that the thermal pattern, T^*, might

"lock on" to a free Rossby wave solution, and result in the thermal forcing being "turned off." The resulting flow regime is characterized by zero surface winds and an equivalent barotropic response. Marshall and So suggest that thermal equilibration is a mechanism by which the atmosphere may approach a free-mode state.

In addition to determining this basic state flow, a new expression for the refractive index is derived in isentropic coordinates making use of the geostrophic momentum approximation. The refractive index is expressed as the gradient of the natural logarithm of the potential vorticity with respect to the Bernoulli function. The attractiveness of this form of the refractive index is that it relates two ***conserved*** properties of steady, inviscid adiabatic flow to a quantity that is significant in terms of characterizing wave propagation.

6.2 Limitations

There are limitations with this work. Perhaps one of the most significant limitations is the fact that the data set is hydrostatically inconsistent at the lower boundary (1000 hPa). One would anticipate that the greatest discrepancies between the extrapolated height and temperature fields would be observed over mountains. This may change the results mentioned in the preceding paragraphs. There is some hope; however, that since time means fields were used to determine the $M = M(\theta)$ relationship, in the time mean, one might expect that the atmosphere profiles of temperature might approximate a standard atmosphere, and the hydrostatic inconsistency between the geopotential and temperature fields may have been reduced. In any case, more study must be done to determine what effect (if any) the NMC extrapolation of heights and temperatures may have on the results.

While geostrophic balance is, for the most part, applicable to middle latitude, synoptic scale systems, in the subtropics and in particular the tropics, it is not the best balance con-

dition to be used. In Chapter 4, the nonlinear balance condition of Charney (1948) was developed in isentropic coordinates. A similar technique could be envisioned to solve that system of equations.

One of the central objectives of this work was to determine a realistic basic state for the study of the dynamics of synoptic scale waves. It was noted that the movement of the principal tropospheric jets (in particular the polar jet) prevents time averages of quantities such as potential vorticity to be smeared out. A comparison of the basic state flow with instantaneous flows reveals that the magnitudes of the basic state flow PV gradients are not nearly as concentrated as the instantaneous gradients. This difference may be attributed to the method used to determine the Q-M relation. The technique involved determining a mean value of Q along contours of M. The assumption made was that there exists a distinct functional relationship between Q *and* M. However, as was noted earlier, the relationship between Q and M is determined, in part, by the synoptic scale eddies. Depending upon the amplitude of these synoptic scale waves, the Q-M relationship may in fact be steeper that the one determined from the technique of averaging along the contour. A steeper Q-M relationship will lead to sharper jets and more concentrated PV gradients.

An alternative way to determine a global Q-M relationship for each isentropic surface, would be to determine a Montgomery potential using the data from the composited cross section (Figure 2.4), and then for each isentropic level identify the corresponding Q for that M.

6.3 Extensions

Given the "realistic" basic state that has been determined, and a refractive index which characterizes wave propagation on this state, there are number of possible directions to be

taken. The most obvious are stability and wave propagation studies. Many studies of the stability of three-dimensional time mean or climatological flows have been undertaken (e.g. Frederiksen, 1983). Given that time mean flows are not the most appropriate to use as basic states for the study of the dynamics of waves, the use of a basic state determined using the technique motivated and outlined in this work, may reveal some interesting results concerning the stability of the observed flow.

While the technique used to determine a basic state yields a realistic flow pattern, an important but unanswered question is "*Is this solution unique?*" Given that there is a relationship between the uniqueness of flows and their stability, if the stability of the flow were assessed, on could then determine whether the solution described in Chapter 4 is unique.

In addition to stability studies, the basic state could be used to test the ideas of the initial value development of perturbations. It has been recognized that the deformation of eddies may lead to their transient development if the effect of the deformation is to make the eddies more isotropic, (Farrell, 1989). The initial growth of the perturbations is highly dependent on the initial structure of the eddy and the orientation of the eddy with respect to the basic flow. The largest regions of deformation tend to be found along the jets associated with shearing deformation, (Dole, 1993), and at the exit and entrance regions of the jets in the associated with stretching deformation. The most optimally configured perturbations for this basic state could be determined.

Appendix A Solution of system of (3.1)

The solution to the system in Section 3.1 is given by

$$C_1 = -q_1 Z - u_s$$

$$C_2 = Y_B q_1 y_s + \Psi_B - \frac{1}{2} q_1 Y_B^2 + Y_B u_s$$

$$C_3 = -q_2 y_s - u_s$$

$$C_4 = Y_T q_2 y_s + \Psi_T - \frac{1}{2} q_1 Y_T^2 + Y_T u_s$$

where Ψ_s satisfies,

$$(-\Delta q)\,\Psi_s^2 + 2\,(y_T q_2 - y_B q_1)\,\Psi_s - q_2 y_T^2 + q_1 y_B^2 + 2\,(\Psi_T - \Psi_B) + 2u_s\,(y_T - y_B) \;=\; 0$$

Appendix B *Q* - *M* relationships

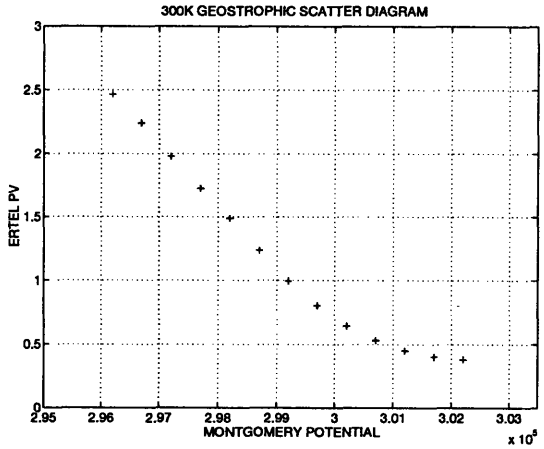

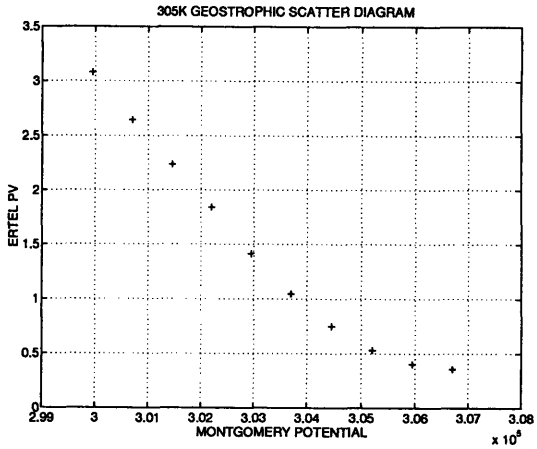

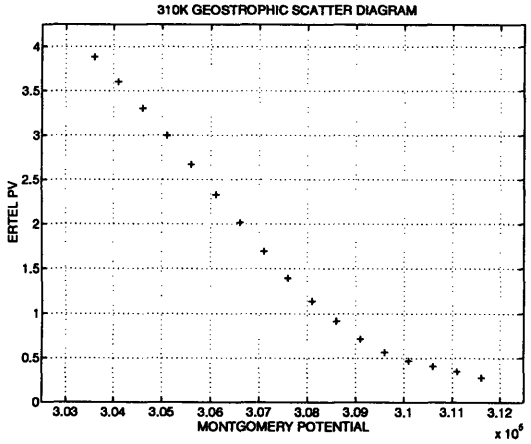

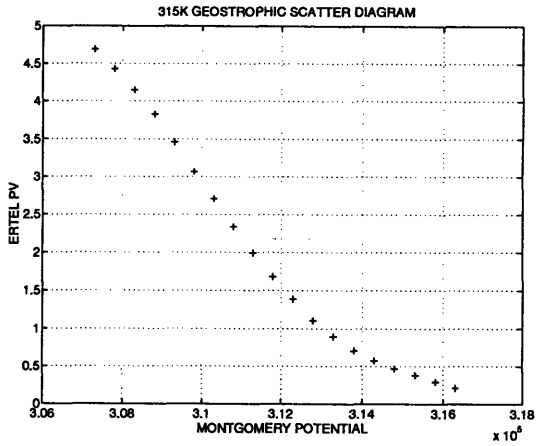

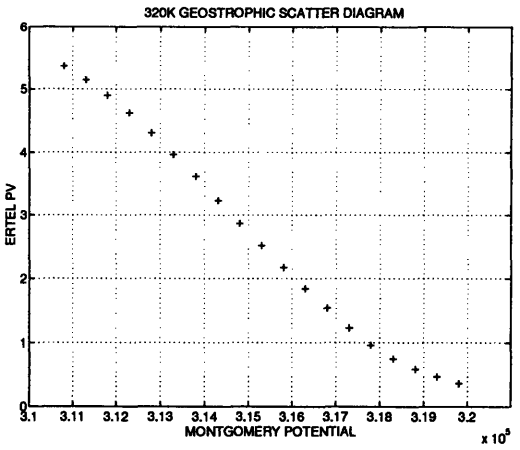

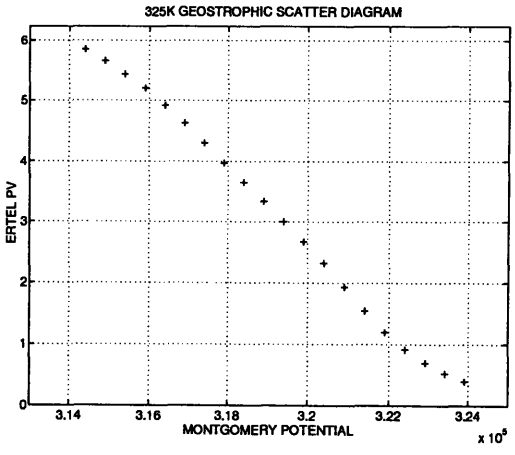

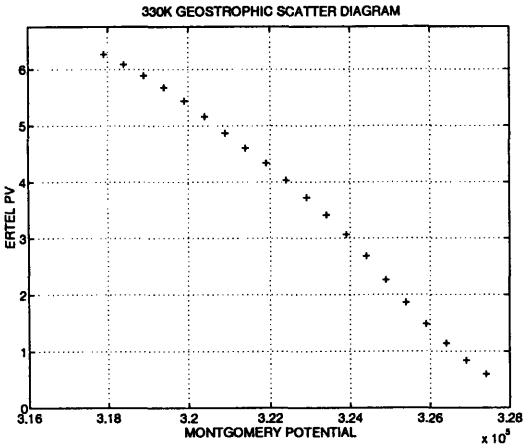
330K GEOSTROPHIC SCATTER DIAGRAM
ERTEL PV
MONTGOMERY POTENTIAL
x 10^5

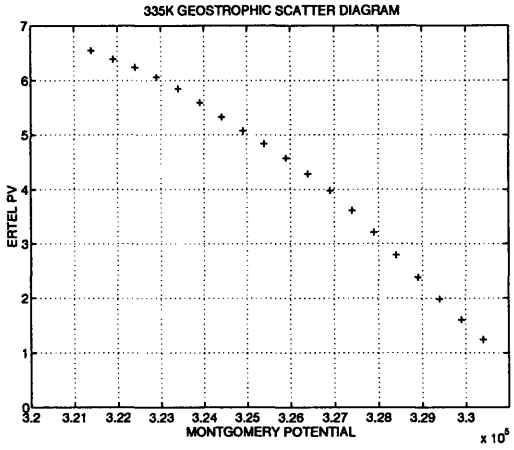
335K GEOSTROPHIC SCATTER DIAGRAM
ERTEL PV
MONTGOMERY POTENTIAL
x 10^5

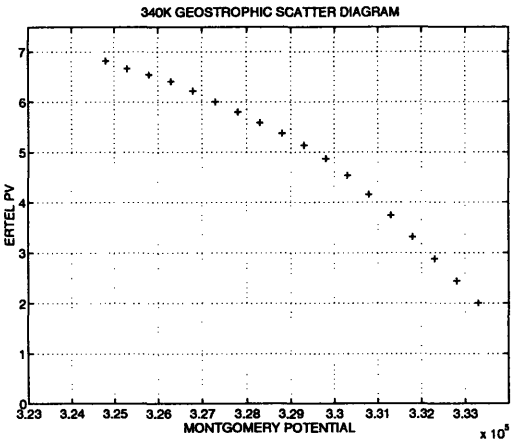
340K GEOSTROPHIC SCATTER DIAGRAM
ERTEL PV
MONTGOMERY POTENTIAL
x 10^5

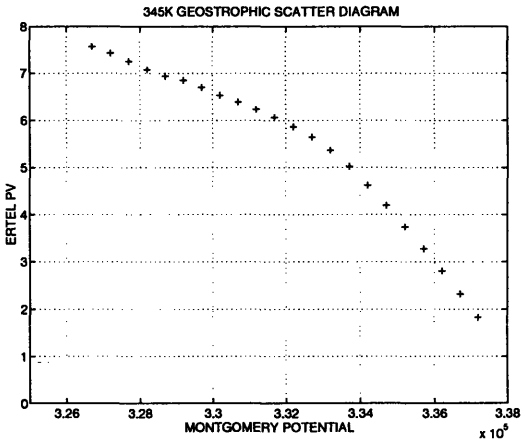
345K GEOSTROPHIC SCATTER DIAGRAM
ERTEL PV
MONTGOMERY POTENTIAL
x 10^5

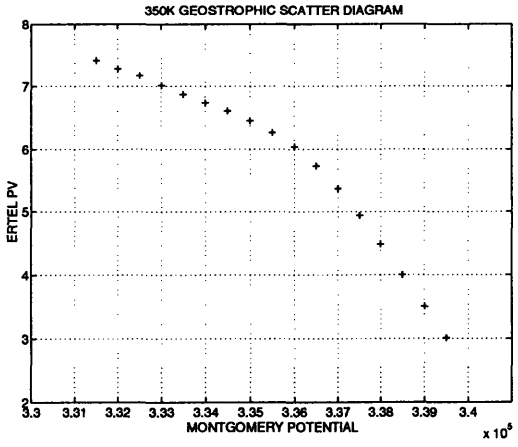
350K GEOSTROPHIC SCATTER DIAGRAM
ERTEL PV
MONTGOMERY POTENTIAL
x 10^5

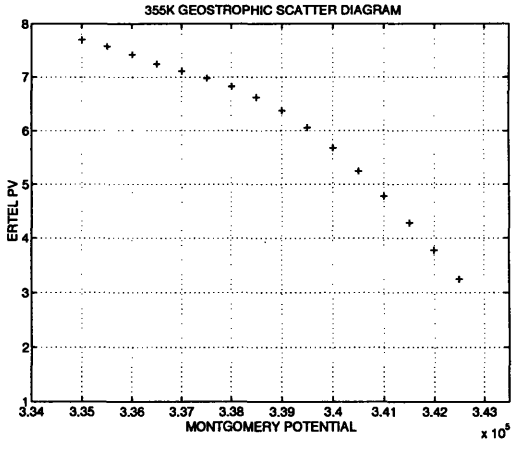
355K GEOSTROPHIC SCATTER DIAGRAM
ERTEL PV
MONTGOMERY POTENTIAL
x 10^5

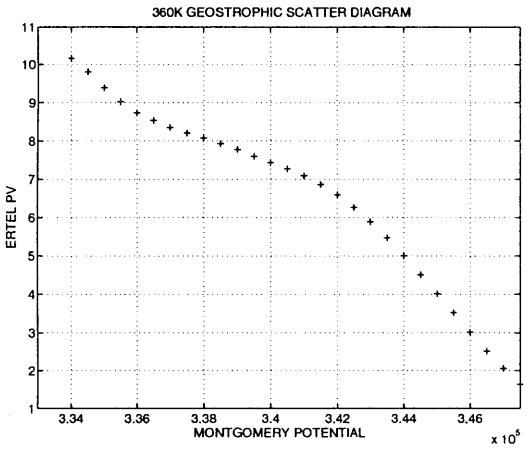
360K GEOSTROPHIC SCATTER DIAGRAM
ERTEL PV
MONTGOMERY POTENTIAL
x 10^5
11
10
9
8
7
6
5
4
3
2
1
3.34
3.36
3.38
3.4
3.42
3.44
3.46

Appendix C

Isentropic surface	q	M
315	.3	315774.204
320	.3	320160.534
325	.4	323814.307
330	.4	328148.823
335	.5	331676.402
340	.5	337966.981
345	.5	339239.826
350	1.25	341373.497
355	1.25	344650.254
360	1.25	347976.011

Table 3.1: Southern lateral boundary contours values

Appendix D Numerics

In this section the numerical technique used in obtaining a solution to the system

$$\frac{1}{f_0}\nabla^2 M - \left(\frac{p_0}{\kappa g c_p^{\frac{1}{\kappa}}}\right) Q_g \left(\frac{\partial M}{\partial \theta}\right)^{\frac{1}{(\gamma-1)}} M_{\theta\theta} = f \tag{D.1}$$

with

$$Q_g = Q_g(M)$$

and

$$\theta = \theta(M)$$

is outlined.

(C.1) is discretized using a centered difference:

$$\nabla^2 M \cong \frac{(M_{i+1,j,k} + M_{i-1,j,k} - 2M_{i,j,k})}{\delta x^2} + \frac{(M_{i,j+1,k} + M_{i,j-1,k} - 2M_{i,j,k})}{\delta y^2} \tag{D.2}$$

$$\left(\frac{\partial M}{\partial \theta}\right)^{\frac{1}{(\gamma-1)}} \cong \left(\frac{(M_{i,j,k+1} - M_{i,j,k-1})}{2\delta\theta}\right)^{2.5} \tag{D.3}$$

$$M_{\theta\theta} \cong \frac{(M_{i,j,k+1} + M_{i,j,k-1} - 2M_{i,j,k})}{\delta\theta^2} \tag{D.4}$$

where $\delta x = \delta s * \cos\phi$, $\delta y = \delta s$ (where $\delta s = 277.5$ km and ϕ is latitude), and $\delta\theta = 5$K. We define

$$\xi = f_0 \left(\frac{p_0}{\kappa g c_p^{\frac{1}{\kappa}}}\right) Q_{g_{i,j,k}}(M_{i,j,k}, \theta) \left(\frac{(M_{i,j,k+1} - M_{i,j,k-1})}{2\delta\theta}\right)^{2.5} \tag{D.5}$$

(C.1) may then be rewritten using (C.2) through (C.5)

$$Res_{i,j,k} = \left(\frac{\delta y}{\delta x}\right)^2 (M_{i+1,j,k} + M_{i-1,j,k} - 2M_{i,j,k}) +$$

$$(M_{i,j+1,k} + M_{i,j-1,k} - 2M_{i,j,k}) +$$

$$\xi \left(\frac{\delta y}{\delta \theta}\right)^2 (M_{i+1,j,k} + M_{i-1,j,k} - 2M_{i,j,k}) + f_0 f_j \delta y^2$$

where $Res_{i,j,k}$ is the residual (the difference between the discretized left and right hand sides of (C.1)) at the grid point *(i,j,k)*, and f_j is the value of the Coriolis parameter at grid latitude *j*.

The solution begins with an initial guess for $M_{i,j,k}$. This initial guess for M is used to determine a value of $Q_{i,j,k} = Q(M_{i,j,k})$. Given a local value of Q, the scheme proceeds to modify the value of $M_{i,j,k}$ in a method quite analogous to successive over-relaxation

$$M_{i,j,k}^{new} = M_{i,j,k}^{old} + \alpha \frac{Res_{i,j,k}^{old}}{\left(2 + 2\left(\frac{\delta y}{\delta x}\right)^2 + 2\xi\left(\frac{\delta y}{\delta \theta}\right)^2\right)} \qquad \text{(D.6)}$$

where the superscripts *new* and *old* indicate whether the new or old values of $M_{i,j,k}$ are to be used (Note here $\alpha > 1$).

References

Anderson, J. L., 1992: Barotropic stationary states and persistent anomalies in the atmosphere. *J. Atmos. Sci.*, **49**, 1709 - 1722.

Arnol'd, V. I., 1965: Conditions for nonlinear stability of stationary curvilinear flows of an ideal fluid. *Soviet Math.*, **6**, 773 - 776.

Blackmon, M., 1976: A climatological study of the 500 mb height of the Northern Hemisphere. *J. Atmos. Sci.*, **33**, 1607 - 1623.

Bretherton, F. P., 1966: Critical layer instability in baroclinic flows. *Quart. J. Royal Meteor. Soc.*, **92**, 325 -334.

Branstator, G., 1983: Horizontal energy propagation in a barotropic atmosphere with meridional and zonal structure. *J. Atmos. Sci.*, **40**, 1689 - 1708.

Butchart, N., K. Haines, and J. Marshall, 1989: A theoretical and diagnostic study of solitary waves and atmospheric blocking. *J. Atmos. Sci.*, **46**, 2063 - 2078.

Charney, J., 1947: The dynamics of long waves in a baroclinic westerly current. *J. of Meteor.* **4**, 135 - 163.

_____, 1955: The use of primitive equations of motion in numerical weather prediction. *Tellus*, **2**, 22 - 26.

_____, J. and P. Drazin, 1961: Propagation of planetary - scale disturbances. *J. Geophys. Res.*, **66**, 83 - 100.

_____, J. and M. Stern, 1962. on the stability of internal baroclinic jets in a rotating atmosphere. *J. Atmos. Sci.*, **19**, 159 - 172.

Danielsen E. and R.S Hipskind, 1980: Stratospheric - tropospheric exchange at polar latitudes in summer. *J. Geophys. Res.*, **85**, 393 - 400.

Davis, C., 1990: Cyclogenesis diagnosed with potential vorticity. Massachusetts Institute of Technology. Department of Earth, Atmospheric, and Planetary Sciences, Center for Meteorology and Physical Oceanography, Ph. D.

_____, and K. Emanuel, 1991: Potential vorticity diagnostics of cyclogenesis. *Mon. Wea. Rev.*, **119**, 1929 - 1952.

Dole, R. M., 1993: Deformation in planetary scale flows. In preprint volume of Ninth Conference on Atmospheric and Oceanic Waves and Stability, AMS, Boston, MA, 1 - 4.

Dowling, T. E., 1993: A relationship between potential vorticity and zonal wind on Jupiter. *J. Atmos. Sci.*, **50**, 14 - 22.

Eady, E., 1949: Long waves and cyclone waves. *Tellus*, **1**, 33 - 42.

Ek, N., and G. Swaters, 1994: Geostrophic scatter diagrams and the application of quasi-geostrophic free - mode theory to a northeast Pacific blocking episode. *J. Atmos. Sci.*, **51**, 563 - 581.

Emanuel, A. Thorpe, and M. Fantini, 1987: Baroclinic instability in an environment of small stability to slantwise moist convection. Part I: Two Dimensional Models. *J. Atmos. Sci.*, **44**, 1559 - 1573.

Eliassen, A, and E. Kleinschmidt, 1959: Dynamic Meteorology. 154 pp.

_____, A, 1983: The Charney-Stern theorem on barotropic-baroclinic instability. *Pure and Applied Geophysics*, 121, 563 - 572.

Farrell, B., 1989: Transient development in confluent and diffluent flow. *J. Atmos. Sci.*, **46** 3279 - 3288.

Frederiksen, J. S., 1983: Disturbances and eddy fluxes in Northern Hemisphere flows: instability of Three-dimensional january and July flows. *J. Atmos. Sci.*, **40**,836 - 855.

Haines, K., P. Malanotte - Rizzoli, and M. Morgan, 1993: Persistent jet stream intensifications: A comparison between theory and data., *J. Atmos. Sci.*, **50**, 146 - 154.

Hoskins, B. J., 1990: Theory of Extratropical Cyclones. In *Extratropical Cyclones: The Erik Palmén Volume*. editors C. Newton, and E. Holopainen., AMS, 63 - 80.

_____, B. J., 1991: Towards a PV-θ view of the general circulation. Tellus, **43A**, 27 - 35.

_____, B. J., M. E. McIntyre, and A. W. Robertson, 1985: On the use and significance of isentropic potential vorticity maps. *Quart. J. Royal Meteor. Soc.*, **111**, 897 - 946.

_____, B., I. James, and G. White, 1983: The shape propagation and mean - flow interaction of large - scale weather systems. *J. Atmos. Sci.*, **40**, 1595 -1612.

Illari, L. and J. Marshall, 1983: On the interpretation of eddy fluxes during a blocking episode. *J. Atmos. Sci.*, **40**, 2232 - 2242.

Ioannou, P., and R. S. Lindzen 1986: Baroclinic instability in the presence of barotropic jets. *J. Atmos. Sci.*, **43**, 2999 - 3014.

Karoly, D. J., and Hoskins, B. J., 1982: Three dimensional propagation of planetary waves. *J. Meteor. Soc. Japan*, **60**, 109 - 123.

Lighthill, J., 1987: *Waves in fluids*, Cambridge University Press. pp. 504.

_____, M. J., 1963: 'Boundary-layer theory', in *Laminar boundary layers* (L. Rosenhead, ed.) Oxford University Press.

Lindzen, R. S., 1993: Baroclinic neutrality and the tropopause, *J. Atmos. Sci.*, **50**, 1148 - 1151.

_____, 1994: Classic problems in dynamics revisited. In the *Proceedings of the International Symposium on the Lifecycles of Extratropical Cyclones.* Bergen, Norway. Vol. 1, 90 - 98.

Marshall, J., and D. So, 1990: Thermal equilibration of planetary waves. *J. Atmos. Sci.*, **47**, 964 - 978.

McIntyre, M.E., and T. G. Shepherd, 1987: An exact local conservation theorem for finite-amplitude disturbances to non-parallel shear slows, with remarks on Hamiltonian structure and on Arnol'd's stability theorems. *J. Fluid. Mech.*, **126**, 527 - 565.

Neilley, P., 1990: Interactions between synoptic - scale eddies and the large - scale flow during the life cycles of persistent flow anomalies. Massachusetts Institute of Technology. Department of Earth, Atmospheric, and Planetary Sciences, Center for Meteorology and Physical Oceanography, Ph. D.

Palmén, E., 1948: On the distribution of temperature and wind in the upper westerlies. *J. of Meteor.*, **5**, 20 - 27.

_____, E. and C. Newton. 1969: *Atmospheric Circulation Systems: Their Structure and Interpretation.* Academic Press, pp. 603.

Pedlosky, J., 1987: *Geophysical Fluid Dynamics*, Springer - Verlag, 2nd ed., pp. 710.

Petterssen, S., 1956: *Weather Analysis and Forecasting.* McGraw - Hill Book Company, Inc. Vol. I, pp. 428.

Platzman, G. W., 1949: The motion of barotropic disturbances in the upper troposphere. *Tellus*, **1**, 53 - 64.

Plumb, R. A., 1986: Three-dimensional propagation of transient quasi-geostrophic eddies and its relationship with eddy forcing of the time mean flow. *J. Atmos. Sci.*, **43**, 1657 - 1678.

Read, P. L., P. B. Rhines, and A. White, 1986: Geostrophic scatter diagrams and potential vorticity dynamics. *J. Atmos. Sci.*, **43**, 3226 - 3240.

Rhines, P. and W. Young, 1982: Homogenization of potential vorticity in planetary gyres. *J. Fluid Mech.*, **122**, 347 - 367.

Rivest, C., 1990: Upper - level waves of synoptic scale. Massachusetts Institute of Technology. Department of Earth, Atmospheric, and Planetary Sciences, Center for Meteorology and Physical Oceanography, Ph. D.

Sanders, F. and J. R. Gyakum, 1980: The synoptic - dynamic climatology of the "bomb." *Mon. Wea. Rev.*, **108**, 1589 - 1606.

Schär, C., 1993: A generalization of Bernoulli's Theorem. *J. Atmos. Sci.*, **50**, 1437 - 1443.

_____, and H. Wernli, 1994: The potential vorticity budget of the general circulation as viewed with the generalized Bernoulli-Theorem. In the proceedings of an *International Symposium on The Life Cycles of Extratropical Cyclones.* 75 - 80.

Shutts, G., 1983: The propagation of eddies in diffluent jetstreams: eddy vorticity forcing of blocking flow fields. *Quart. J. Royal Meteor. Soc.*, **109**, 737 - 761.

_____, G. J., 1986: A case study of eddy forcing. in Anomalous Atmospheric Flows and Blocking, ed. by Barry Saltzman, 135 - 161.

_____, G. J., 1987: Some comments on the concept of thermal forcing. *Quart. J. Royal Meteor. Soc.*, **113**, 1387 - 1394.

Smagorinsky, J., 1953: The dynamical influence of large-scale heat sources and sinks on the quasi-stationary mean motions of the atmosphere. *Quart. J. Royal Meteor. Soc.*, **79**, 342 - 366.

Stamp, A. P. and T. E. Dowling, 1993: Jupiter's Winds and Arnol'd's Second Stability Theorem: Slowly Moving Waves and Neutral Stability. *J. Geophys. Res.*, **98**, 847 - 855.

Sun, D., and R. S. Lindzen, 1994: A PV view of the zonal mean distribution of temperature and wind in the extratropical troposphere. *J. Atmos. Sci.*, **51**, 757 - 772.

Verkley, W. T. M., 1994: Tropopause dynamics and planetary waves. *J. Atmos. Sci.*, **51**, 509 - 529.

Whitham, G., 1960: A note on group velocity. *J. Fluid Mech.*, **22**, 273 - 383.